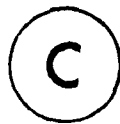^{127}I MÖSSBAUER SPECTROSCOPIC STUDIES OF SOME

CATIONS AND ANIONS OF IODINE

by

(C) Ronald D. Myers (B.Sc.)

A Thesis
Submitted tö the Faculty of Graduate Studies
in Partial Fulfilment of the Requirements
for the Degree
Doctory of Philosophy

McMaster University

February 1982

^{127}I MÖSSBAUER SPECTROSCOPIC STUDIES OF SOME

CATIONS AND ANIONS OF IODINE

TO MY PARENTS AND MY BROTHERS AND SISTER

DOCTOR OF PHILOSOPHY (1982)   McMASTER UNIVERSITY

  (Chemistry)   Hamilton, Ontario.

TITLE: ^{127}I Mössbauer Spectroscopic Studies of Some Cations

                and Anions of Iodine

AUTHOR: Ronald D. Myers, B.Sc. (McMaster University)

SUPERVISOR: Professor T. Birchall

NUMBER OF PAGES: xv;   221

ii

ABSTRACT

The ^{127}I Mössbauer spectra have been recorded at liquid-helium temperature for several series of iodine compounds. The Mössbauer spectra of a number of apparently cubic inorganic iodine compounds were measured and many were found to give abnormally broad lines. This was attributed to distortions from true cubic symmetry present in the compounds. KI gave the narrowest line and it was selected as the reference compound for ^{127}I Mössbauer spectroscopy.

The Mössbauer spectra of a series of linear iodine compounds, including the trihalide [X-I-Y]⁻ anions were measured and the magnitude of the quadrupole coupling constant was found to vary with the electronegativity of the attached ligands. Semi-empirical relationships had been developed to convert isomer shifts and quadrupole coupling constants into s- and p-orbital populations and these relationships have been re-established using the data for these linear iodine compounds. It was found that these semi-empirical relationships do not have general applicability when they were tested with a series of interhalogen, cations and some iodine-chalcogen cations.

Several new interhalogen cations of iodine were also prepared and characterized. The ^{127}I Mössbauer parameters for these square planar iodine(III) cations revealed that, while secondary or bridging inter-

actions are important in determining the sign of the quadrupole coupling constant, it is the primary bonds to iodine which determine the magnitude of the quadrupole coupling constant.

Finally, ^{127}I Mössbauer spectroscopy was applied to some interesting chemical problems. Mössbauer measurements on frozen solutions of $[I_2]^+$ suggest that the new species formed is a square or rectangular dimer of $[I_2]^+$, namely $[I_4]^{2+}$. ^{127}I Mössbauer measurements in conjunction with recent ^{129}Xe and ^{125}Te NMR and ^{129}Xe Mössbauer have conclusively shown that the =OTeF$_5$ ligand is less electronegative than -F.

ACKNOWLEDGEMENTS

LIST OF TABLES

LIST OF FIGURES

xiv

CHAPTER 1

INTRODUCTION

A. General

Iodine occurs in nature as iodide in brines and also as the iodates of sodium and calcium. It is the only halogen which exists naturally in the +5 oxidation state, mainly as the mineral lauterite (calcium iodate). Many forms of marine life concentrate iodine, the rarest of the three common halogens. The production of iodine occurs mainly through the oxidation of I^-, and a suitable laboratory preparation involves oxidation of I^- in acid solution with MnO_2.

Iodine is the only halogen which exhibits the Mössbauer effect. It is a very attractive element for Mössbauer spectroscopic studies for several reasons. It occurs in a number of widely different oxidation states, from I^- in the iodides to I^{7+} in the periodates, and electron configurations often turn out to be relatively simple, having been interpreted as involving only the 5(sp) shell. Iodine is also unique in that it is the fourth member in a series of five consecutive main group elements of the fifth row of the Periodic Table (from ^{119}Sn to ^{129}Xe) which exhibit the Mössbauer effect. Thus it is often possible to make useful comparisons of Mössbauer parameters among isoelectronic compounds from one group to another.

B. Polyhalogen Ions of Iodine

It is possible to view polyhalogen ions in general as being derived from the self-ionic dissociation of the parent neutral halogens or interhalogen compounds. These ionic dissociations could be described by the following equations. In the case of the parent halogens there are several ionic equilibria which may be assumed:

$$3X_2 \rightleftharpoons [X_3]^+ + [X_3]^- \qquad (1.1)$$

$$4X_2 \rightleftharpoons [X_5]^+ + [X_3]^- \qquad (1.2)$$

$$5X_2 \rightleftharpoons 2[X_2]^+ + 2[X_3]^- \qquad (1.3)$$
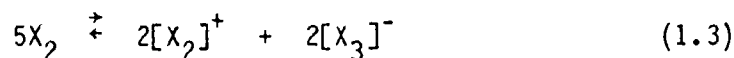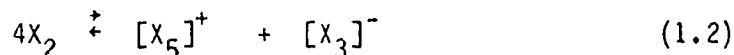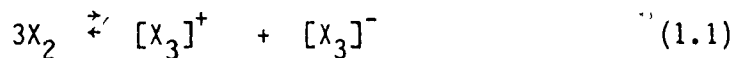
The interhalogen compounds could dissociate according to the following equilibria:

$$2XY_n \rightleftharpoons [XY_{n-1}]^+ + [XY_{n+1}]^- \qquad (1.4)$$

$$\text{if } n = 1, \text{ then} \quad 3XY \rightleftharpoons [X_2Y]^+ + [XY_2]^- \qquad (1.5)$$

$$4XY \rightleftharpoons [X_3Y_2]^+ + [XY_2]^- \qquad (1.6)$$
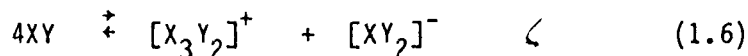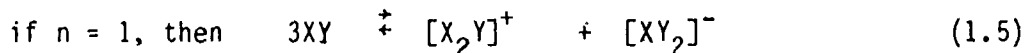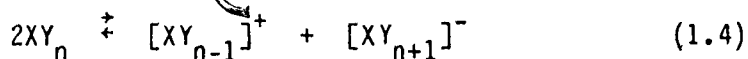
·That these types of equilibria actually exist in the neutral halogen compounds is perhaps demonstrated by ICl_3 which does not exist as a monomer but rather as a chlorine bridged dimer. This dimer could formally be regarded as being comprised of resonance hybrids of the form:

$$(ICl_3)_2 \leftrightarrow [ICl_2]^+[ICl_4]^- \leftrightarrow [ICl_4]^-[ICl_2]^+ \qquad (1.7)$$
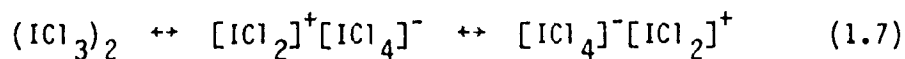
This propensity of the halogens and interhalogens to associate is further illustrated in the X-ray crystal structures of ICl and IBr where there are many secondary interactions from individual molecules to halogen atoms of neighbouring molecules.

From the above equilibria it is easy to see that the addition of a Lewis acid halide acceptor to the parent compound would shift the existing equilibrium, resulting in an increase in the formation of the polyhalogen cation, whereas the addition of a Lewis base would have the opposite effect, namely increasing the formation of polyhalogen anion.

(i) [XIY]⁻ Polyhalogen Anions

The ability of halide ions to associate with either halogen or interhalogen molecules and thus form complex polyhalide anions has been recognized for some time. In fact, soon after the discovery of iodine, Pelletier and Caventou [1] reported the addition complex between iodine and strychnine, which was undoubtedly strychninium tri-iodide, $C_{21}H_{22}O_2N_2 \cdot HI_3$. The polyhalogen complex anions have been reviewed by A. I. Popov [2] and Table 1.1 lists those anions which have been identified. For the purposes of Mössbauer spectroscopy the linear trihalide anions [XIY]⁻ (X,Y = F,Cl,Br,I) were selected for this study since apart from $[I_3]^-$ they contain at most two unique iodine sites and they are well characterized compounds. The X-ray crystal structures of several salts of the $[I_3]^-$ anion have been reported. Early work by Mooney [3] has shown that in $[NH_4][I_3]$ the anion is essentially linear, but is not centro-symmetric. This difference in the I-I bond lengths also occurs in the

Table 1.1.

Polyhalogen Anions of Iodine

$[X_3]^-$	$[X_5]^-$	$[X_7]^-$	$[X_9]^-$	$[X_n]^-$
$[I_3]^-$	$[I_5]^-$	$[I_7]^-$	$[I_9]^-$	$[I_4]^-$
$[I_2Br]^-$	$[I_4Cl]^-$	$[I_6Br]^-$		
$[I_2Cl]^-$	$[I_4Br]^-$	$[IF_6]^-$		
$[IBr_2]^-$	$[I_2Br_3]^-$	$[Br_6Cl]^-$		
$[ICl_2]^-$	$[I_2Br_2Cl]^-$			
$[IBrCl]^-$	$[I_2BrCl_2]^-$			
$[IBrF]^-$	$[IBrCl_3]^-$			
$[Br_3]^-$	$[ICl_4]^-$			
$[Br_2Cl]^-$	$[ICl_3F]^-$			
$[BrCl_2]^-$	$[IF_4]^-$			
$[Cl_3]^-$	$[BrF_4]^-$			
	$[ClF_4]^-$			

cesium salt,[4] while the tetraphenylarsonium salt [5] contains a symmetrical, linear $[I_3]^-$ anion. The crystal structures of $K[ICl_2]$,[6] $Cs[I_2Br]$,[7] $Cs[IBr_2]$,[8] and more recently $[(C_6H_5)_4P][IBr_2]$ [9] have also been reported and all contain essentially linear anions. It has been found by X-ray analysis, in conjunction with vibrational data, that the least electronegative halogen, namely iodine, is always in the central position of the anion. While there is no spectroscopic evidence for the $[BrIF^-]$ anion, Cremer and Duncan [10] observed that CsF absorbs IBr to produce a yellow solid thought to be $Cs[BrIF]$. The linearity of many of these trihalide anions has been confirmed and in some cases inferred on the basis of extensive vibrational spectroscopic studies.[11-13] The iodine Mössbauer spectra of $K[ICl_2] \cdot H_2O$ [14] and $Cs[I_3]$ [15] have been measured, using the 129-isotope in the latter case. The Mössbauer parameters are consistent with the linear geometry which has been established by X-ray crystallography and vibrational spectroscopy.

(ii)   Interhalogen Cations of Iodine

The polyhalogen cations have been reviewed recently by Shamir.[16] As previously mentioned the most convenient method for preparing polyhalogen cations involves the addition of Lewis acid halide acceptors to the neutral compounds. In these reactions the formal oxidation state of the central halogen generally remains unchanged and thus the formation of hetero-polyhalogen cations from neutral interhalogen compounds may be described by the following equation:

$$XY_n + MY_m \rightarrow [XY_{n-1}]^+[MY_{m+1}]^- \qquad (1.8)$$
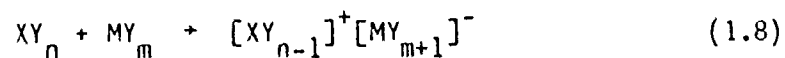
where XY_n is the neutral parent interhalogen compound and MY_m is a Lewis acid such that M = Sb, As, Al, etc. Polyhalogen cations may also be prepared by oxidative reactions whereby the Lewis acid itself can act as the oxidizer. Such is the case in the preparation of $[I_2][Sb_2F_{11}]$ [17] according to the following equation:

$$2I_2 + 5SbF_5 \rightarrow 2[I_2][Sb_2F_{11}] + SbF_3 \qquad (1.9)$$
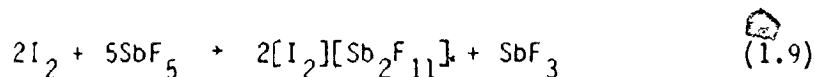
The polyhalogen cations are highly hygroscopic and hydrolyze easily and hence must be handled and stored under rigorously dry conditions. Table 1.2 lists the known polyhalogen cations of iodine, many of which will be discussed in this thesis.

(iii) $[IX_2]^+$ and $[I_3X_2]^+$ Symmetric Cations

Various physical measurements such as single-crystal X-ray structures, vibrational spectra, multinuclear NMR and Mössbauer spectroscopy of $[XY_2]^+$ cations in general support a mainly ionic structural model in which the cation is bent and possesses C_{2v} symmetry. However some cation-anion interaction does exist via halogen bridges of varying strength from two separate anions to the cation. VSEPR theory [18] would then predict an octahedral geometry $AX_2Y_2E_2$ with the two non-bonding electron pairs occupying the axial positions. As in the anions it has been found without exception that the least electronegative halogen occupies the central position of the cation, while the terminal positions are occupied by the more electronegative halogens. This observation can be extended to the general case for any interhalogen cation.

Table 1.2.

Polyhalogen Cations of Iodine

$[I_2][Sb_2F_{11}]$ $[IF_2][BF_4]$ $[I_2Cl][SbCl_6]$ $[IF_4][SbF_6]$

$[Ta_2F_{11}]$ $[AsF_6]$ $[AlCl_4]$ $[Sb_2F_{11}]$

$[SbF_6]$ $[SO_3F]$ $[SO_3F]$

$[GaCl_4]$ $[SnF_6]$

$[I_3][AlCl_4]$

$[AsF_6]$ *$[ICl_2][SbF_6]$ $[TaCl_6]$ $[PtF_6]$

$[SbF_6]$ $[SbCl_6]$ $[CrF_4Sb_2F_{11}]$

$[AlCl_4]$ $[I_2Br][SO_3F]$

$[I_5][AlCl_4]$ $[Sb_2F_{11}]$ $[IF_6][SbF_6]$

$[SbF_6]$ $[SO_3F]$ $[BrICl][SbCl_6]$ $[Sb_2F_{11}]$

$[SO_3Cl]$ $[SO_3F]$ $[AsF_6]$

$[I_7][SO_3F]$ $[BF_4]$

*$[IBr_2][Sb_2F_{11}]$ *$[Br_{0.75}ICl_{1.25}][SbCl_6]$ $[AuF_6]$

$[SO_3F]$

$[SO_3CF_3]$ *$[I_3Cl_2][SbCl_6]$

$[I_3Br_2][SbCl_6]$

$[AlCl_4]$

* These cations were prepared and characterized in the course of this work.

The X-ray crystal structures of $[ICl_2][SbCl_6]$ and $[ICl_2][AlCl_4]$ have been reported [19] and they are isostructural in that they both contain iodine in a square-planar environment. In this square, two positions are occupied by two terminal chlorines of the $[ICl_2]^+$ cation and two others by bridging chlorines of two separate anions. This geometry has been observed in the X-ray crystal structures of several $[XY_2]^+$ interhalogen cations [20-24] which do not contain iodine. The $[IF_2]^+$ cation [25] and $[IBr_2]^+$ cation [26,27] have been identified on the basis of ^{19}F NMR and Raman spectroscopic studies, respectively.

The $[I_3]^+$ cation was first postulated in 1938 by Masson [28] and since 1960 several groups have confirmed the existence of this ion in solution, by conductimetric and cryoscopic methods.[29-31] The X-ray crystal structure of the hexafluoroarsenate salt of $[I_3]^+$ was recently reported by Passmore and co-workers.[32] The structure is similar to that of $[ICl_2]^+$ in that the central iodine is in a square-planar environment with bonds to two terminal iodines and weaker bridging interactions to two fluorines of two separate $[AsF_6]^-$ anions.

In view of the geometry observed in these square-planar iodine-(III) compounds there are several possible bonding models. A purely ionic model in which localized p-orbitals of the central halogen form primarily p-σ bonds would be expected to result in a bond angle of 90°. This angle could undergo some distortion as a result of mutual repulsion between the two terminal halogens of the cation. Alternatively, a more covalent, bridging model with sp^3d^2 hybridization of the central halogen would result in a pseudo-octahedral structure. This again would result

in bond angles of 90° with some distortion due to the asymmetry in the bond lengths of the terminal and bridging halogens. Finally, a bond angle near 109° 27' corresponding to the tetrahedral angle would be expected if an ionic model with sp^3 hybridization were operative. On the basis of existing X-ray data for these compounds no exclusive model may be assumed, however, because of the unusual strength of the bridging bonds, the high degree of planarity of the $[IX_4]$ unit, and the volatility of some of these compounds, there must be considerable covalent character in the bonds of which the sp^3d^2 description would be a contributor.

It has also been reported [33-35] that under suitable conditions iodine monochloride combines with antimony pentachloride to produce compounds with the general formula $I[SbCl_6]\cdot nICl$ (n = 2-4), i.e., containing the cations $[I_3Cl_2]^+$, $[I_4Cl_3]^+$ and $[I_5Cl_4]^+$.

(iv) $[I_2X]^+$ and $[XIY]^+$ Asymmetric Cations

The asymmetric $[I_2X]^+$ and $[XIY]^+$ cations are less well characterized than the symmetric cations, having been identified on the basis of vibrational spectroscopy and conductivity measurements. The $[I_2Cl]^+$ cation has been reported by several groups, [26,27,36-40] and although no X-ray structural data is yet available it has been assumed that it has the same bent geometry as the symmetric cations. Similar spectroscopic evidence has been reported for $[I_2Br]^+$ and $[BrICl]^+$. [26,27,38]

C. The Mössbauer Effect

(i) Nuclear Resonant Absorption

The phenomenon of absorption or emission of gamma-ray photons with no loss of energy due to thermal broadening or recoil of the nucleus is known as the Mössbauer effect. R. L. Mössbauer [41] first observed recoiless nuclear resonant absorption in 1957. This process is of fundamental importance in chemical studies since it provides a means of measuring the comparatively weak interactions between the nucleus and surrounding electrons. This is possible because of the production of monochromatic radiation having an extremely high intrinsic resolution of one part in 10^{13}. There are several mechanisms which can act to degrade this radiation, particularly the effects of nuclear recoil and thermal broadening. [42]

Consider the hypothetical situation of an isolated nucleus of a particular mass and energy moving at constant velocity. Subsequent to the emission of a gamma-ray photon the nucleus undergoes recoil and has a new velocity and a new total energy. The energy of the emitted photon is thus given by:

$$E_\gamma = E - E_R - E_D \qquad (1.10)$$

where E_R is the recoil kinetic energy and E_D is the thermal or Doppler energy. Since momentum must be conserved during emission, the energy of recoil [43] is given by:

$$E_R = \frac{E_\gamma^2}{2Mc^2} \qquad (1.11)$$

The Doppler energy E_D which also degrades the radiation, is dependent on the thermal motion of the nucleus and has a distribution of energies as a result of its temperature dependence. An average value of E_D can be defined [43] which is related to the average kinetic energy per translational degree of freedom, $\overline{E}_k = 1/2\ kT$, by:

$$\overline{E}_D = 2\sqrt{(\overline{E}_k E_R)} = E_\gamma \sqrt{\frac{2\overline{E}_k}{Mc^2}} \qquad (1.12)$$

where k is Boltzman's constant and T is the absolute temperature. As a result of these two nuclear effects the statistical energy distribution of the emitted gamma-rays is displaced from the true excited state energy by $-E_R$ and is broadened by E_D into a Gaussian distribution of width $2\overline{E}_D$. The distribution for absorption has the same shape but is displaced to $+E_R$. Thus nuclear resonant absorption will only have a significant probability of occurring if these two energy distributions overlap strongly. The problem of recoil is however minimized when the nucleus is embedded in a rigid crystal lattice rather than being in an isolated situation. In this case the entire crystal takes up the recoil and because of the large effective mass, both the kinetic recoil energy and Doppler broadening become small and less than the line width at half maximum, Γ (equations 1.11 and 1.12). The statistical energy distribution is governed by the Heisenberg uncertainty principle so that:

$$\Gamma = \frac{\hbar}{\tau} \qquad (1.13)$$

where $h = 2\pi\hbar$ is Planck's constant and τ is the lifetime of the excited state.

The kinetic recoil energy is much less than chemical binding energies but is similar in magnitude to lattice vibration phonon energies. The Debye theory [44] for solids requires that these lattice vibrations be quantized so that recoil energy can only be transferred to the lattice if it corresponds closely to an allowed quantum jump. The recoil-free fraction f_A is therefore defined as the fraction of emissions which do not excite lattice vibrations and where recoiless emission of gamma-rays occurs. It is possible to relate f_A to the vibrational properties of the crystal lattice by:[45,46]

$$f_A = \exp\left(\frac{-E_\gamma^2 \langle x^2 \rangle}{(\hbar c)^2}\right) \qquad (1.14)$$

where $\langle x^2 \rangle$ is the mean square vibrational amplitude of the nucleus in the direction of the gamma-ray emission. The mean square vibrational amplitude of the nucleus is temperature dependent [43] and f_A is therefore inversely proportional to temperature. It is critical that f_A be as large as possible and it is maximized for a rigidly bound atom at low temperature with a small mean square displacement, and when the gamma-ray energy is small.

D. Hyperfine Interactions

(i) Isomer Shift

The nucleus has a finite size which can change fractionally during a gamma-ray transition. Similarly, the s-electron wave function also has a finite value inside the nuclear radius and is directly responsible for the change in electrostatic energy observed. If during a nuclear transition from the excited to the ground state the nuclear radius changes by a small amount, the corresponding change in electrostatic energy is given by:[43]

$$\Delta W = \frac{1}{5\varepsilon_0} Ze^2 R^2 \frac{\delta R}{R} |\psi_s(0)|^2 \qquad (1.15)$$

where ε_0 is the permittivity of a vacuum and $|\psi_s(0)|^2$ is the non-relativistic Schroedinger wavefunction at $r = 0$ and represents the s-electron density at the nucleus. The Mössbauer experiment then compares the difference in energy between the nuclear transitions in the source and absorber and when the s-electron density is different in the source from that of the absorber, a Doppler velocity must be applied to the source in order to observe resonance. The isomer shift is given by:[47]

$$I.S. = \delta = \frac{4\pi}{5} Ze^2 R^2 \left(\frac{\delta R}{R}\right) \left(|\psi_s(0)_{abs}|^2 - |\psi_s(0)_{source}|^2\right) \qquad (1.16)$$

where R is the radius of the nucleus and δR is the change in nuclear radius during emission. There have been various estimates [48,49] of $\delta R/R$ for ^{127}I, ranging from -5.6×10^{-5} to -4.8×10^{-4} and while there is

no general agreement as to the absolute value for $\delta R/R$ the sign is known to be negative. This means that the ^{127}I nucleus expands upon de-excitation and hence an increase in chemical isomer shift corresponds to a decrease in s-electron density at the iodine nucleus. Since the above equation (1.16) is the product of a chemical term and a nuclear term, the latter of which is constant for a particular transition, it is possible to study changes in electron density directly. $|\psi_s(o)|^2$ includes contributions from all occupied s-electron orbitals of the atom and is sensitive to changes occurring in the valence orbitals. Although $|\psi(o)|^2$ for p-, d- and electrons in higher orbitals is zero these orbitals affect the net s-electron density indirectly since they can penetrate the inner core and hence shield the s-electrons from the nucleus. Any factor which can alter the s-electron density at the nucleus will consequently affect the isomer shift.

The isomer shift is also temperature dependent and is affected by two factors. One is the second order Doppler shift [47] which arises from the temperature dependence of the lattice vibration term $\langle x^2 \rangle$, affecting the gamma-ray energy to a small extent.

$$\delta E_\gamma = \frac{-\langle x^2 \rangle}{2c^2} E_\gamma \qquad (1.17)$$

Since c^2 is much larger than $\langle x^2 \rangle$ this term will be very small. So for a series of chemically similar compounds measured at the same temperature, the second order Doppler shift will be essentially zero because $\langle x^2 \rangle$ is

nearly constant. A second temperature dependent effect which is often

difficult to detect arises from chemical or physical changes in the

compound itself due, for example, to a phase change in the crystal

structure.

(ii) Quadrupole Splitting

As well as interacting with extra-nuclear electrons the nuclear

energy levels may also be affected by the surrounding chemical environ-

ment interacting with the electric quadrupole moment. The quadrupole

moment is a measure of the deviation from spherical symmetry of the

nuclear charge, and may be positive or negative depending on the

distribution. Only those nuclear states with spin $I > 1/2$ have a non-

spherical charge distribution and hence a quadrupole moment. For ^{127}I

the ground state quadrupole moment eQ is negative and thus the nucleus is

flattened along the spin axis. If the surrounding molecular electric

field changes rapidly as a function of the angle from some molecular

axis, then the various orientations of the non-spherical nucleus with

respect to this axis lifts the degeneracy of the levels. This may be

expressed by the following Hamiltonian:[43]

$$H = \frac{-1}{6} eQ \cdot \nabla E \qquad (1.18)$$

where eQ is the electric quadrupole moment and ∇E represents the electric

field gradient at the nucleus. It is only necessary to specify two

components to completely describe the electric field gradient in its

principal axis system. $V_{zz} = eq$ is taken to be the largest value of $|V_{ii}|$ and the asymmetry parameter η is defined as follows:[ ]

$$\eta = (\frac{V_{xx}-V_{yy}}{V_{zz}}) \quad (0 < \eta < 1) \tag{1.19}$$

The previous Hamiltonian in equation (1.18) may now be expressed as

$$H = \frac{eQ}{2I(2I-1)} [V_{zz}I_z^2 + V_{yy}I_y^2 + V_{xx}I_x^2]$$

$$= \frac{e^2qQ}{4I(2I-1)} [3I_z^2 - I(I+1) + \eta(I_x^2 - I_y^2)] \tag{1.20}$$

If the electric field gradient has axial symmetry ($\eta = 0$) the the energy levels are given by:[43]

$$E_Q = \frac{e^2qQ}{4I(2I-1)} [3I_z^2 - I(I+1)] \tag{1.21}$$

Therefore for ^{127}I where $I_g = \pm5/2$ the ground state is split into three levels and the excited state which has $I_e = \pm7/2$ is split into four levels. The relative energies of the transitions between the ground and excited states are thus determined by the magnitude of the ground and excited state quadrupole moments. For ^{127}I the ground state quadrupole moment is quite large (-0.79 barn) and the ratio $^{127}Q_e/^{127}Q_g = 0.892$ [50] so that moderate deviations from cubic symmetry result in some splitting of the resonance into the eight component lines. The relative intensities of the respective lines are in the ratios of the squares of

the Clebsch-Gorden [51] coefficients of the transitions. The M1 dipole selection rule restricts transitions so that $\Delta I_z = 0, \pm 1$ when $n = 0$. If the electric field is not axially symmetric about the principal axis, i.e. $n \neq 0$, then all twelve possible transitions between the excited state and ground state become allowed since the quantum numbers which determine the nuclear spin states are no longer good and the states are mixed. Also if $n > 0$ the relative intensities of all the lines are modified and some transitions may become degenerate. Figure 1.1 illustrates in a series of computer simulated [52] ^{127}I Mössbauer spectra how n affects the absorption envelope when all other parameters are held constant. In these spectra the quadrupole coupling constant is fixed at a large positive value (3000 MHz), the isomer shift is fixed at -0.5 mms^{-1} and the source and absorber line widths are fixed at the natural value (1.27 mms^{-1}). Eta varies from 0.0 - 1.0 (Figure 1.1a-d) and the overall effect is to make the absorption envelope more symmetric as n approaches unity. Thus a quadrupole spectrum of ^{127}I yields the magnitude as well as the sign of the quadrupole coupling constant $e^2 q^{127} Q_g'/h$, and hence the electric field gradient, as well as the magnitude of the asymmetry parameter n. When $n = 1$ the sign of $e^2 q^{127} Q_g/h$ has no meaning.

(iii) Line Width

The natural line width is governed by the uncertainty principle where the ideal source would produce radiation with a Lorentzian distribution of energy. Assuming that the absorber is ideally thin then
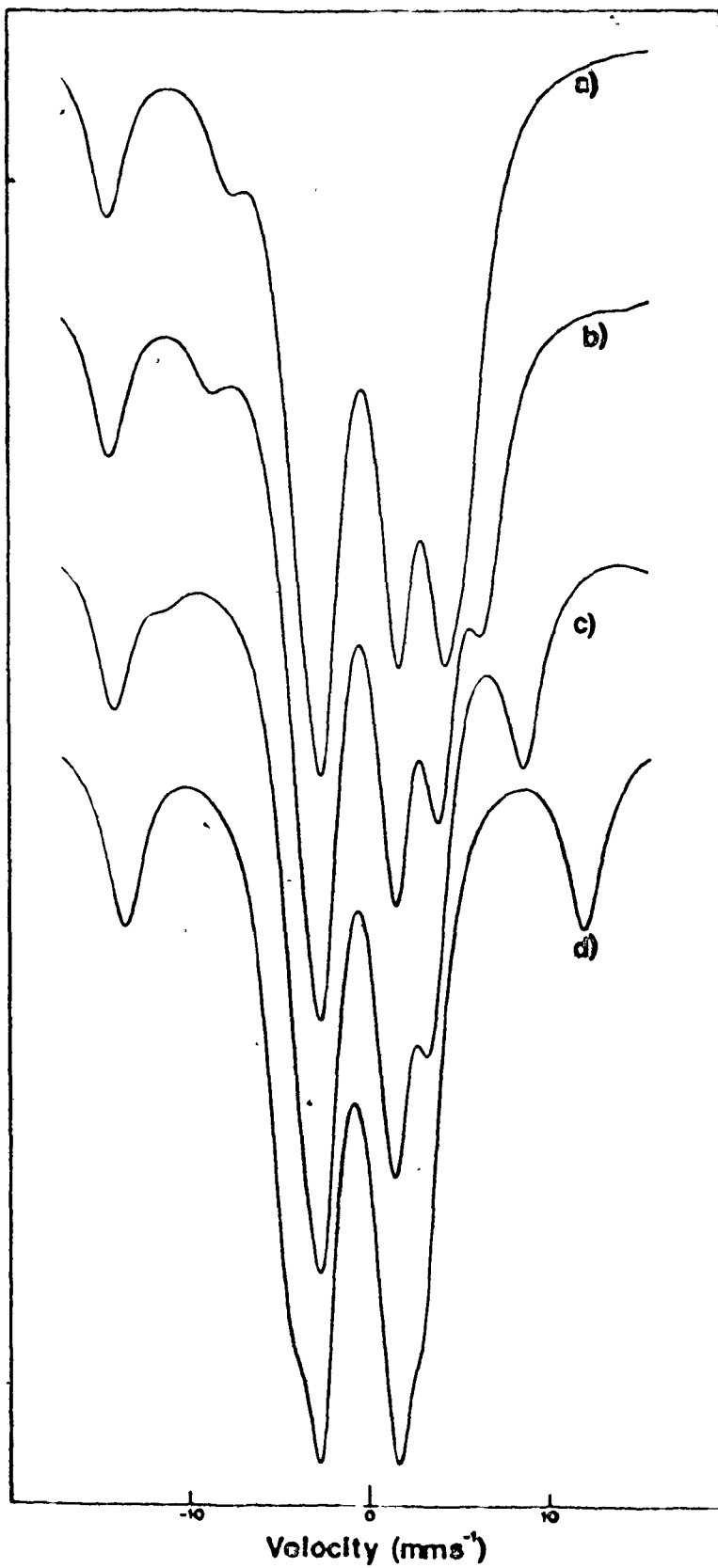
Figure 1.1.   Simulated ^{127}I Mössbauer spectra where $e^2q \, ^{127}Q'_g/h = 3000$ MHz, isomer shift $= -0.5$ mms^{-1}, and $2\Gamma = 2.54$ mms^{-1}: a) $\eta = 0.0$ b) $\eta = 0.3$ c) $\eta = 0.6$ d) $\eta = 1.0$

the absorption band would have a width at half intensity, $\Gamma_{exp} = 2\Gamma_{nat}$. It is rare that the natural line width is observed, for several reasons. Non-homogeneity of the chemical environments of the resonant atoms in the source and/or absorber, i.e., disorder or multiple sites, will result in small variations in the hyperfine parameters and hence apparently broadened lines. Geometric effects, thermal effects and the presence of hyperfine structure due to extra-nuclear field effects may also contribute to the apparent line width.

It has become customary to treat Mössbauer spectra as if they were sums of Lorentzian lines, however it has long been recognized [46,53] that this procedure is unsatisfactory for thick absorbers with overlapping lines. For well resolved spectra no serious problems arise from such a treatment since individual line positions are accurately known and the effect of absorber thickness on the intensity and width of a single line is well understood.[53,54] In the case of ^{127}I however where the hyperfine interactions are generally small compared to the observed line width the individual parameters become correlated and thickness effects become much more subtle. Lazarus and Thomas [55] and others [56,57] have shown that reliable data can be obtained if transmission integral procedures are employed in the fitting procedures and if thickness effects are considered. For an absorption spectrum produced by a single Lorentzian source and a multiple line Lorentzian absorber, the transmission integral as a function of the velocity v is given by:[55]

$$I(v) = I_0 \left((1-f_S) + \frac{f_S}{\pi} \int_{-\infty}^{\infty} \frac{(\Gamma_0/2)dE}{(E + vE_0/c)^2 + (\Gamma_0/2)^2}\right.$$

$$\left. \exp\left[-\sum_k W(k)T_A \frac{(\Gamma_0/2)^2}{[E-E_A(k)]^2 + (\Gamma_0/2)^2}\right]\right) \tag{1.22}$$

I_0 is the intensity of the unattenuated radiation, f_S is the recoil-free fraction of the source, Γ_0 is the full width of a half-maximum, assumed to be the same for source and absorber, $W(k)$ is the Clebsch-Gorden intensity for the kth line located at $E_A(k)$, E_0 is the energy of the incident radiation at zero velocity and c is the velocity of light. The effective thickness of the absorber, T_A is a dimensionless quantity equal to $f_A n_A a \sigma_0 t_A$ where f_A is the recoil-free fraction of the absorber, n is the number of atoms per cubic centimeter, a is the fractional abundance of resonant atoms, σ_0 is the cross section at resonance and t_A is the thickness of the absorber in centimeters. Therefore if T_A is small the transmission function reduces to a sum of Lorentzians, each with width $2\Gamma_0$ and intensity given by $W(k)$.

E.   Chemical Interpretation of ^{127}I Mössbauer Spectra

The chemical isomer shift and quadrupole coupling constant in ^{127}I compounds are largely determined by the valence shell (5sp) electron configuration.   It has become customary to use semi-empirical relationships to convert isomer shifts and quadrupole coupling constants into s- and p-orbital populations.   The "hole numbers", $h_{p_{x,y,z}}$ and h_s refer to the amount of $5p_{x,y,z}$ and 5s charge, expressed in units of electrons,

missing from the closed shell $5s^2p^6$ electron configuration of I^-. The semi-empirical relationships for the isomer shift have been developed by Hafemeister et al.[58] and later by Perlow and Perlow,[14] and that for the electric field gradient by Townes and Dailey.[59,60] It is possible to write the isomer shift with respect to I^- as:

$$\delta_{I^-} = K[-h_s + \gamma(h_p + h_s)(2 - h_s)] \tag{1.23}$$

K and γ are constants so that $-Kh_s$ represents the change in isomer shift due to loss of 5s-electrons. The $(2-h_s)$ 5s-electrons remaining are then deshielded by a total decrease in the number of electrons $(h_p + h_s)$. In order to use expression (1.23) the values of K and γ must be evaluated. The accepted value [43,47,61] for γ is 0.07. In most cases $h_s \ll h_p$ so (1.23) may be written as:

$$\delta_{I^-} = 2K\gamma h_p \tag{1.24}$$

The relative populations of the s- and p-orbitals are not given by the isomer shift, but may be derived in conjunction with the quadrupole coupling constant to which h_s does not contribute. According to Townes and Dailey,[60] the principal value of the molecular electric field gradient (eq_{mol}) is related to the atomic electric field gradient arising from a 5p-hole in the $5s^2p^6$ configuration, eq_{at} by:

$$eq_{mol} = eq_{at}U_p \tag{1.25}$$

where U_p is the imbalance in the 5p-shell. U_p has been assigned a directional property in terms of U_x, U_y and U_z as given by:

$$U_p = -U_z + \frac{U_x + U_y}{2} \qquad (1.26)$$

Thus the asymmetry parameter is given by:

$$\eta = \frac{V_{xx} - V_{yy}}{V_{zz}} = \frac{3}{2} \left(\frac{U_x - U_y}{U_p} \right) \qquad (1.27)$$

The value of $e^2 q_{at}{}^{127}Q_g/h$ is known [62] accurately from nuclear quadrupole resonance spectroscopy to be +2293 MHz. Having evaluated U_x, U_y and U_z, h_p can be calculated from:

$$h_p = 6 - (U_x + U_y + U_z) \qquad (1.28)$$

Perlow and Perlow [14] have used U_p, calculated from the measured quadrupole coupling constants, together with the isomer shifts for HI (anhydrous), I_2, $K[ICl_2] \cdot H_2O$, ICl and $K[ICl_4] \cdot H_2O$ to obtain a value for $2K\gamma$ of -0.56 mms^{-1}. This then leads to the following expression for the isomer shift:[47]

$$^{127}\delta_{ZnTe} = 4.0[-h_s + 0.07 (h_p + h_s)(2 - h_s)] + 0.16$$
$$= 3.44 h_s - 0.56 h_p + 0.16 \qquad (1.29)$$

The above expression has been used exclusively to describe the bonding in a wide variety of iodine compounds.

F.   Purpose of This Work

In 1962 Jha et al. [63] reported the 27.77 KeV gamma-ray transition of ^{129}I, a radio-isotope with a half-life of 1.7×10^7 y. Soon after this Hafemeister et al. [58] conducted extensive experiments which yielded chemical, solid state and nuclear results. The 57.60 KeV gamma-ray transition of ^{127}I, the naturally occuring isotope present in 100% abundance, was observed by Barros et al. [64] in 1964. By far the greatest use for chemical studies has been made with the 129-isotope because of the superior spectral resolution that it offers. However the 129-isotope suffers a major disadvantage in chemical studies in that one must carry out chemical reactions with a radio-isotope on a small scale, and it is rare that the products of such reactions are chemically analyzed. This disadvantage of course does not arise for the stable 127-isotope and the paucity of chemical investigations with this isotope is probably due to the large natural line width.($2\Gamma = 2.54$ mms^{-1} [65]) coupled with the high transition energy which results in lower recoil-free fractions and necessitates carrying out measurements at liquid He temperatures.

The main objective of the work presented in this thesis was to examine in a systematic way some series of iodine compounds whose structures are well known from X-ray crystallography and spectroscopy. In order to confidently interpret the effect which different ligands surrounding a particular iodine nucleus have on the Mössbauer parameters it is imperative that the same gross structure be maintained in the series of compounds. The linear trihalide [X-I-Y]$^-$ anions were

initially examined to, first, determine the feasibility of doing ^{127}I

Mössbauer spectroscopy and second, to test the semi-empirical

relationships which have been used in interpreting iodine Mössbauer

parameters, and thereby monitor the effect of the terminal halogens on

the Mössbauer parameters of the central nucleus.

Several new iodine interhalogen cations were prepared and

characterized in order to clarify some problems existing in this area of

chemistry and to investigate the iodine nucleus when it is situated in a

square-plane of halogens, as is found in the series of $[IX_2]^+$ cations.

The chalcogen-iodine cations which were examined, provided a series of

well characterized compounds whose ^{127}I Mössbauer parameters gave

information as to the nature of the bonding between the iodine and

chalcogen atoms. Once again the semi-empirical relationships were

examined as to their general applicability.

By conducting an extensive survey of well characterized compounds

it became possible to apply this technique to some interesting chemical

problems. Using the results of the study of the $[X-I-Y]^-$ anions and

related compounds, it was possible to determine the relative electro-

negativities of the -F and -OTeF$_5$ ligands using ^{127}I Mössbauer spectro-

scopy, in conjunction with other spectroscopic techniques. The $[I_2]^+$

cation was examined in the solid state and frozen fluorosulfuric acid

solution in order to try and understand the structure and the bonding of

the cation, particularly in the frozen solution.

Finally, one of the biggest problems in comparing ^{127}I Mössbauer data from different laboratories arises because of the lack of a suitable reference compound. The Mössbauer spectra of several nominally cubic inorganic iodine compounds were measured in order to select a good reference compound.

CHAPTER 2

EXPERIMENTAL SECTION

A. General Preparative Techniques

(i) Vacuum System

The majority of the preparative work presented in this thesis was carried out with the use of a pyrex vacuum system. The vacuum line consisted of an all pyrex high-vacuum section and a greaseless pyrex section equipped with teflon Rotaflow valves. Both sections were maintained under dynamic vacuum with a rotary pump and a two-stage mercury diffusion pump. Connections were made to the high-vacuum section by 9 mm i.d. ball joints while those to Rotaflo valves were made by 1/4" standard wall pyrex tubing which was attached by means of 1/4" teflon nuts and ferrules to a straight Swagelock union or to a teflon diaphragm valve.

(ii) Dry Atmosphere System

All starting materials and samples which hydrolyze in air were handled in a dry-nitrogen Labconco glove-box fitted with a constant circulation liquid nitrogen drying system. The glove-box was filled with "extra-dry nitrogen" supplied by Specialty Gases, or with dry nitrogen from the liquid nitrogen reservoir boil-off. An evacuable port provided access to the glove box.

(iii) Reaction Vessels

Since many of the compounds prepared for this thesis are highly moisture sensitive and very strong oxidants it was necessary to prepare them in the absence of air and in a weakly basic solvent. The solvent used was SO_2 (or SO_2ClF) and a Dean type reaction vessel [66] as shown in Figure 2.1 was used to prepare the compounds. Depending on the aims of a particular reaction, the vessel was modified by attaching NMR tubes, etc., directly to the vessel. The stopcocks used on the vessels were either teflon Rotaflo valves or teflon diaphragm valves, as previously described.[67] Prior to use the reaction vessels were carefully dried by repeated flamings while pumping under dynamic vacuum.

B.   Experimental Techniques and Apparatus

(i) Mössbauer Spectrometer

The Mössbauer spectra were recorded using an Elscint Mössbauer Function Generator and Driving Unit, Model MFD-4, and an Elscint transducer. Constant acceleration motion was used and the sense of the acceleration was controlled by a multichannel analyzer operating in the multiscaling mode. A Northern-900 series multichannel analyzer was used and spectra were either accumulated in 256 channels of the mutichannel analyzer with automatic folding of the triangular waveform or in 512 channels with no folding. The velocity and hence the gamma-ray energy varied linearly with time. The complete system was comprised of a preamp/amplifier, single channel analyzer, analog-to-digital converter, a

TEFLON
STOPCOCK

TEFLON PLUG

TEFLON
SWAGELOCK
UNION

MEDIUM SINTERED
GLASS

TEFLON
COATED
STIRRING
BAR

5mm NMR TUBE
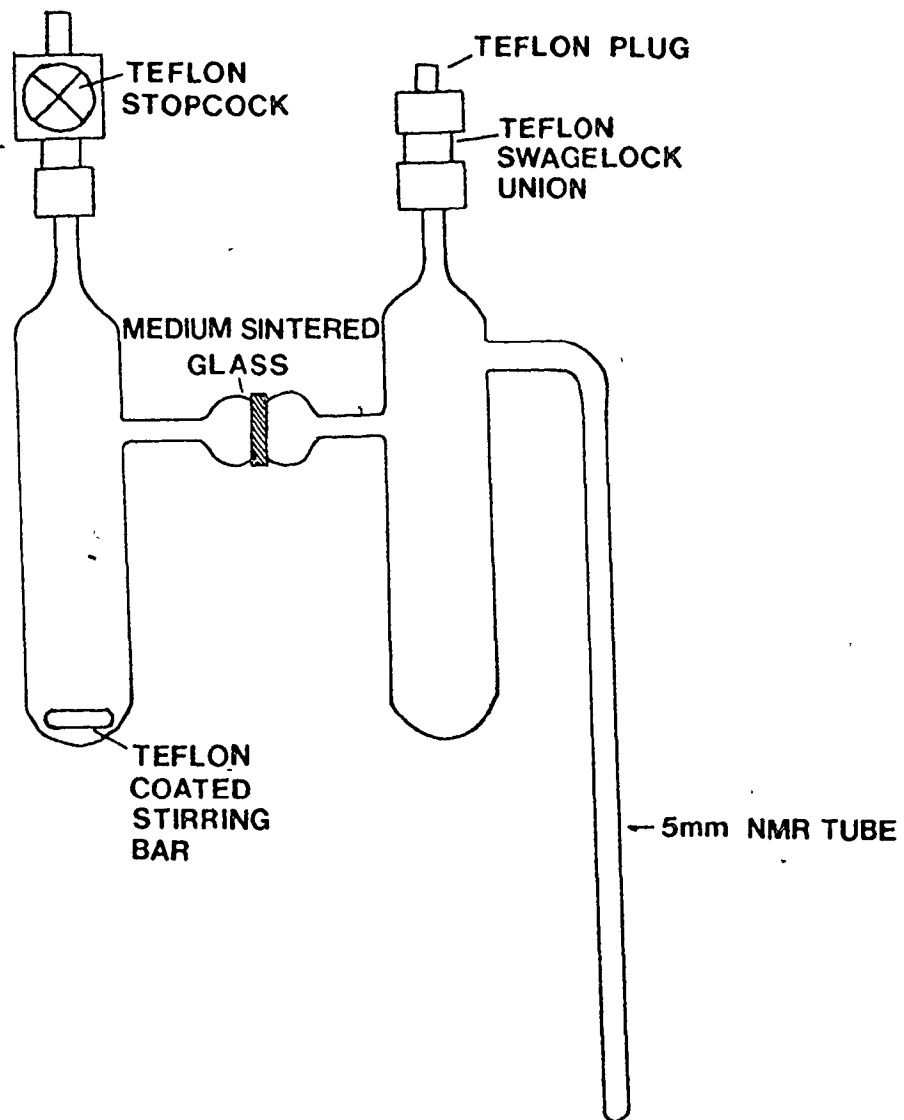
Figure 2.1.   Dean reaction vessel with attached NMR tube.

complete core memory package, readout drives and a cathode ray tube display. The Northern-900 analyzer was used in conjunction with a Northern-458 dual input multichannel scaling controller. The block diagram, Figure 2.2, shows the essential components of the Mössbauer spectrometer.

The gamma-ray source used was either a 10 or 20 mCi $Zn^{127m}Te$ emitter produced by New England Nuclear Corporation. Attempts to produce a suitable source in the McMaster University Nuclear Reactor by neutron irradiation of $^{66}Zn^{126}Te$ were unsuccessful because of the low thermal neutron fluxes available. The single channel analyzer was set on the 57.6 keV gamma-ray line as shown in Figure 2.3. The partial decay scheme of ^{127m}Te is also given in the inset. The transmitted radiation was detected by a Harshaw NaI(Tl) crystal and matched photomultiplier tube. The crystal thickness was 2 mm. The appropriate energy was selected by adjusting the upper and lower input voltage of the single channel analyzer. The signal from the single channel analyzer was amplified, counted, and stored in the core memory.

The Mössbauer spectra consist of a plot of count rate versus velocity (energy). Since the constant acceleration motion has opposite signs in alternate halves of the memory a mirror image appears in the memory halves with one spectrum being counted during acceleration and the other during deceleration of the drive in the nonfolding mode.

The accumulated data was then transferred onto a teletypewriter, TTY33, which included a typewriter and paper tape punch. The data were subsequently transferred to computer cards for final processing.
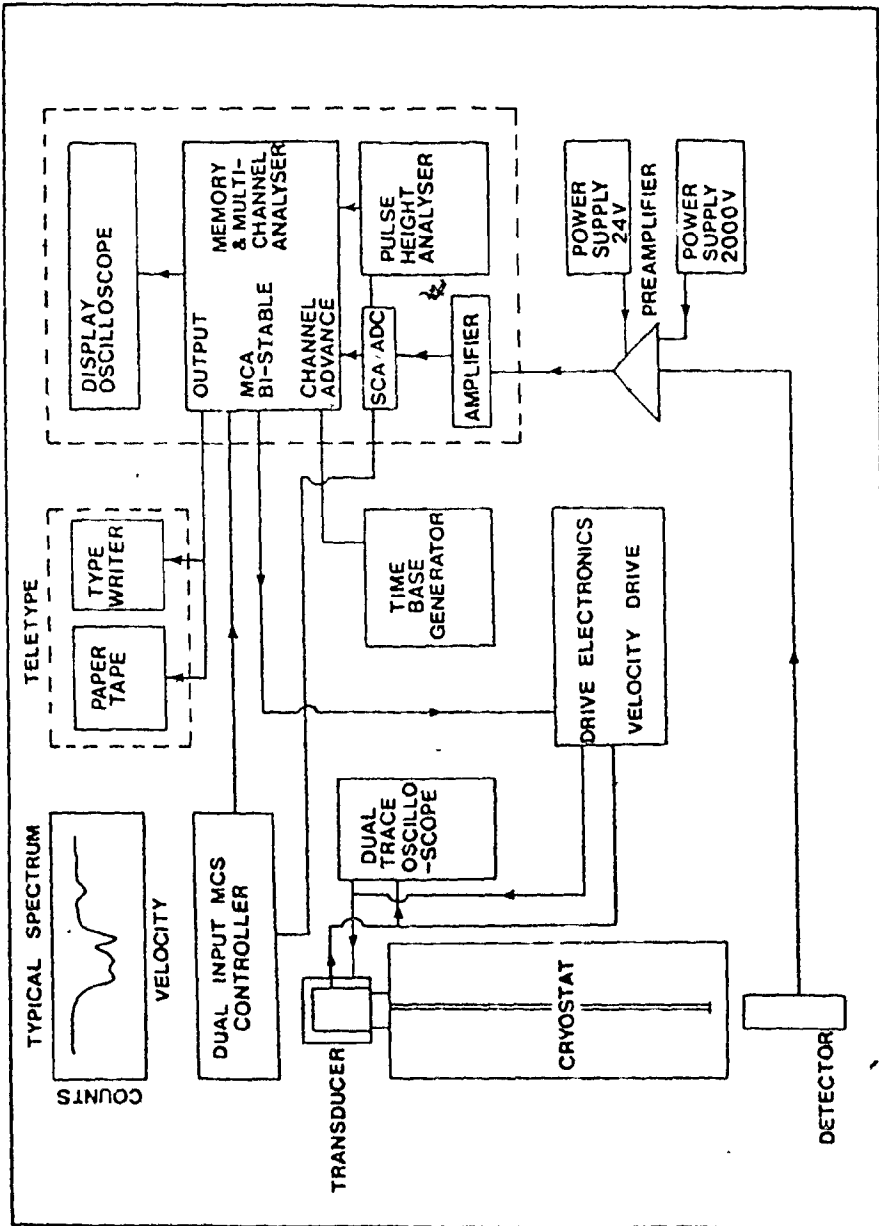
Figure 2.2. Schematic diagram of Mössbauer spectrometer used to record ^{127}I Mössbauer spectra.
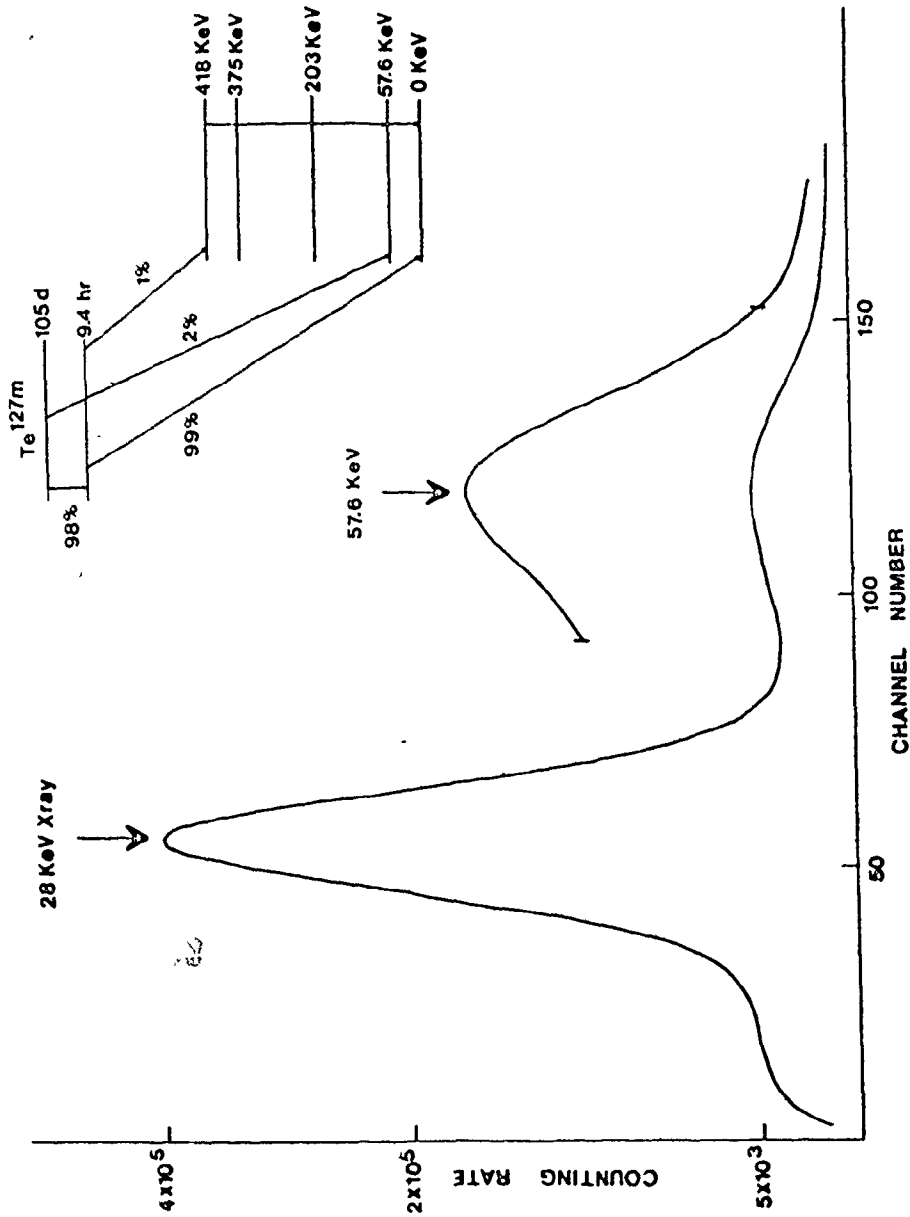
Figure 2.3. Gamma-ray spectrum of ^{127m}Te. The partial decay scheme of ^{127m}Te is shown in the inset.

The drive velocity was calibrated by recording the spectrum of iron foil on the opposite end of the transducer using a ^{57}Co in Pd source supplied by New England Nuclear Corporation. The ^{127}I Mössbauer spectra were then referenced with respect to a suitable single line absorber such as KI, recorded at 4.2°K.

Samples containing about 30 mg of natural iodine per cm^2 were prepared. The air stable compounds were finely ground and mixed thoroughly with Al_2O_3 while those samples which were moisture sensitive were prepared in a glove-box by grinding them and mixing them intimately with dried prefluorinated teflon powder. The samples were then placed in a 20 mm i.d. threaded Kel-F sample holder. Solution samples were prepared in a similar Kel-F sample holder which contained a screw plug on the side for easy loading by syringe, and subsequently frozen to 78° K.

Both source and sample were maintained at liquid helium temperature (4.2° K) in a detachable tail research cryostat manufactured by Janis Research Company. Figure 2.4 shows a schematic of the liquid helium cryostat, indicating the geometry of the experiment. The temperature was continuously monitored by means of a calibrated Allen-Bradley 47 ohm, 1/4 watt, carbon resistor and a Cryogenic Research Company temperature controller, and this ensured that the source and sample were immersed in liquid helium at all times. The level of the main liquid helium reservoir was continuously monitored by a series of carbon resistors located at different levels in the reservoir. A liquid helium boil-off rate of 200-300 cc/hr was typical. The liquid nitrogen reservoir level was automatically maintained with a Torr Vacuum Products Inc., Model L-21 liquid nitrogen level controller.

TRANSDUCER — — DRIVE CABLE

8 PIN ELECTRICAL
FEEDTHRU

SAFETY PRESSURE — HELIUM BATH
RELIEF — PUMPING ARM

EVACUATION
VALVE — THERMAL ANCHOR

NITROGEN RESERVOIR

HELIUM RESERVOIR

VACUUM SPACE

NEEDLE VALVE — DRIVE ROD
ABSORBER — SOURCE
CAPILLARY — INDIUM SEALED FLANGE

MYLAR WINDOW — NaI(Tl) CRYSTAL

SCINTILLATION
DETECTOR
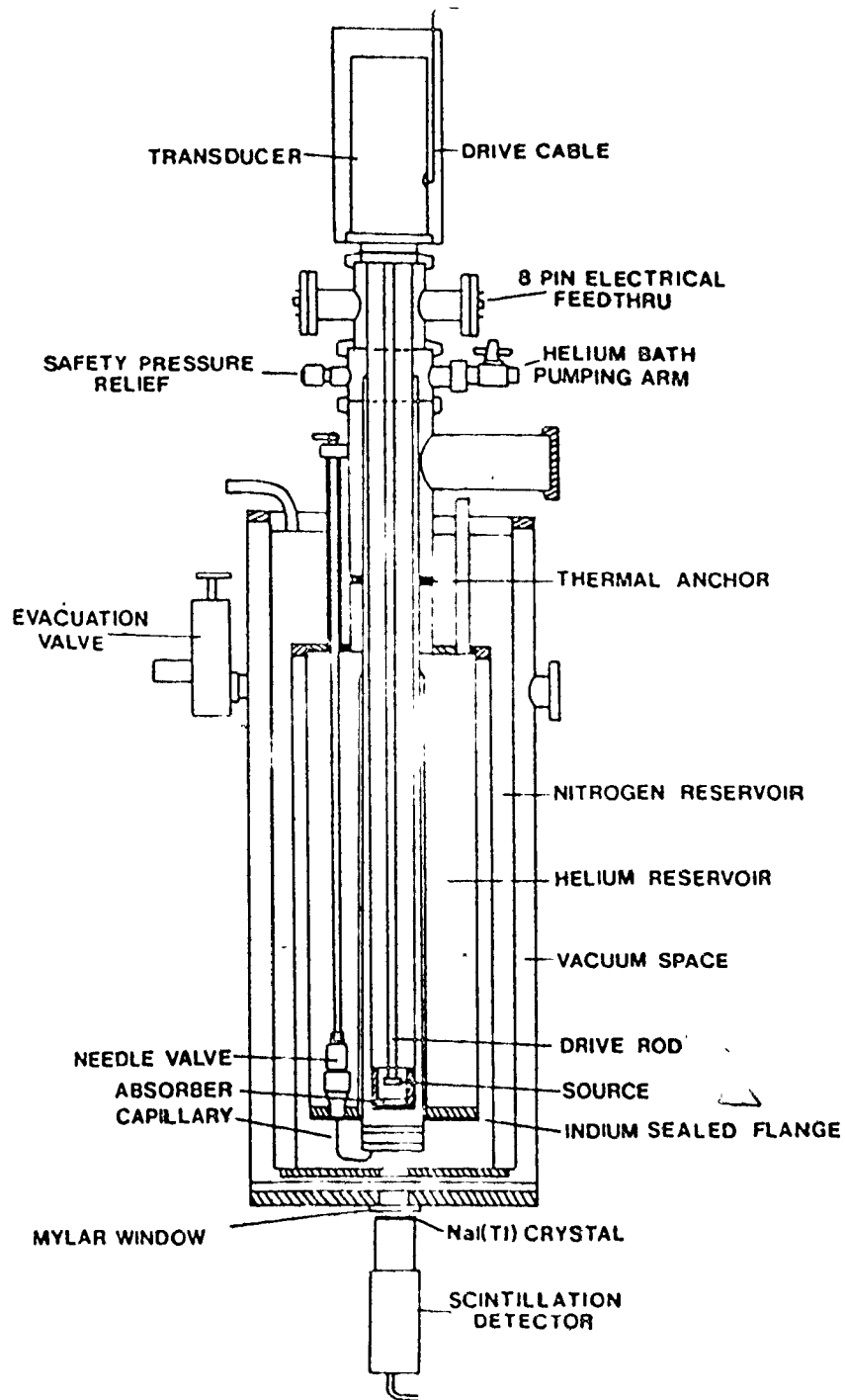
Figure 2.4.   Schematic diagram of liquid He cryostat
used to measure ^{127}I Mössbauer spectra.

- The $Zn^{127m}Te$ source was attached to a stiff 90 cm long stainless steel rod so that the source to detector distance was about 10 cm. This resulted in 57.6 keV gamma-ray count rates which varied from 20-30 counts s^{-1} channel^{-1} depending on the chemical composition of the absorber and the activity of the source. Typical spectra were recorded in 24-36 h and when folded gave 1×10^6 - 5×10^6 counts channel^{-1} with about 1% absorption.

All spectra were computer fitted using programs [52,57] previously described, which incorporate full transmission integral procedures. In the fitting procedure the source line width was constrained to the natural value (Γ_{nat} = 1.27 mms^{-1}), and while the absorber line widths were allowed to vary in quadrupole split spectra, the individual lines were constrained to have equal but variable width. The absorber thickness (T_A), isomer shift, quadrupole coupling constant, and where appropriate, eta (η), were allowed to vary although in the initial stages η was fixed at zero. When two unique iodine sites were present, the relative intensities of the two sites were initially assumed to be equal to their molar ratios in the molecule. This constraint was removed in later stages since it is unlikely that the different sites would have the same recoil-free fractions. In addition to the usual goodness of fit criterion x^2, the misfit criterion of Ruby [68] was employed in the fitting procedure. In each Table of Mössbauer data the x^2 value is presented as a function of the degrees of freedom, with a value of one representing an acceptable computer fitted spectrum.

(ii)   Laser Raman Spectrometer

The laser Raman instrumentation has been extensively described elsewhere.[69,70] Cylindrical sample tubes were mounted vertically so that the angle between the incident laser beam and the sample tube was 45° and Raman scattered radiation was observed at 45° to the laser beam or 90° to the sample tube direction. Spectra were recorded while spinning the sample tube and at -196°C by mounting the sample tube vertically in an unsilvered pyrex glass dewar filled with liquid nitrogen.

(iii)   Nuclear Magnetic Resonance Spectrometer

^{19}F NMR spectra were obtained using a Bruker WH-90 Fourier transform multinuclear spectrometer equipped with a Nicolet 1080 computer, a Nicolet 294 disk memory and quadrature phased detection. All spectra were ^{2}H locked and accumulated in 16K of memory. The spectrometer frequency was 84.66 MHz and spectra were obtained using 5 mm o.d. NMR tubes and were locked to an external d_6-acetone capillary in the probe head housing. Spectra were recorded at -120°C using a Bruker temperature controller, and the temperature was monitored using a copper constantan thermocouple inserted directly into the sample region of the probe and was accurate to ±1°C.

Tellurium-125 and xenon-129 NMR spectra were obtained on natural-abundance compounds using a Bruker WM-250 Fourier-transform multinuclear spectrometer. The spectra were recorded by Professor G. J. Schrobilgen. All spectra were run unlocked (field drift < 1Hz/hr) and accummulated in

16K of memory. Xenon-129 and tellurium-125 spectra were obtained at 69.20 and 78.97 MHz, respectively, in 5,000 to 10,000 scans using a spectral width of 45 KHz (2.8 Hz/data point; pulse repetition time, 0.18 sec) for ^{129}Xe, a spectral width of 83 KHz (5.1 Hz/data point; pulse repetition time, 0.20 sec) for ^{125}Te and pulse widths of 20 μ sec for both nuclei. Line broadenings of 3 Hz (^{129}Xe) and 5 Hz(^{125}Te) were applied in the exponential smoothing of the free induction decays.

Nuclear magnetic resonance samples were prepared by Professor G. J. Schrobilgen in 10 mm o.d. precision glass NMR tubes (Wilmad) joined by 1/4" o.d. standard wall tubing and attached by means of 1/4" Teflon nuts and ferrules to a Teflon diaphragm valve. Samples were prepared by distilling the appropriate solvent through all Kel-F and Teflon connections into a sample tube containing the solute at -196°C. Samples were sealed under vacuum and stored at -196°C until their spectra could be recorded.

Xenon-129 spectra were referenced externally with respect to pure $XeOF_4$ liquid at 24°C. Tellurium-125 spectra were referenced externally with respect to saturated aqueous $Te(OH)_6$ at 24°C.

(iv) Visible Absorption Spectrometer

A Cary Model 14 spectrophotomer was used to obtain the visible absorption spectra. Spectra were recorded on very dilute solutions of the solute in liquid SO_2 solvent using matched quartz cells having a sample thickness of 1 cm.

(v) <u>X-ray Crystallography</u>.

Since the compounds examined by X-ray crystallography in this thesis are all highly moisture sensitive, crystals had to be sealed in capillaries to prevent decomposition. Crystals of $[ICl_2][SbF_6]$ and $[IBr_2][Sb_2F_{11}]$ were mounted in rigorously dried Lindemann capillaries. $[I_3Cl_2][SbCl_6]$ and $[IBr_{0.75}Cl_{1.25}][SbCl_6]$ are volatile solids and crystals of these compounds were obtained by sublimation. Samples were placed in a sublimation vessel to which fine (0.2-0.3 mm) quartz capillaries had been attached. By applying a small temperature gradient across the vessel, crystals were eventually sublimed into the capillaries.

The instrumentation, and details regarding data acquisition for determining crystal structures have been thoroughly described [71] previously. The theory of the solution of crystal structures is described in great detail in the book by Stout and Jenson.[72] All structures were solved by conventional heavy atom methods. The iodine and/or antimony atoms were located using a Patterson map. Subsequent Fourier maps revealed the positions of the remaining atoms and confirmed the positional assignments of the heavy atoms.

All calculations were performed on a CDC 6400 or Cyber 170/730 computer using the program SHELX [73] in the initial stages, while the final refinements were completed using the series of programs in the XRAY package.[74]

(vi) Chemical Analysis

The iodine content of the polyhalide anions $[X-I-Y]^-$ $(X,Y = F,$ Cl, Br, I) was determined by the addition of a weighed quantity of the polyhalide salt to an excess solution of aqueous KI and titration of the liberated iodine with standard $Na_2S_2O_3$ solution.

The total halide content of $[I_3Cl_2][SbCl_6]$ was determined by a method similar to that described by Vonk and Wiebenga.[75]

C. Purification of Starting Materials

(i) Antimony Pentafluoride

Antimony pentafluoride (Ozark-Mahoning) was doubly distilled in an all-pyrex apparatus described previously.[76] The fraction boiling at 142-143°C was collected and stored in a pyrex flask in the glove box for subsequent use in a dry atmosphere.

(ii) Antimony Pentachloride

Antimony pentachloride (J. T. Baker Co. Reagent) was used as supplied without purification.

(iii) Antimony Trihalides

Antimony trifluoride (Alfa Inorganics) was sublimed at 319°C under vacuum and stored in a dry nitrogen atmosphere until used.

Antimony trichloride (Allied Chemical) was sublimed at 50°C under vacuum and stored in the glove-box until required.

Antimony tribromide (Alfa Inorganics) was sublimed at 200°C under vacuum and stored in the glove-box until used.

(iv) <u>Halogens</u>

Iodine (Fischer Scientific Co.) was freshly sublimed before use.

Bromine (McArthur Chemical Co.) was stored over P_2O_5 for several days prior to use.

Chlorine (Matheson Co.) was dried by storage over P_2O_5 for several days prior to use.

(v) <u>Solvents</u>

Sulfur dioxide (Matheson Co.) was dried and stored over P_2O_5 before use. When required, it was distilled into the reaction vessel.

SO_2ClF was purified by trap-to-trap distillation through a -78°C dry-ice acetone slush bath and collected in a trap cooled to -196°C.

(vi) <u>Iodine Pentafluoride</u>

Iodine pentafluoride (Matheson) was purified by Professor G. J. Schrobilgen using the procedure outlined for bromine pentafluoride.[77]

D. Preparation of Polyhalide Anions

(i) $[IBrCl]^-$, $[I_2Br]^-$, $[I_2Cl]^-$ and $[IBr_2]^-$

Samples of $[N(CH_3)_4][IBrCl]$, $[N(CH_3)_4][I_2Br]$, $[N(CH_2CH_3)_4][I_2Cl]$ and $[N(CH_2CH_3)_4][IBr_2]$ were prepared according to standard methods [78,79] by mixing tetra-alkyl ammonium halide salts with the appropriate halogen or interhalogen. These compounds (or those containing a similar cation) have all been characterized by vibrational spectroscopy-infrared and Raman,[11-13] X-ray crystallography,[3-9,80-82] and chemical analysis.

$[N(CH_2CH_3)_4][IBr_2]$: calc., I, 30.45; found, I, 30.30

$[N(CH_3)_4][I_2Br]$: calc., I, 62.25; found, I, 63.65

$[N(CH_3)_4][IBrCl]$: calc., I, 40.10; found, I, 39.95

$[N(CH_2CH_3)_4][I_2Cl]$: calc., I, 60.5; found, I, 59.65

(ii) $[IBrF]^-$ and $[IClF]^-$

The cesium salts of $[IBrF]^-$ and $[IClF]^-$ were prepared by mixing CsF with a large excess of IBr and ICl respectively and warming to ca. 50°C. After allowing the CsF to react completely, the excess IBr or ICl was removed by grinding the material to powder and pumping under high vacuum. All manipulations were carried out under a dry nitrogen atmosphere in a glove-box. The compounds were characterized by chemical analysis, Mössbauer spectroscopy and Raman spectroscopy.

Cs[IBrF] : calc., I, 35.40; found, I, 36.80

Cs[IClF] : calc., I, 40.40; found, I, 45.25

(iii) [IF$_2$]$^-$

The tetraethylammonium salt of the difluoroiodide anion was prepared by halogen exchange between tetraethylammonium dichloroiodide and silver fluoride in acetonitrile solution as described by Meinert and Klamm.[83] The compound was characterized by Raman spectroscopy and Mössbauer spectroscopy.

E. Preparation of Polyhalogen Cations of Iodine

(i) [I$_2$][Sb$_2$F$_{11}$]

The salt [I$_2$][Sb$_2$F$_{11}$] was prepared by the method of Gillespie and co-workers [17] by treating I$_2$ with SbF$_5$ in SO$_2$ solvent and the purity was established by Raman spectroscopy.

(ii) [I$_3$][AsF$_6$]

The sample of [I$_3$][AsF$_6$] was kindly provided by Passmore et al.[32] who have described its preparation and X-ray crystal structure.

(iii) I$_2$Cl$_6$

I$_2$Cl$_6$ was prepared according to the method of Birk [84] by treating finely ground I$_2$ with excess liquid Cl$_2$ at -78°C.

(iv) [ICl$_2$][SbCl$_6$]

The compound [ICl$_2$][SbCl$_6$] was prepared by the method of Vonk and Wiebenga [75] by heating I$_2$Cl$_6$ in a large excess of SbCl$_5$.
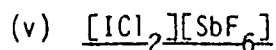
(v) [ICl$_2$][SbF$_6$]

[ICl$_2$][SbF$_6$] was prepared as follows: 3.6694 g (16.93 mmol) of SbF$_5$ was added by means of a glass syringe to one side of a Dean reaction vessel equipped with a 5 mm thin walled NMR tube. This manipulation was carried out under a dry nitrogen atmosphere in a glove-box. Then 1.9753 g (4.233 mmol) of I$_2$Cl$_6$ was added to the other side by vacuum sublimation from a preweighed glass vessel, on a vacuum line. SO$_2$ClF was then distilled onto the SbF$_5$ and the SbF$_5$/SO$_2$ClF solution was quickly poured onto the I$_2$Cl$_6$ through the sintered glass frit. After stirring for six hours a clear cherry-red solution remained. The ^{19}F NMR sample was obtained by pouring some of this solution into the attached NMR tube and sealing it off under vacuum. The SO$_2$ClF solvent was removed from the remaining solution by slow distillation, which left behind a viscous red paste. After some time it was noticed that red crystals had begun to grow and the vessel was then pumped under dynamic vacuum to remove any remaining SbF$_5$. The melting point of a single crystal of [ICl$_2$][SbF$_6$] is 83°C giving a red liquid with no decomposition. [ICl$_2$][SbF$_6$] was characterized by ^{19}F NMR spectroscopy, Mössbauer spectroscopy, Raman spectroscopy and X-ray crystallography.

(vi) [IBr$_{0.75}$Cl$_{1.25}$][SbCl$_6$]
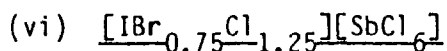
[IBr$_{0.75}$Cl$_{1.25}$][SbCl$_6$] was prepared in a Dean reaction vessel comprised of two 100 ml pyrex round bottom flasks. 12.0629 g (40.34 mmol) of SbCl$_5$ was added to one side of the reaction vessel. Then 8.2915 g (40.07 mmol) of IBr was added to the SbCl$_5$. Following this

2.8050 g (39.56 mmol) of dry Cl_2 was distilled onto the mixture at
-196°C. The reaction mixture was allowed to warm up to room temperature
over a period of several hours. SO_2 solvent was then introduced into the
vessel and the reaction product was stirred and then carried over to the
other side of the vessel. After the SO_2 was removed by slow distillation
a very dark red-brown crystalline solid remained. The melting point of a
single crystal of $[IBr_{0.75}Cl_{1.25}][SbCl_6]$ is 50°C. A Raman sample was
prepared by subliming a large crystal of the material into a 1/4" pyrex
tube. $[IBr_{0.75}Cl_{1.25}][SbCl_6]$ was characterized by Raman spectroscopy,
Mössbauer spectroscopy and X-ray crystallography.

(vii) $\underline{[IBr_2][Sb_2F_{11}]}$

$[IBr_2][Sb_2F_{11}]$ was prepared as follows: 6.5057 g (30.014 mmol)
of SbF_5 was added to one side of a Dean reaction vessel. Then 2.4630 g
(11.904 mmol) of IBr was prepared from I_2 and Br_2, using the method
described by Brauer,[85] in the other side of the vessel. SO_2 was
distilled onto the SbF_5 and the SbF_5/SO_2 solution was poured through the
frit, onto the IBr. After stirring for one week a very dark green, clear
solution remained which contained a fine white precipitate of SbF_3. The
solution was filtered to the other side of the vessel and the SO_2 was
slowly removed in an attempt to induce crystallization. A dark thick
paste remained which, when SO_2ClF was added, produced a dark green clear
solution. When the SO_2ClF was removed by slow distillation shiny, dark,
needle-like crystals of $[IBr_2][Sb_2F_{11}]$ formed. The melting point of a

single crystal of $[IBr_2][Sb_2F_{11}]$ is 139°C. This compound was characterized by Raman spectroscopy, Mössbauer spectroscopy and X-ray crystallography.

(viii) $[I_3Cl_2][SbCl_6]$

$[I_3Cl_2][SbCl_6]$ was prepared as follows: 3.4303 g (15.03 mmol) of resublimed $SbCl_3$ were added to one side of a Dean reaction vessel under a dry nitrogen atmosphere in a glove-box. Then 3.4134 g (7.31 mmol) of I_2Cl_6 were added to the other side of the vessel by vacuum sublimation from a preweighed glass vessel. SO_2 was distilled onto the $SbCl_3$ and when the latter had dissolved, the $SbCl_3/SO_2$ solution was poured onto the I_2Cl_6 through the sintered glass frit. After stirring overnight a fine brown precipitate was formed which after repeated washing to the other side of the vessel remained as dark brown crystals. After cooling to 0°C, to ensure maximum crystal formation, the SO_2 was decanted to the other side of the vessel which was then sealed under vacuum. $[I_3Cl_2][SbCl_6]$ is highly moisture sensitive and attempts to mount crystals in rigorously dried Lindemann capillaries inside a glove-box containing an atmosphere with less than 2-3 ppm of moisture resulted in rapid crystal decomposition. Part of the driving force of this decomposition is thought to be due to the loss of the partial vapour pressure of the -volatile crystals when the glass vessel is opened. To overcome this problem a sample of the material was placed in a sublimation vessel and crystals were sublimed into quartz capillaries. The melting point of a single crystal of $[I_3Cl_2][SbCl_6]$ under its own vapour pressure is 47°C

giving a brown liquid with no decomposition. The compound gave satisfactory gravimetric analysis for total halide present by precipitation of AgI and AgCl. $[I_3Cl_2][SbCl_6]$ was characterized by Raman spectroscopy, X-ray crystallography, Mössbauer spectroscopy and visible absorption spectroscopy.

F. <u>Attempted Reactions of I_2Cl_6 with Other Group(V) Trihalides</u>

The following reactions were attempted in an effort to produce cations similar to $[I_3Cl_2]^+$. The reaction of I_2Cl_6 with SbF_3 resulted in the formation of a very dark viscous oil which was not characterized. Halogen exchange was found to occur when I_2Cl_6 was mixed with $SbBr_3$, according to the following reaction:

$$I_2Cl_6 + 2SbBr_3 \rightarrow 2SbCl_3 + 2IBr + 2Br_2 \qquad (2.1)$$
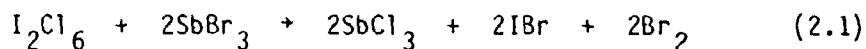
No reaction was obvserved between I_2Cl_6 and $AsCl_3$.

G. <u>Preparation of Diphenyliodonium Halides</u>

(i) <u>$[(C_6H_5)_2IX]_2$, where X = Cl, Br, I</u>

These compounds were prepared using the method described by Beringer <u>et al</u>.[86] To a stirred mixture of potassium iodate, benzene and acetic anhydride, cooled to below 10°C, was added a cold solution of acetic acid in sulfuric acid. After working up the reaction mixture it was divided into three portions. Upon the addition of aqueous ammonium

halide solution the diphenyliodonium halide salts were precipitated. The authenticity of the products was confirmed by their melting points.

$[(C_6H_5)_2ICl]_2$: mp, 223°C

$[(C_6H_5)_2IBr]_2$: mp, 208°C

$[(C_5H_5)_2II]_2$: mp, 171°C
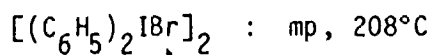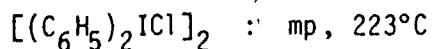
H.   Compounds Containing Chalcogen Cations of Iodine

Samples of $[S_7I][AsF_6]$,[37] $[S_7I][SbF_6]$,[87] $[(S_7I)_4S_4][AsF_6]_6$,[88] $[(S_7I)_2I][SbF_6]_3 \cdot 2AsF_3$,[89] $[S_2I_4][AsF_6]_2$,[90] $[Se_2I_4][AsF_6]_2$,[91] $[SeI_3][SbF_6]$ [92] and $[TeI_3][AsF_6]$ [93] were kindly provided by Prof. J. Passmore and co-workers.

I.   Sulfenyl Iodine Compounds

(i) $\underline{C_7H_{13}NSI-X}$, where X = Br, I
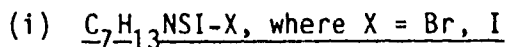
Samples of these compounds were kindly prepared by Prof. B. E. McCarry according to the procedure described by Rogstad and Augdahl.[94] Their authenticities were confirmed by their melting points.

J.   Preparation of Miscellaneous Iodine Compounds
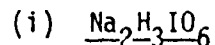
(i) $\underline{Na_2H_3IO_6}$

The disodium salt of H_5IO_6 was prepared by oxidizing a solution of $NaIO_3$ in aqueous NaOH with liquid Cl_2. The $Na_2H_3IO_6$ was precipitated and collected by filtration. The compound was characterized by chemical analysis. $Na_2H_3IO_6$: calc., I, 46.70; found, I, 46.31.

(ii) <u>CuI</u>

CuI was prepared by slowly adding an aqueous solution of KI to an
aqueous solution of $CuSO_4$. The CuI precipitated immediately and was
collected by filtration.

(iii) <u>CsI</u>

CsI was made by titrating an aqueous solution of Cs_2CO_3 with
aqueous HI until the resulting solution had a neutral pH. Upon
concentrating the solution CsI precipitated.

(iv) <u>$[I(C_5H_5N)_2][NO_3]$</u>

The sample of $[I(C_5H_5N)_2][NO_3]$ was prepared by the method of
Arotsky and Symons.[95]

(v) <u>$FI(OTeF_5)_4$</u>

$FI(OTeF_5)_4$ was prepared by Prof. G. J. Schrobilgen using the
method described by Seppelt.[96]

(vi) <u>$IO_2F_3 \cdot SbF_5$</u>

A sample of $IO_2F_3 \cdot SbF_5$ was obtained from Prof. R. J. Gillespie <u>et</u>
<u>al</u>.[97]

(vii) <u>$K[ICl_4]$</u>

$K[ICl_4]$ was prepared using the method described by Brauer [85] by
bubbling Cl_2 through a saturated, acidic, aqueous solution of KI. Upon
cooling long needle-like crystals of $K[ICl_4]$ precipitated.

CHAPTER 3

SINGLE LINE ABSORBERS

A. Introduction

        As mentioned in Chapter 1 the chemical isomer shift in

Mössbauer spectroscopy is given by

$$\delta = A\{|\psi_s(0)|^2_A - |\psi_s(0)|^2_S\} \frac{\delta R}{R} \qquad (3.1)$$

where A is a constant, $\{|\psi_s(0)|^2_A - |\psi_s(0)|^2_S\}$ is the difference in the

electron density between absorber and source, and $\delta R/R$ is a nuclear term

which depends upon the difference in nuclear radii of excited and ground

states.

        In order to interpret isomer shift data and to compare new data

with old, in the absence of an absolute velocity calibration such as that

provided by a laser, it is necessary that a suitable reference material

be chosen as a universal standard. This is particularly important for

^{127}I Mössbauer spectra because isomer shift differences are generally

small and less than the natural line width. Agreement on the reporting

of isomer shift data is universal for other common Mössbauer isotopes

such as ^{57}Fe, ^{119}Sn and ^{121}Sb but this is not the case for ^{127}I. Some

workers have reported isomer shifts with respect to the source and

although the sources used may be nominally the same, the source quality may vary considerably. Ivantchev et al.[64] found a substantial difference in the line width of a sample recorded using a polycrystalline $Zn^{127m}Te$ source compared to an amorphous source of the same material. This of course could lead to small discrepancies in the measured isomer shift. Stevens [98] has collected isomer shift data for the various Mössbauer isotopes in an attempt to provide reliable values.

The following criteria then determine the usefulness of a material as a reference:

i)   It must be a single line absorber, i.e., the nucleus of interest must be in a cubic environment so that the electric field gradient and hence the quadrupole coupling constant are zero.

ii)   The absorber line width should be as close to natural as possible.

iii) The compound should be easily obtainable and be stable.

iv)   The recoil-free fraction f_A should be high and any other elements present in the compound should not be strong gamma-ray absorbers, i.e., preferably small Z nuclei.

With the above criteria in mind a number of inorganic compounds which contain iodine in a nominally cubic environment were selected for examination and their ^{127}I Mössbauer spectra were recorded.

B. Results and Discussion

The compounds which were examined in order to select an appropriate reference compound were CuI, KI, CsI, KIO_4, H_5IO_6 and $Na_2H_3IO_6$. The Mössbauer parameters obtained for these compounds are given in Table 3.1. All of the samples were prepared so that they each contained approximately 230 mg of iodine. This was done so that the absorber thickness, T_A, reflects the recoil-free fraction for each sample. In the fitting procedure the quadrupole coupling constant $e^2q^{127}Q_g/h$ was fixed at zero since in these "cubic" systems the electric field gradient, eq, should vanish.

As far as the isomer shift is concerned there are two classes of compounds found in Table 3.1. The oxygen containing compounds all have positive isomer shifts with respect to the source. The oxygen bonded periodates may be regarded as being formally either sp^3 or sp^3d^2 hybridized with strong s-orbital involvement in the bonding. Oxygen is much more electronegative than iodine and hence the electrons in the bonds will be polarized towards the oxygen nuclei. Since the s-electrons are involved in the bonding they are effectively removed from the iodine nucleus, thereby lowering the s-electron density. This reduction in s-electron density causes the isomer shift to become positive with respect to the source, since $\delta R/R$ is negative. Of course p- and d-electrons are also removed from the iodine nucleus causing a deshielding of the remaining s-electron density. This would act in the opposite sense to the former effect, i.e., cause an increase in s-electron density, but since the isomer shift is directly dependent upon the s-

Table 3.1.

^{127}I Mössbauer Parameters for Selected Single Line Absorbers

Compound	χ^2/degrees of freedom	$T_A{}^a$	$e^2q^{127}Q_g/h$ (MHz)	Isomer shift (mms^{-1})	Γ (mms^{-1})
KI	1.01	0.33(1)	0	-0.14(2)	3.06(10)
CsI	1.02	0.53(1)	0	-0.14(1)	3.32(7)
CuI	0.91	0.38(1)	0	-0.16(1)	5.20(12)
H_5IO_6	1.30	0.36(1)	0	0.70(2)	7.33(22)
$Na_2H_3IO_6$	2.38	0.60(2)	0	0.75(2)	7.76(14)
KIO_4	1.06	0.40(1)	0	0.47(2)	6.07(16)
KIO_4	1.02	0.42(1)	-465(80)	0.51(3)	5.12(31)

a Dimensionless absorber thickness, see Ref. 52.

electron density at the nucleus, the removal of s-electrons will be the major factor determining the isomer shift. The second group of compounds consists of the almost ionic iodides, two alkali metal iodides and cuprous iodide. The isomer shifts of these compounds are slightly negative with respect to the source, indicating that the s-electron density is somewhat higher in these compounds than in the source. This is reasonable if one considers that in the source ($Zn^{127m}Te$) the s-electrons are involved in some degree of covalent bonding while in the iodides the iodine atom has the noble gas electron configuration $5s^2p^6$ with no s-electrons removed. The s-electron density at iodine in these iodides is of course much higher than in the periodates because of the substantial electron withdrawing ability of the oxygen atoms in the latter case. The isomer shifts of these compounds have been measured by other workers [14,47,99] and there are small variations in the measured values.

The most striking aspect of these data is the wide range in the line widths observed for these apparently cubic iodine systems. As Table 3.1 indicates the absorber line widths vary from 3.06 mms^{-1} for KI to 7.76 mms^{-1} for $Na_2H_3IO_6$. This is also illustrated in Figure 3.1 where the ^{127}I Mössbauer spectra of KI, CuI, KIO_4 and H_5IO_6 are presented. While it has been assumed that these compounds contain iodine in a cubic environment it is possible that resonant nuclei in different parts of the source and/or absorber have slightly different crystalline environments. This would cause the source and/or absorber line to be broadened due to a variance in say, chemical shift, thermal shift, or quadrupole splitting.
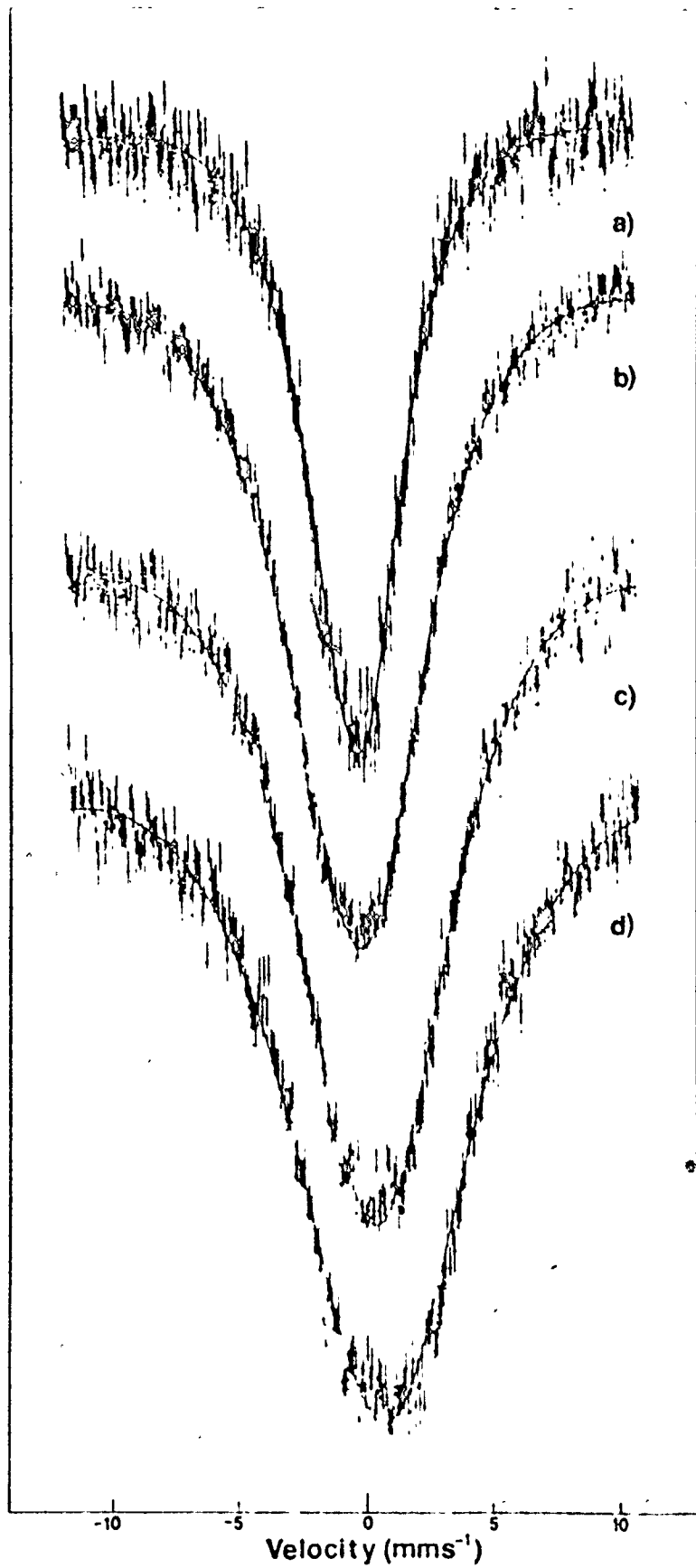
Figure 3.1. ^{127}I Mössbauer spectra of selected single line absorbers: a) KI b) CuI c) KIO_4 d) H_5IO_6.

The powder X-ray diffraction pattern of CuI has been indexed and it has the zinc blende (ZnS) structure, i.e., tetrahedrally coordinated iodine. However like ZnS, CuI exhibits polytypism and in addition to the phases known as α, β and γ (cubic), two other polytypes have been detected by diffraction methods. Kurdyumova and Baranova [100] have detected the polytype (6H) by electron diffraction from a single crystral while recently Batchelor and Birchall [101] have solved the single crystal X-ray structure of cuprous iodide (12R). The latter polytype consists of close-packed layers of iodine atoms on two crystallographically independent sites while the copper atoms are disordered equally over four crystallographically independent sites comprising the tetrahedral holes between the iodine layers. In view of the extensive polytypism CuI probably exhibits and the high probability of disorder in the crystal structures, it is not surprising that the resonance observed for CuI is very broad compared to the natural value. It was further observed that the absorber line width of CuI varied considerably depending upon the particular conditions under which it was prepared. Thus, contrary to what has been suggested by Stevens and Gettys,[102] CuI is not a suitable reference material for ^{127}I Mössbauer spectroscopy because of the difficulty in preparing a pure sample of known structure reproducibly, and because of the broad line which results due to polytypism and disorder.

As Table 3.1 indicates the ^{127}I Mössbauer resonance of H_5IO_6 has a line width of 7.33 mms^{-1}. This is at first somewhat surprising since the $[IO_6]^{5-}$ anion would be expected to have perfect O_h symmetry and hence a zero electric field gradient. A single crystal X-ray study of

H_5IO_6 by Feikema [103] has shown that the structure consists of a slightly deformed oxygen octahedron with iodine in the center, such that the I-O distances vary from 1.73 to 1.90Å. A subsequent neutron diffraction study [104] of H_5IO_6 by the same author confirmed the above analysis and located the hydrogen atoms. This latter study found five oxygen atoms directly bonded to hydrogen so that the distance from these oxygen atoms to the central iodine was 1.89(2)Å, while the remaining I-O distance was 1.78(2)Å. Extensive hydrogen bonding between neighbouring molecules was also present. It seems then that this hydrogen bonding coupled with the asymmetry present in the octahedron around iodine generates a small electric field gradient, and hence a broad line. The ^{127}I Mössbauer spectrum of the related compound $Na_3H_2IO_6$ has also been reported by a number of groups.[14,48,64,99] and there seems to be little agreement as to the isomer shift or absorber line width. It has not been possible to prepare this particular compound, although two different procedures were tried. However, it was possible to prepare the salt, $Na_2H_3IO_6$. Oxidation of $[IO_3]^-$ with chlorine in strongly basic (NaOH) solution resulted in the formation of the disodium salt and not $Na_3H_2IO_6$ as was previously reported.[85] Titration of H_5IO_6, the parent acid, with three equivalents of NaOH, followed by crystallization also failed to yield the trisodium salt. Indeed a pH titration curve of H_5IO_6 (Figure 3.2) shows that two protons are easily removed while at higher pH two further protons are titrated. The disodium salt therefore seems to be the most likely product in a simple acid-base reaction and this was confirmed by the chemical analysis of the salt remaining after titration with two mole
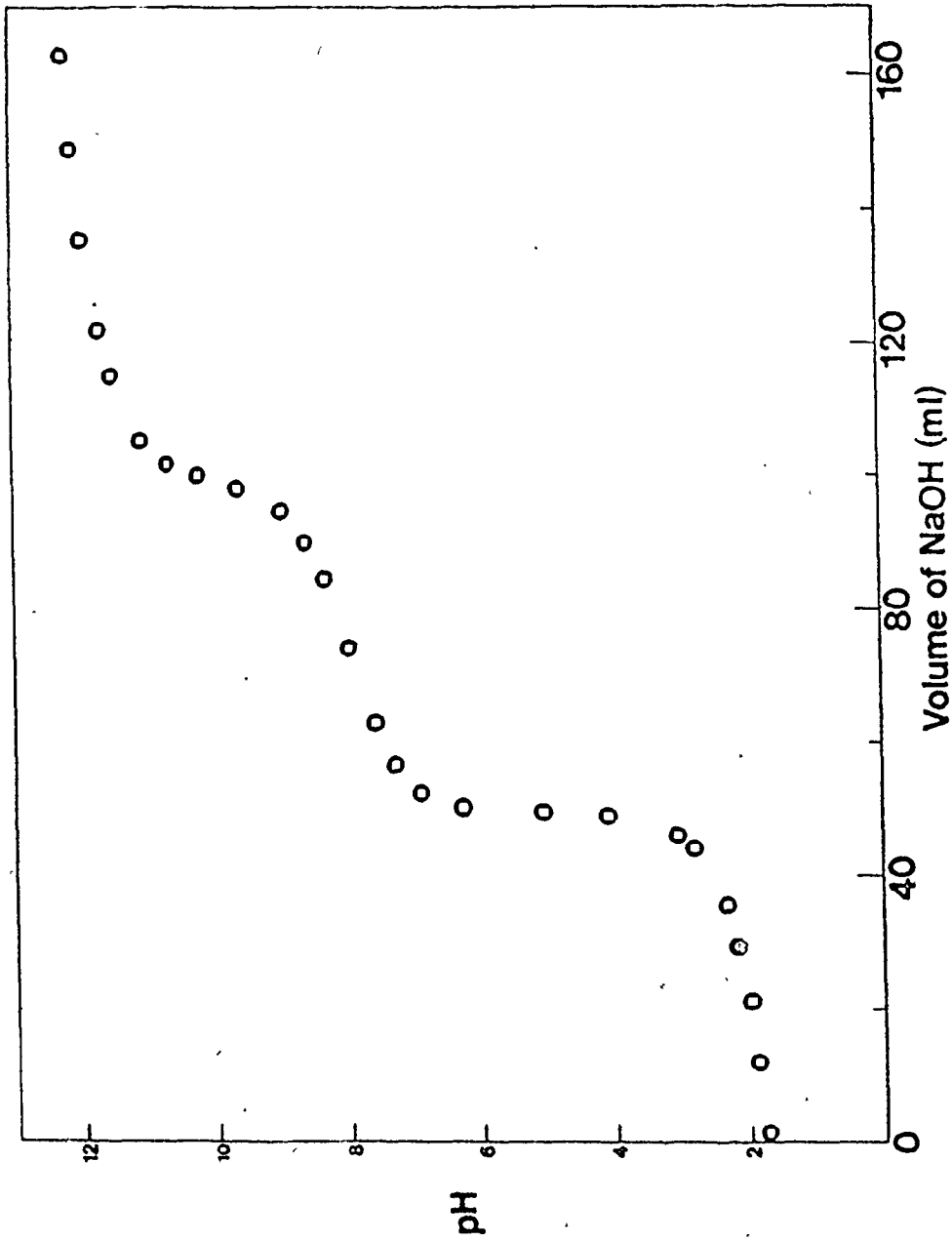
Figure 3.2.   pH titration curve of H_5IO_6.   1.1327 g (4.968 m moles) of H_5IO_6 were titrated with 0.1000 M NaOH. pka_1 = 4.8, pka_2 = 10.4.

equivalents of base. In view of the uncertainty of the composition of $Na_3H_2IO_6$ this substance does not appear to be useful as a reference material. It is also interesting to note that the single crystal X-ray structure of the diammonium salt $[NH_4]_2[H_3IO_6]$ has been reported [105] while there is no report of a structure analysis of the trisodium or triammonium salts. In the diammonium salt the author reports the presence of different iodine-oxygen bond lengths, however the environment around iodine was described as octahedral within experimental error. The reported line width of the trisodium salt varies from about 4.1 to 7.0 mms^{-1} [64,99] while that presented here for the disodium salt was 7.76 mms^{-1}. This very broad line can be attributed to the same structural characteristics which are present in H_5IO_6, i.e., the octahedron of oxygen atoms is distorted and possibly to a larger extent than in H_5IO_6 because of the presence of the larger sodium cations, and now only three oxygen atoms are directly bonded to hydrogen. Therefore H_5IO_6 and any of its known derivatives are not useful as reference standards because the very broad line results in a large uncertainty in the isomer shift.

The remaining iodine (VII) compound found in Table 3.1, namely KIO_4 also exhibits a very broad ^{127}I Mössbauer resonance. Because of the expected tetrahedral symmetry one would anticipate the electric field at the central nucleus to be zero for the anion and very small in the crystalline solid. The actual arrangement about the iodine atom in KIO_4 has been described [106] as disphenoid tetrahedral within experimental

error. A more recent single crystal X-ray study [107] of $NaIO_4$ has shown that the periodate tetrahedron is compressed along the $\underline{c}$ direction so that O-I-O is 114°. That there is an electric field gradient at the nucleus in various periodates has been established by several workers. Weiss and Weyrich [108] have found from an NMR study of single crystals of $NaIO_4$ that the ^{127}I quadrupole coupling constant must be large. They conclude from their work that the ionic charge distribution in the crystal contributes only a minor part to the electric field gradient at the ^{127}I nucleus. The largest contribution is from the distortion of the ideally tetrahedral arrangement of the I-O bonds by the crystal lattice. Burkert [109,110] has observed pure iodine quadrupole resonance in KIO_4, $NaIO_4$ and several other periodates. The observed electric field gradient was attributed to two factors. An electrostatic term would arise from the field at a given atom of the remaining charged species throughout the lattice and a covalent contribution would arise from asymmetric distribution of valence electrons. The electric field in the above periodates was found to be temperature dependent and the quadrupole coupling constant for KIO_4 at room temperature was 20.8 MHz. Since it is not possible to determine the sign of the electric field gradient from NQR measurements, the quadrupole coupling constant of KIO_4 was determined from its ^{127}I Mössbauer spectrum by fitting $e^2q^{127}Q_g/h$ and allowing Γ to vary. This result is found in Table 3.1. The quadrupole coupling constant for KIO_4 was measured to be -465 MHz with a line width of 5.12 mms^{-1}. The quadrupole coupling constant is substantially larger than that found by NQR but this can be attributed to the strong

correlation between the quadrupole coupling constant and the line width when the coupling constant is small. It is clear however that $e^2q^{127}Q_g/h$ is negative and since $e^{127}Q_g$ is negative this means that V_{zz} is positive and there is an excess of electron density along the z axis, which may be taken as the two fold axis of the disphenoid tetrahedron.

Much of the X-ray work on these oxygen containing species is relatively old and hence the accuracy of the final parameters is some-times not adequate to detect asymmetry in the structures. It is apparent that in these compounds, perhaps because of the relatively high covalency of the iodine-oxygen bond, small distortions of the structure from ideal cubic geometry result in substantial electric field gradients, and hence broad absorption envelopes due to unresolved quadrupole splittings.

The remaining two compounds examined were the alkali metal iodides KI and CsI. These compounds have been studied by Mössbauer spectroscopy previously [61] using the 129-isotope. The line widths obtained for KI and CsI were the narrowest observed with that for KI being the smallest. Both salts have cubic structures [111] with KI having the NaCl structure while CsI has the CsCl structure. The 3.06 mms^{-1} wide resonance observed for KI is still broader than the natural width and this may be due to distortions in the crystal lattice of the source or of the absorber. KI is preferable to CsI as a reference material because it is more readily obtainable, but most importantly CsI contains heavy Cs atoms which act to absorb the 57.6 keV gamma-ray and hence reduce the counting rate. KI would also be a convenient reference material for ^{129}I Mössbauer measurements since the radio-isotope is commercially

available in this form. It is recommended that KI be adopted as the reference material for both ^{127}I and ^{129}I Mössbauer spectroscopy and throughout this thesis all isomer shifts will be quoted with respect to that of KI taken as zero.

Examination of Table 3.1 shows that $Na_2H_3IO_6$ has the highest value for T_A while KI has the smallest value. Since T_A is directly related to the recoil-free fraction f_A which determines the strength of the Mössbauer signal one would, on this basis, choose $Na_2H_3IO_6$ as the standard reference material. However as the previous discussion showed this material gives a very broad resonance and hence it is difficult to ascertain the centre of the absorption envelope with the certainty necessary for a reference substance. CsI gives a much higher recoil-free fraction than KI but because of the higher atomic number of cesium compared to potassium, the number of recoil-free events transmitted in CsI is less than that for KI so that a statistically acceptable spectrum is obtained much faster for KI. Hence KI represents the best reference material.

The apparent broadness in the resonances of many of the compounds discussed above has been attributed to an asymmetric distribution of valence electrons at the iodine nucleus. In CuI there is also a high probability of disorder and the presence of multiple sites, arising from polytypism. There is as well the possibility that the crystal lattice in some of these compounds undergoes some phase transition at low temperature, further removing the iodine nucleus from ideal cubic geometry.

CHAPTER 4

^{127}I MÖSSBAUER STUDIES OF [X-I-Y]$^-$ ANIONS AND RELATED SPECIES

A.   Introduction

Most of the applications of ^{127}I Mössbauer spectroscopy have centred around the correlation of the Mössbauer parameters with the structure of the molecule and the nature of the bonding to the iodine atom. It has become customary to use the semi-empirical relationships mentioned in Chapter 1 to establish s- and p-orbital populations at the iodine nucleus by utilizing the isomer shift and quadrupole coupling constant parameters. However these relationships were established by examining a limited number of iodine compounds of widely differing structure and it is rare that they are questioned.[112] For example in developing equation (1.29) it was assumed that there was no involvement of s-electrons in the bonds to iodine in the various compounds examined. This may not be a reasonable assumption, particularly for anhydrous HI. Also any participation, or contribution of the iodine 5d-electrons to the bonding has been assumed to be negligible.

There is also some question as to which value for the isomer shift of iodine was used in Figure 2 of reference 14, in order to obtain the value for 2Ky (equation (1.24)). Greenwood and Gibb [47] have plotted $\delta(^{127}$I) _versus_ $\delta(^{129}$I) for a series of compounds and it is seen that only iodine deviates significantly from their straight line. A number of workers have measured the Mössbauer spectrum of ^{129}I$_2$ and are in good

agreement as to its isomer shift relative to ZnTe, namely

0.91 mms^{-1}.[47,61,112] Conversion of this value into the 127-iodine

equivalent using the data of Jones and Warren [113] gives $\delta(^{127}I_2)$ of

-0.31 mms^{-1}. Relative to the KI standard of Perlow and Perlow,[14] a shift

of -0.31 -(0.14) = -0.45 mms^{-1} is found for $\delta(^{127}I_2)$. This is somewhat

closer to the value used to establish equation (1.29) but is slightly

more positive than the measured value. These discrepancies are further

complicated by the lack of internal consistency in reference 14. The

data obtained using the ZnTe source are claimed to be more reliable than

those for the Te(OH)$_6$ source,[14] yet it is interesting to note that with

this latter source $\delta(^{127}I_2)$-$\delta(^{127}KI)$ is -0.48 mms^{-1}, in rather good

agreement with the value calculated from ^{129}I data and with the value

measured here.

It is apparent from the above that a number of anomalies exist

which required further study. Since Mössbauer data existed for the

[ICl$_2$]$^-$ [14] and [I$_3$]$^-$ [15] anions it seemed appropriate to examine more

extensively the [X-I-Y]$^-$ series of anions, where X and Y can be F, Cl, Br

or I, as well as some related compounds. The linear trihalide anions can

be considered as addition complexes etween a halide ion and a halogen or

interhalogen molecule. The bonding in these complexes could be described

using a simplified MO treatment [114] such that the halogen p-orbitals

along the bond axis of the system are combined to form three molecular

orbitals which may accommodate four electrons. Thus, as in XeF$_2$ it may

be viewed as a three centre-four electron bond, of bond order one-half.

Just as the linear $[X-I-Y]^-$ anions are isoelectronic with the xenon dihalides, the following systems would be regarded as comprising an isoelectronic series of compounds.

$$Z^- \quad + \quad XY \quad \rightarrow \quad [XYZ]^- \qquad (4.1)$$

$$R_3N \quad + \quad XY \quad \rightarrow \quad R_3N-XY \qquad (4.2)$$

$$2R_3N \quad + \quad X^+ \quad \rightarrow \quad [R_3N-X-NR_3]^+ \qquad (4.3)$$

$$R_2S \quad + \quad XY \quad \rightarrow \quad R_2S-XY \qquad (4.4)$$
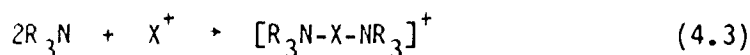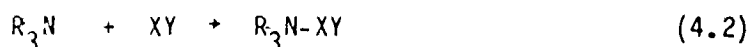
Charge transfer complexes between I_2 and various amines have been examined using ^{129}I Mössbauer, by May et al.[115] In the present study the ^{127}I Mössbauer parameters of $[I(py)_2][NO_3]$ wil be compared to those of the trihalide anions. The $[I(py)_2]^+$ cation is known from crystallographic data [116] to contain a linear N-I-N segment and Jones [112] has measured the ^{129}I Mössbauer spectrum. Similarly, the addition complexes between the thioketone N-methylthiocaprolactam $(C_7H_{13}NS)$ and I_2 and IBr will provide a useful comparison since they may be regarded as complexes of the type R_2S-XY (4.4). A single crystal X-ray study [117] of the I_2 addition complex has shown the S-I-I unit to be essentially linear, the S-I-I angle being 176.21(04)° and it is assumed that the IBr complex is similar in this respect.

These linear iodine systems then provide a series of well characterized compounds in which systematic changes made in the ligands surrounding the central iodine atom could possibly be correlated with the Mössbauer parameters. The isomer shift expression previously

established and assumed to have general applicability will be tested and re-evaluated using new data. The shifts used are relative to KI as zero isomer shift.

B. Results and Discussion

(i) Mössbauer Spectroscopy

The data from the computer analysis of the spectra are summarized in Table 4.1. Also included are literature data for $K[^{127}ICl_2] \cdot H_2O$,[14] $^{127}I_2$,[14] $Cs[^{129}I_3]$,[15] $^{129}I_2$,[112] ^{129}IBr,[118] $[^{129}I(py)_2][NO_3]$,[112] and $RS^{129}I$ [119] where R = N-p-chlorophenyl-2-(benzyloxycarbonamide)-3-methyl-butanamide: the ^{129}I isomer shifts have been converted to the corresponding ^{127}I isomer shifts by multiplying the former data by -0.345.[113] The absorber line widths which were allowed to vary in the transmission integral fitting are slightly greater than the natural width (Γ_{nat} = 1.27 mms^{-1}) except for two fluoro-complexes and $C_7H_{13}NSIBr$ which have widths about twice the natural value. The spectra for these compounds are also not fitted quite as well as the others and these aspects will be discussed.

The ^{127}I Mössbauer data obtained for iodine are compared to the literature data obtained at 4.2°K. There is generally good agreement for the $e^2q^{127}Q_g/h$ and η parameters, however there is some disparity between the isomer shift obtained in this study and those reported in the literature. The major source of error here is probably the lack of an

Table 4.1.

[127]I Mössbauer Data for [X-I-Y]⁻ Anions and Related Species

Compound	Isomer Shift (mms^{-1})	$e^2q^{127}Q_g/h$ (MHz)	η	Γ (mms^{-1})	T_A	χ^2/deg. of freedom	U_p	h_p (h_s=0)	h_s (h_p=U_p)
I$_2$	-0.49(2)	-2137(11)	0.22(1)	1.99(7)	0.84(2)	1.22	0.93	0.61	0.05
	-0.48(13)[a]	-2238(20)	0.12(2)						
	-0.72(7) [b]								
	-0.45(2) [c]	-2145(18)	0.16(3)						
Cs[I$_3$]	-0.34(4) [d]	-2515(20)					1.10		
	0.01(4) [d]	-1460(14)					0.64		
	0.14(4) [d]	- 820(25)					0.36		
[N(CH$_3$)$_4$][BrI$_2$]	-1.12(11)	-2583(55)		1.43(20)	0.84(9)	0.93	1.13	1.64	-0.08
	0.05(13)	-1580(75)		1.43(20)			0.69	-0.29	0.16
[N(C$_2$H$_5$)$_4$][ClI$_2$]	-0.71(7)	-2769(37)		1.47(17)	1.49(14)	1.09	1.21	0.97	0.04
	-0.53(12)	-1264(75)		1.47(17)			0.55	0.67	0.02
[N(CH$_3$)$_4$][IBrCl]	-0.73(5)	-3048(18)		1.58(14)	1.49(10)	0.99	1.33	1.00	0.05
K[ICl$_2$]·H$_2$O	-0.72(4) [b]	-3189(20)					1.39		
Cs[IClF]	-0.95(5)	-3029(36)	0.16(3)	2.47(17)	1.45(7)	1.36	1.32	1.36	-0.01
Cs[IBrF]	-0.84(5)	-2769(18)	0.24(2)	2.25(16)	1.75(9)	1.66	1.21	1.18	0.00
[N(C$_2$H$_5$)$_4$][IF$_2$]	-0.85(2)	-1380(12)	1.0	1.69(8)	0.63(2)	1.36	0.60	1.20	-0.09
[N(C$_2$H$_5$)$_4$][IBr$_2$]	-0.67(5)	-2695(36)	0.19(3)	1.95(17)	1.21(8)	1.16	1.18	0.90	0.05

<u>Table 4.1</u>: (Contd.)

Compound	Isomer Shift (mms^{-1})	$e^2q^{127}Q_g/h$ (MHz)	η	Γ (mms^{-1})	T_A	x^2/deg. of freedom	U_p	h_p ($h_s=0$)	h_s ($h_p=U_p$)
IBr	-0.28(2) [e]	-2892(10)	0.06(2)				1.26		
[I(C$_5$H$_5$N)$_2$][NO$_3$]	-0.93(3)	-3159(18)	0.08(4)	1.42(10)	1.69(10)	1.15	1.38	1.33	0.01
	-0.77(3) [c]	-3237(20)	0.03(3)						
C$_7$H$_{13}$NSIBr	-0.69(3)	-2471(20)	0.27(2)	2.25(12)	0.30(1)	1.25	1.08	0.93	0.02
C$_7$H$_{13}$NSI$_2$	-0.90(5)	-2601(26)		1.95(12)	0.35(1)	1.26	1.13	1.28	-0.02
	-0.31(5)	-1561(30)		1.95(12)			0.68	0.31	0.06
RSI	0.00(2) [f]	-2153(15)	0.07(3)						
KI	0	0		3.06(10)	0.33(4)	1.01			
	-0.14(2) [g]								

[a] Reference 14 (Te(OH)$_6$ source). [b] Reference 14 (ZnTe source).

[c] Reference 112 (converted from ^{129}I$_2$ data).

[d] H. de Waard and R.L. Spanhoff, unpublished results (converted from ^{129}I data),

[e] Reference 118.

[f] Reference 119 (R = N-p-chlorophenyl-2-(benzyloxycarbonamide)-3-methylbutanamide, converted from ^{129}I data).

[g] Isomer shift of KI relative to ZnTe source.

internal reference which would adjust all isomer shifts appropriately. This clearly illustrates the need for a universal reference material such as KI.

The semi-empirical relationship (1.29) has been widely used to calculate h_p or h_s by assuming that $U_p = h_p$. As previously mentioned however, this expression may not be completely general. It is satisfactory for $[ICl_2]^-$ since this particular anion was used to establish the equation, but for the structurally related $[I_3]^-$ the values of h_p for the central iodine atom, calculated from $e^2q^{127}Q_g/h$ and the isomer shift are 1.10 and 1.29 respectively. Hence the agreement is not as good. Therefore to further test this relationship, compounds containing all of the possible $[X-I-Y]^-$ anions for which Mössbauer data did not previously exist were examined. The Mössbauer data, in conjunction with the Raman data are the first spectroscopic evidence for $Cs[ClIF]$, $Cs[BrIF]$ and $[N(Et)_4][IF_2]$. Figures 4.1 and 4.2 show the ^{127}I Mössbauer spectra of $[N(CH_3)_4][BrICl]$ and $[N(Et)_4][I_2Cl]$ respectively. Except for $[N(Et)_4][IF_2]$ all spectra are similar in that the line due to transition number 2 is resolved at high positive velocity. This means that $e^2q^{127}Q_g/h$ is negative for all of the compounds, as would be expected for a central iodine atom with the X and Y ligands along the internuclear axis taken as z, and the non-bonding electron pairs in the xy plane.

It is apparent from Table 4.1 that the quadrupole coupling constant for the central iodine in the $[X-I-Y]^-$ anions increases as the electronegativities of the terminal halogens increase. For example

Figure. 4. 1. ^{127}I Mössbauer spectrum of. $[N(CH_3)_4]$ [BrICl] measured at 4.2°K. The solid line represents the best, fit to the data.
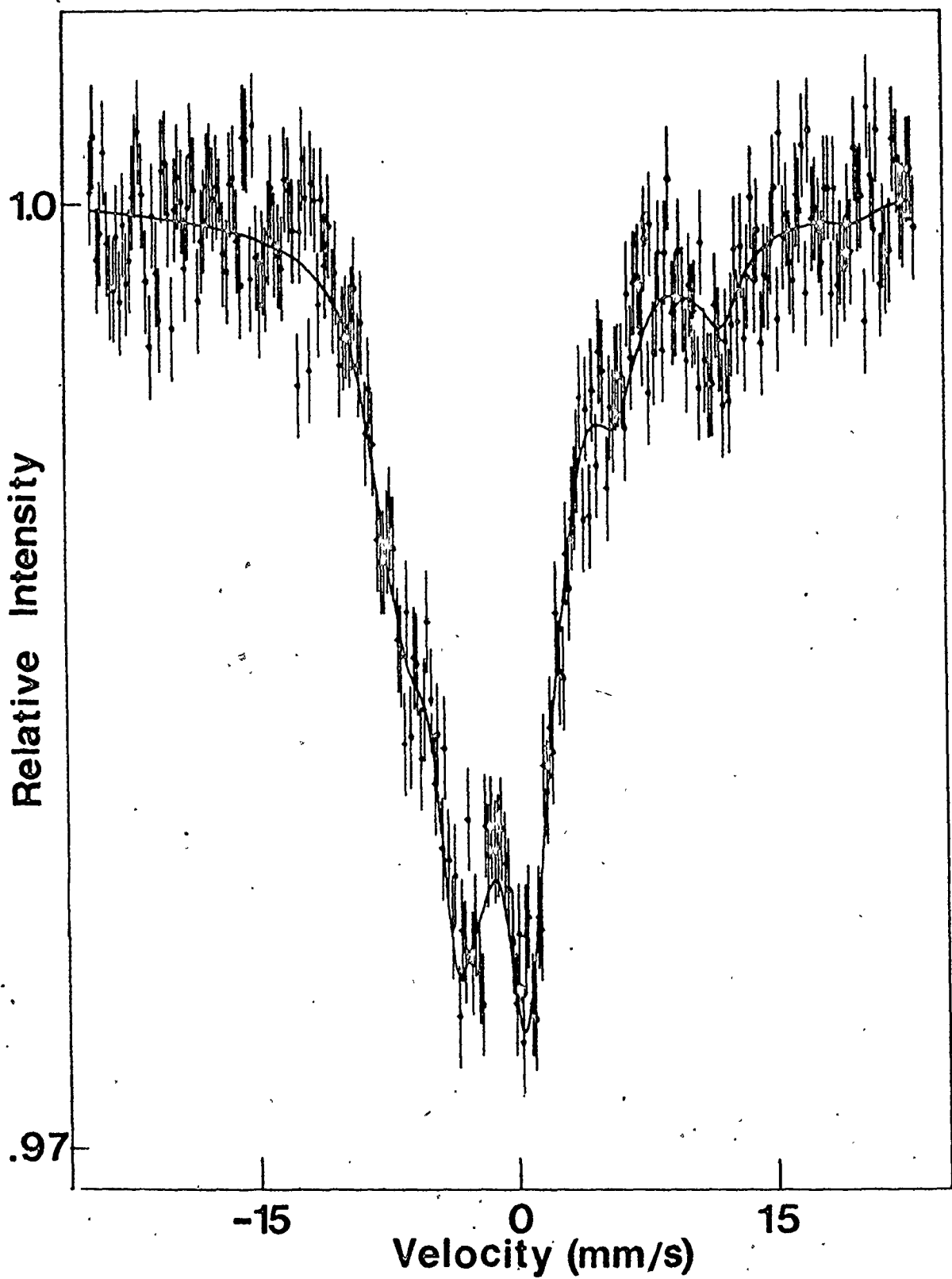
Figure 4.2. ^{127}I Mössbauer spectrum of $[N(CH_2CH_3)_4][I_2Cl]$ measured at 4.2°K. The solid line represents the best fit to the data.

$e^2q^{127}Q_g/h$ for $[I_3]^- < [IBr_2]^- < [ICl_2]^-$ and $[I_3]^- < [I_2Br]^- < [I_2Cl]^-$. Only the fluoro-anions deviate significantly from this trend. This relationship is further illustrated in Figure 4.3 where U_p, the reduced quadrupole coupling constant, is plotted against the sum of the electronegativities of the terminal atoms bonded to the central iodine in these linear anions. The electronegativity data of Pauling was used but a similar correlation is obtained using the Allred-Rochow values. The straight line corresponds to the best least-squares fit to the data, excluding the fluoro-anions, where the errors for each datum point are included in the fit. While there is some scatter in the data it is apparent that the effective charge on the central iodine nucleus is dependent upon the electronegativities of the ligands bonded to it. This same dependence has been observed by Jones [112] for a series of iodine compounds. It was also reported by this author [112] that a two centre-two electron bond, as is found in I-Cl, is equivalent to a three centre-four electron bond as in $[ICl_2]^-$ in terms of the number of elec-trons removed from the central iodine. A similar result is found in this study in that the quadrupole coupling constant of $[IBr_2]^-$ (-2695(36) MHz) is very close to that which has been reported for IBr (-2892(10) MHz).[118]

The fluoro-anions $[ClIF]^-$, $[BrIF]^-$ and $[IF_2]^-$ deviate markedly from the least-squares fit of the data in Figure 4.3, having much lower coupling constants and hence lower U_p values than would have been expected in view of the high electronegativity of fluorine, and the trend observed for the other trihalide anions. In fact the first two anions have coupling constants which are ca. 100 MHz smaller than those of the
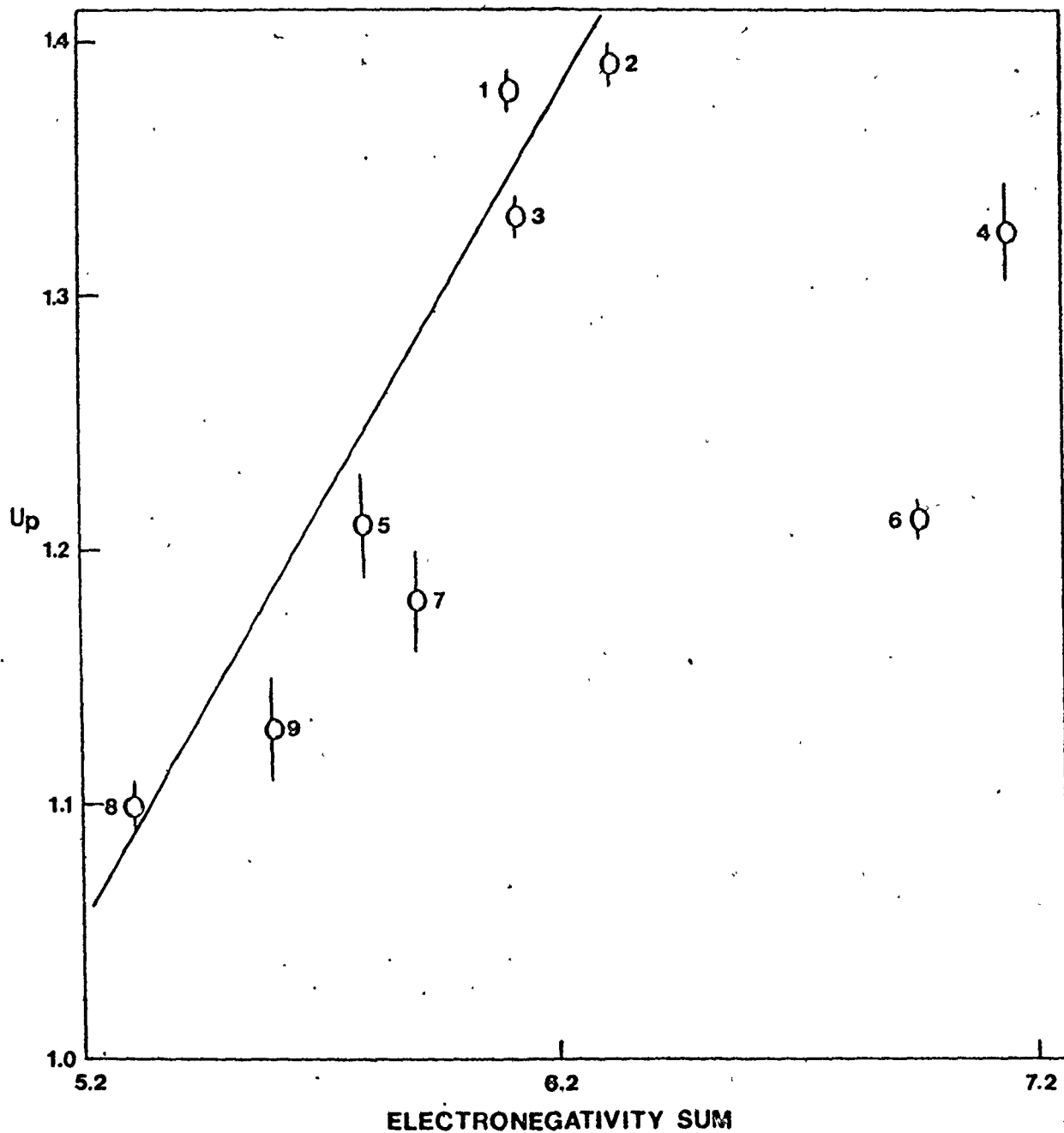
Figure 4.3.   · Plot of U_p versus the sum of Pauling electronegativities of terminal halogens in $[X-I-Y]^-$. The line drawn is best least squares fit to the data taking into account the errors, and excluding the fluoro-anions. Ions = (1) $[I(py)_2]^+$; (2) $[ICl_2]^-$; (3) $[IBrCl]^-$; (4) $[IClF]^-$; (5) $[I_2Cl]^-$; (6) $[IBrF]^-$; (7) $[IBr_2]^-$; (8) $[I_3]^-$; (9) $[I_2Br]^-$.

parent ICl and IBr molecules.[118] This apparently anomalous behaviour may possibly be explained by considering the Mössbauer spectrum of $[IF_2]^-$ and the X-ray crystal structures of ICl and IBr. In β-ICl there is, in addition to the short I-Cl bond (2.351Å), another longer I-Cl bond (2.939Å) which is almost colinear with the first. Other ICl molecules in the lattice have an iodine atom rather than a chlorine atom colinear with the I-Cl bond, and there are therefore two unique iodine environments in the crystal lattice.[120] A similar molecular structure with two non-equivalent iodine sites is also found in α-ICl.[121] The first of these two sites should have a coupling constant similar to that of $[ICl_2]^-$ while the latter should resemble that of the central iodine in $[I_2Cl]^-$. IBr should be similar to ICl in this respect. Thus when the reaction between ICl and CsF takes place to produce Cs[ClIF] the secondary I---Cl bond in ICl is replaced by a much weaker I---F⁻ interaction. It is also likely that F⁻ would interact with more than one ICl molecule so that its potential electronegativity is not reached and the withdrawal of electron density along the bonding axis is less than expected. The [ClIF]⁻ and [BrIF]⁻ anions have significantly larger asymmetry parameters than the other trihalide anions. This is probably indicative of the presence of significant additional interactions to the iodine atom which are off the intramolecular axis. These interactions would arise from the fluorine bridging mentioned above. Since $e^2q^{127}Q_g/h$ is still large and negative however, the [F---I-X]⁻ (X = Cl, Br) interaction must be essentially linear. As was previously mentioned it has been found that the quadrupole coupling constant remains essentially the same in going from

IX to $[IX_2]^-$. · A similar relationship would be expected to occur ·from IX(Y) to $[XIY]^-$, such that the coupling constant for $[XIY]^-$ should lie between that of IX and IY, or as the previous correlation suggests $1/2(e^2q^{127}Q_g/h)$ for $[IX_2]^-$ + $1/2(e^2q^{127}Q_g/h)$ for $[IY_2]^-$ should give approximately $e^2q^{127}Q_g/h$ for $[XIY]^-$. Since $e^2q^{127}Q_g/h$ for $[ClIF]^-$ is smaller than that of ICl this then suggests that the coupling constant due to an I-F interaction should be even smaller. The diatomic molecule IF is not isolable probably because of the weakness of the I-F bond and the stability of the disproportionation products. However $[IF_2]^-$ can be stabilized by large non-polarizing cations and the tetra-ethylammonium salt has been reported.[83] The ^{127}I Mössbauer parameters of $[IF_2]^-$ should then reflect those which would be expected for IF and the ^{127}I Mössbauer spectrum $[N(CH_2CH_3)_4][IF_2]$ is shown in Figure 4.4. The small coupling constant and very large asymmetry parameter observed continue the trend found for the other fluoro-anions and must be a reflection of the very high degree of asymmetry present, which is probably due to extensive fluorine bridging. This extensive bridging would preclude fluorine from exhibiting its maximum electron withdrawing power, and hence the rather small coupling constant. Since in the case of $[IF_2]^-$,. eta has a value of one it is not possible to determine the sign of the quadrupole coupling constant. It has been assigned a negative sign because it is assumed that while there is the presence of extensive fluorine bridging, the principal interactions occur along ·the z axis. The $[IF_2]^-$ anion is not included in Figure 4.3 but it is readily apparent that it would lie well off the straight line. In view of the very
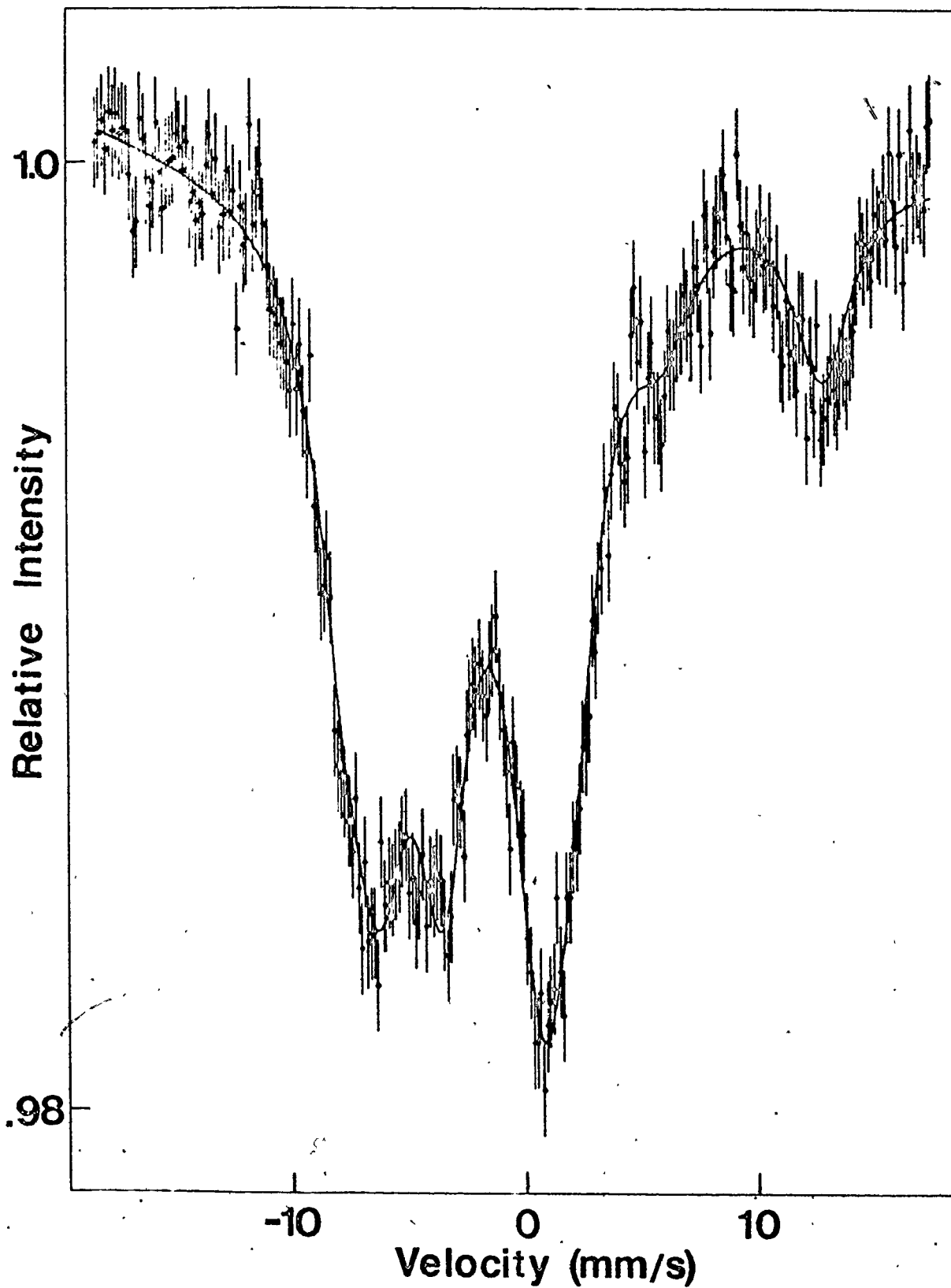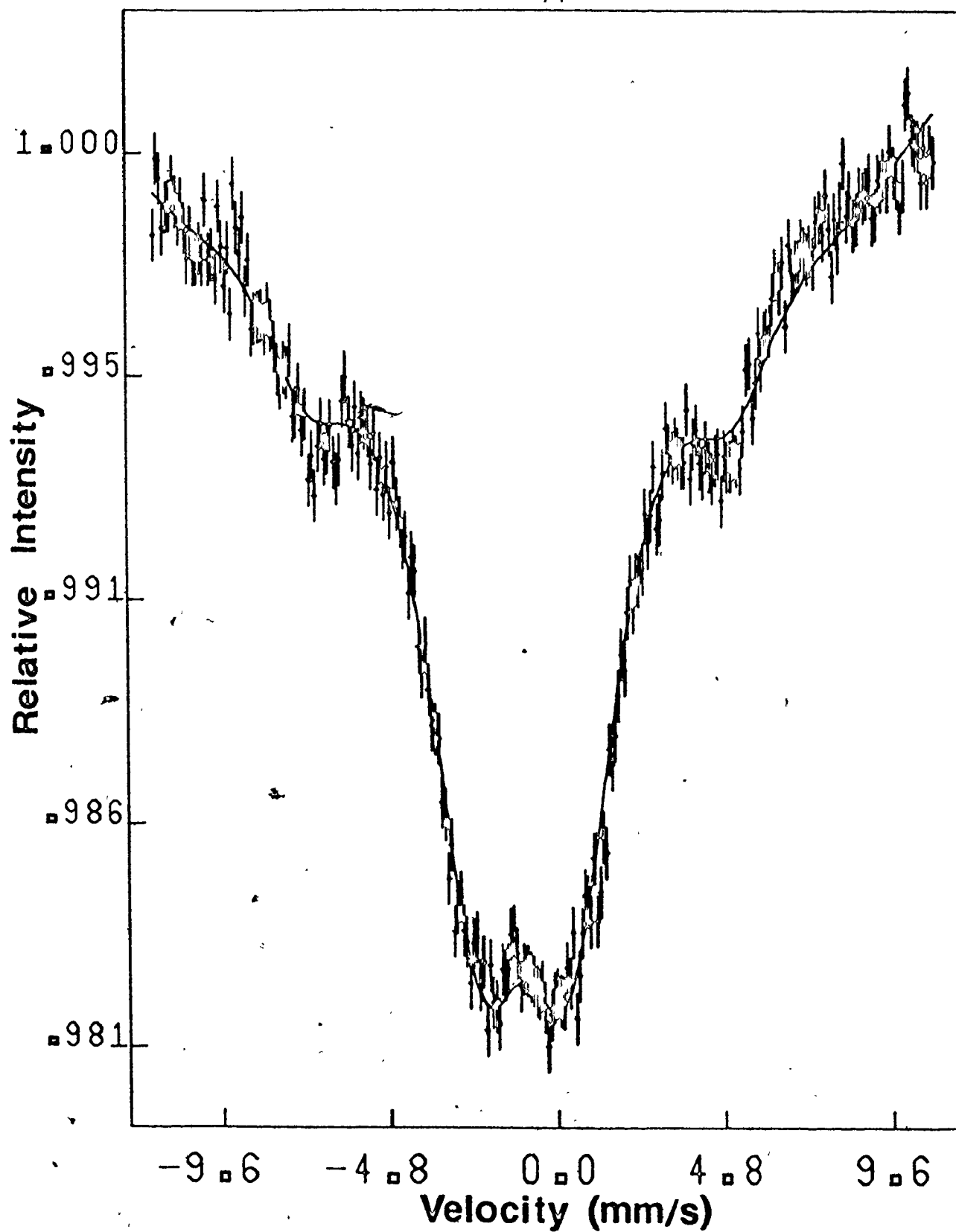
Figure 4.4. ^{127}I Mössbauer spectrum of $[N(CH_2CH_3)_4][IF_2]$ measured at 4.2°K. The solid line represents the best fit to the data.

unusual Mössbauer parameters obtained for these fluoro-anions, and in particular $[IF_2]^-$ the X-ray crystal structures of these compounds would be of great interest.

It was previously suggested that in the iodine-chlorine series of compounds $e^2q^{127}Q_g/h$ was a property of the I-Cl bond only.[118] Jones [112] has already commented on this and the results presented here clearly show that the quadrupole coupling constant does depend upon the nature of all coordinated ligands. For example the coupling constants for anions containing an I-I bond range from -2515 to -2767 MHz, for an I-Br bond, from -2471 to -3048 MHz and for an I-Cl bond from -2765 to -3189 MHz.

Dipyridineiodine(I) nitrate shows the largest quadrupole coupling constant of the compounds examined. It is slightly smaller than that measured by Jones [112] who used the ^{129}I isotope. The p-electron imbalance is very large at 1.38, consistent with that for an iodine cation linearly bonded between two pyridine-nitrogen atoms.

The charge transfer complexes between N-methylthiocaprolactam and I_2 and IBr exhibit the expected Mössbauer parameters -- the quadrupole coupling constants are large and negative. The IBr complex has a coupling constant somewhat smaller than the parent interhalogen compound which is as expected since the electronegativity of sulfur is slightly less than that of bromine. Potasek [119] has measured the ^{129}I Mössbauer spectrum of $RS^{129}I$ (R = N-p-chlorophenyl-2-(benzyloxycarbonamide)-3-methylbutanamide) and found $^{129}\delta_{ZnTe}$ = -0.41 mms^{-1} and $e^2q^{129}Q_g/h$ = -1510 MHz. After conversion to their 127-iodine equivalents the

values are $^{127}\delta_{ZnTe}$ = -0.14 mms^{-1} and $e^2q^{127}Q_g/h$ = -2153 MHz. Thus the iodine-sulfur bond in this compound has the effect of removing much less electron density from iodine than does the iodine-bromine bond in I-Br, and this is reflected in the much smaller quadrupole coupling constant in the former compound. This is consistent, since the coupling constant for $C_7H_{13}NSIBr$ lies between that of $RS^{127}I$ and IBr. The iodine addition complex $C_7H_{13}NSI_2$ seems at first somewhat anomalous in that the central iodine in the S-I-I segment has a coupling constant larger than that of the iodine atom in $C_7H_{13}NSIBr$. This could possibly be due to a problem associated with the fitting procedure in that the presence of two iodine sites prevents the precise resolution of the two components. However in view of the high level of success achieved in fitting two site spectra this is probably not the case. Perhaps because the electrons in the iodine-iodine bond found in the I_2 addition complex are not polarized towards the terminal iodine (R=S-I-I) to the same extent that they might be towards bromine in the IBr complex (R=S-I-Br) there is more efficient transfer of charge from the central iodine atom to the sulfur atom in the former compound. This higher transfer of charge would result in a larger p-electron imbalance at the central iodine and hence a larger quadrupole coupling constant.

The isomer shift data for this series of compounds is much more difficult to interpret than the quadrupole coupling constant data. Unlike the latter parameter, the shifts are dependent upon the source, upon the reference compound used, if any, and also upon whether the source and absorber are at the same temperature. It is generally very

difficult to compare data from one research group to another because of these variables and also the measured shifts are usually much smaller than the natural line width. It is important that these problems and the anomalies mentioned earlier be cleared up before relationships such as (1.29) can be used to estimate s- and p-orbital occupation numbers.

All of the compounds examined in Table 4.1 have negative isomer shifts ranging from ca. -0.3 to -1.0. This implies that the s-electron density in these linear compounds is higher than that in the source. This is consistent with a bonding model involving p-orbitals principally which thereby deshields the s-electrons causing an effective increase in s-electron density at the nucleus.

In order to evaluate the constants in equation (1.23) one can plot the isomer shift $\underline{versus}$ U_p for a series of compounds. If the bonding is principally of p-character then $U_p \equiv h_p$, equation (1.23) reduces to equation (1.24) and a plot of δ $\underline{versus}$ h_p (i.e. U_p) gives a line of slope $2K\gamma$. Since $\gamma = 0.07$ [43,47,122] the value of K may be determined. Equation (1.29) was established such that the data were relative to the ZnTe source. This relationship has been re-evaluated here using the isomer shift data relative to the KI standard and only data from this work have been considered because they are internally consistent. In Figure 4.5 the straight line represents a least-squares fit of all the data where errors associated with each datum have been considered. The slope of this line is -0.61 ± 0.03 mms^{-1} with an intercept of -0.12 ± 0.04 mms^{-1}. In view of the scatter of the data the intercept is fortuitously close to the isomer shift measured for KI in
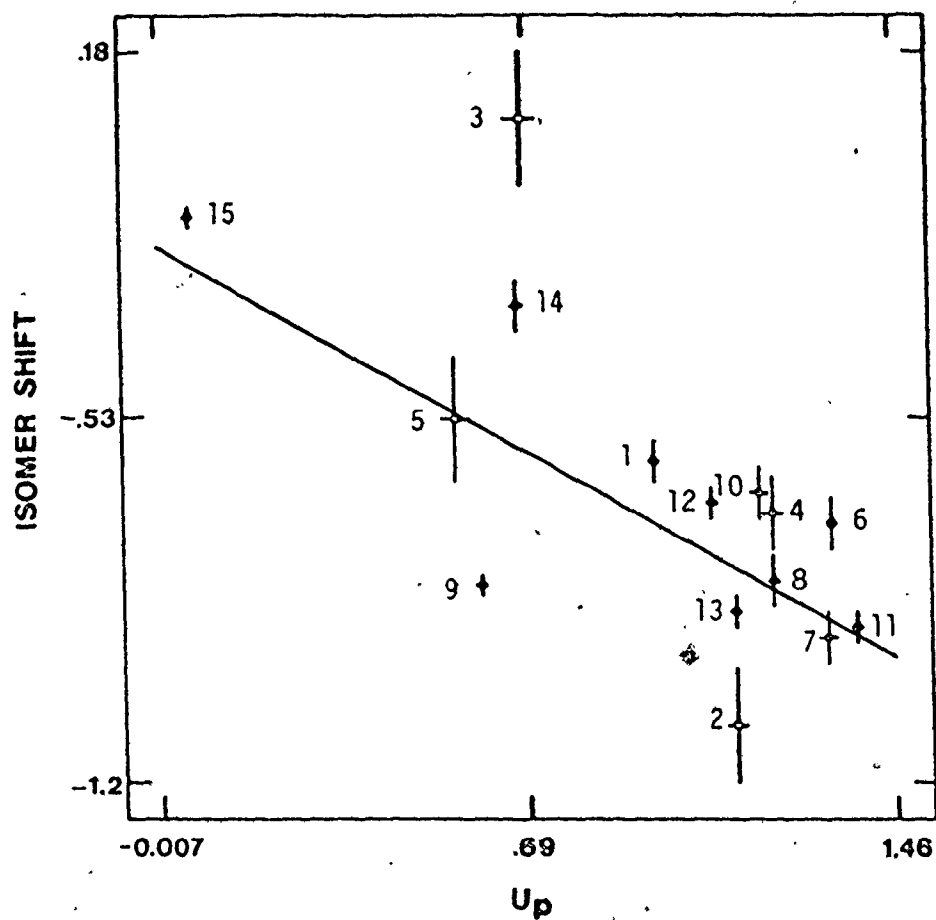
Figure 4.5.   Plot of isomer shift _versus_ U_p. . The line drawn

is the best least squares fit to the data.   Compounds:

(1) I_2; (2) $[I\overset{*}{-}I-Br]^-$; (3) $[\overset{*}{I}-I-Br]^-$; (4) $[Cl-\overset{*}{I}-I]^-$;

(5) $[Cl-I-\overset{*}{I}]^-$; (6) $[Br-I-Cl]^-$; (7) $[Cl-I-F]^-$;

(8) $[Br-I-F]^-$; (9) $[F-I-F]^-$; (10) $[Br-I-Br]^-$;

(11) $[I(py)_2]^+$; (12) $C_7H_{13}NSIBr$; (13) $C_7H_{13}NS-\overset{*}{I}-I$;

(14) $C_7H_{13}NS-I-\overset{*}{I}$; (15) KI.

·this work, namely -0.14 ± 0.02 mms^{-1}. This line should be parallel to the line which has been determined previously [14],[122] and the different intercepts arise because in this work the isomer shifts are relative to KI. The slope of the line is very close to what has been determined previously (-0.56 mms^{-1},[14] -0.50 mms^{-1} [122]) and gives a value for 2KY of -0.61 mms^{-1}. This may be regarded as the ^{127}I shift per 5p-electron hole. The value of K is then -4.36 mms^{-1} and equation (1.23) becomes (4.5) or (4.6):

$$^{127}\delta_{I^-} = -4.36 \left[-h_s + 0.07 (h_p + h_s)(2 - h_s) \right]$$
$$\approx 3.74 h_s - 0.61 h_p \tag{4.5}$$
$$^{127}\delta_{KI} = 3.74 h_s - 0.61 h_p - 0.12 \tag{4.6}$$

It is apparent from Figure 4.5 that there is considerable scatter in these data. The largest deviations are observed for the two sites in $[BrI_2]^-$ where the two isomer shifts are strongly correlated in the fitting procedure. If these two isomer shifts are constrained to be equal an isomer shift value of -0.67 mms^{-1} is found which correlates much better with the line drawn. However there is no reason to expect these shifts to be the same and indeed a lower χ^2 value is obtained when the two isomer shifts are allowed to vary in the fitting procedure. The fluoro-anions deviate slightly but again this can probably be attributed to additional interactions between anions, via fluorine·bridges, as discussed above for the quadrupole coupling constant data. Equation (4.6) can then be used to calculate h_p, assuming that h_s = 0, or to

estimate h_s by equating h_p and U_p, and these calculated values are found
in Table 4.1. One can see that the agreement between the values for U_p
and h_p calculated in this way varies quite considerably. This is not too
surprising because the value of x^2 per degree of freedom for the
correlation upon which the calculation depends is very high (32.5), even
though the compounds which were included in the analysis all have a
similar structure and presumably very similar bonding. The differences
between U_p and h_p cannot be accounted for by either s-involvement in the
bonds or by π character in the bonds. Negative values for h_s have no
meaning and while π character to the bonding is usually invoked when $h_p >$
U_p, this is clearly not the case. These discrepancies then may be due to
inaccurate assumptions made initially, and at best the correlation
discussed above should be treated as a semi-empirical scheme, useful for
making general descriptions of the bonding in iodine compounds.

(ii) Raman Spectroscopy

The linear trihalide anions have been examined quite extensively
using vibrational spectroscopy.[11-13] Until now there has been no
vibrational spectroscopic data reported for the fluorine containing
anions. It was not possible to obtain good elemental analysis for the
fluoro-anions, however this seems to be a common problem associated with
the analysis of other elements in the presence of fluorine. Also no X-
ray crystallographic data is available for these compounds but it is
assumed that they are linear compounds like the other trihalide anions.

The linear symmetrical molecules X_3 and YXY (symmetry $D_{\infty h}$)
exhibit three fundamental modes of vibration; ν_1, the symmetric stretch-
ing mode is Raman·active only, while ν_3, the asymmetric stretching mode,
and ν_2 the YXY deformation are exclusively infrared active. The linear
triatomic molecule XYZ (symmetry $C_{\infty v}$) has all three modes of vibration
both Raman and infrared active. The above rules can however break down
if say the YXY molecule becomes unsymmetric due to crystal packing
effects or if the site symmetry for the·ions in the crystal is lower than
the point group symmetry of the free ions. Raman data obtained for
Cs[BrIF], Cs[ClIF] and [N(CH$_2$CH$_3$)$_4$][IF$_2$] are given in Table 4.2.

It becomes useful at this point to digress back to the ^{127}I
Mössbauer spectrum of [N(CH$_2$CH$_3$)$_4$][IF$_2$]. Close examination of the
absorption envelope for this particular compound reveals two possible
interpretations. The very symmetric nature of the spectrum (Figure 4.4)
could be caused by the presence of a very large asymmetry parameter, and
this in fact was the interpretation given. This type of spectrum, in
theory could also arise from a nearly equimolar mixture of two compounds
whose quadrupole coupling constants have opposite signs, and in this case
would almost certainly have to be [IF$_2$]$^-$ and [IF$_4$]$^-$. This latter
interpretation is untenable for two reasons. It is not likely that the
iodine(I) compound used to produce [IF$_2$]$^-$ would be oxidized to
iodine(III) under the mild exchange conditions employed, nor is there
anything present that can be reduced. Also, the Raman spectrum of
Cs[IF$_4$] has been reported [123] and there are no coincidental bands in the
spectrum obtained here for [IF$_2$]$^-$. The Raman spectrum of

Table 4.2.

Raman Data for Cs[ClIF], Cs[BrIF] and $[N(CH_2CH_3)_4][IF_2]$

	Frequency (cm^{-1})	Intensity	Assignment
$[N(CH_2CH_3)_4][IF_2]$			
	106	22	lattice
	113	17	
	167	100	ν_2
	304	33	
	334	14	
	344	28	
	415	34	ν_1
	461	53	ν_3
Cs[ClIF]			
	95	94	ν_2 bend
	262	100	I-Cl st.
	425	2	I-F st.
Cs[BrIF]			
	27	6	lattice
	36	5	
	46	15	
	72	9	
	130	20	
	146	49	
	180	100	I-Br st.
	188	58	

$[N(CH_2CH_3)_4][IF_2]$ is consistent with the Mössbauer data in that the presence of more than one band suggests the molecule is severely distorted from $D_{\infty h}$ symmetry. The interpretation of the Raman spectrum of $[IF_2]^-$ may be facilitated by comparison with that of the isoelectronic compound XeF_2 ($D_{\infty h}$ symmetry) whose vibrational data have been assigned [124] as follows: ν_1 (R) 497 cm^{-1}, ν_2 (IR) 213 cm^{-1} and ν_3 (IR) 555 cm^{-1}. The asymmetric stretch of $[IF_2]^-$ has been assigned to the band at 461 cm^{-1}. By comparison with the same band in XeF_2 one sees that it occurs at a lower frequency than XeF_2, contrary to what would be expected. This lowering in frequency may be attributed to the high degree of fluorine bridging previously suggested. This trend is also followed by the two bands which have been assigned as ν_1 and ν_2. The two lowest frequency lines have been assigned as lattice vibrational modes and in the absence of crystallographic data it is very difficult to assign the remaining lines in the Raman spectrum of $[N(CH_2CH_3)_4][IF_2]$. The Raman lines due to the vibrations of the cation were also observed but they are not included here.

The remaining two anions $[ClIF]^-$ and $[BrIF]^-$ should have $C_{\infty v}$ symmetry and hence all three vibrational modes should be observable in the Raman. Once again precise assignments of these vibrational modes is difficult in the absence of X-ray crystal structure information. The band at 262 cm^{-1} in the Raman spectrum of $[ClIF]^-$ has been assigned to the I-Cl stretch. Close examination of this band reveals the presence of a small shoulder at ca. 258 cm^{-1} which is probably due to the I-^{37}Cl stretch. These iodine-chloride stretching frequencies are reasonable.

when compared to the I-Cl stretching frequency [125] of ICl which is 381 cm^{-1}. The band assigned to the I-F stretch is very weak but is in the same region as that found in $[IF_2]^-$. The remaining strong band at 95 cm^{-1} is probably the deformation mode of $[ClIF]^-$.

The Raman spectrum of $[BrIF]^-$ is again somewhat complex. There is no peak in the spectrum above 200 cm^{-1}, so the I-F stretch in this anion is not observable. The I-Br stretching frequency in various $[BrICl]^-$ salts [12] ranges from 174 to 180 cm^{-1}. In the Raman spectrum of $[BrIF]^-$ there are two strong bands at 180 and 188 cm^{-1}, the former of which has been arbitrarily assigned as the I-Br stretch. The band at 130 cm^{-1} is thought to be ν_2, the deformation mode, while the lines below 130 cm^{-1} are assigned as lattice vibrational modes. The remaining two lines at 146 cm^{-1} and 188 cm^{-1} are difficult to assign but probably arise because of the additional interactions which have been mentioned previously.

CHAPTER 5

THE PREPARATION AND CHARACTERIZATION OF THE SQUARE PLANAR

IODINE(III) CATIONS

$[ICl_2][SbCl_6]$, $[IBr_2][Sb_2F_{11}]$ and $[IBr_{0.75}Cl_{1.25}][SbCl_6]$
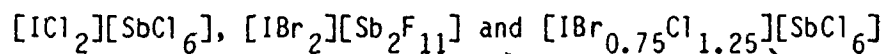
A.   Introduction

A review of polyhalogen cations has recently been published by

Shamir.[16] Several interhalogen cations of iodine(III) have been prepared

and identified by various physical measurements (Table 1.2). In this

Chapter the preparation and characterization of three new iodine(III)

compounds will be presented and the structure and bonding will be

discussed in light of their X-ray crystal structures, Mössbauer, Raman

and NMR spectra.

The X-ray crystal structures of $[ICl_2][SbCl_6]$ and $[ICl_2][AlCl_4]$

have been reported [19] and both contain iodine in a square-planar

environment. In these compounds cation-anion interactions are quite

strong with the bridging I---Cl bond distances varying from 2.85-3.00Å.

These distances are only slightly longer than the bridging I---Cl

distances in I_2Cl_6 which average 2.70Å.[126]

Recently Aubke and co-workers [27] allowed I_2Cl_6 to react with a

large excess of SbF_5 and obtained a compound which was formulated as

$[ICl_2][Sb_2F_{11}]$ with some cation-anion interaction. Such an interaction

should result in a square geometry about the iodine, from two terminal

chlorines and two bridging fluorines. This particular reaction was

repeated here in an attempt to prepare $[ICl_2][Sb_2F_{11}]$ and while evidence for the $[Sb_2F_{11}]^-$ anion was found in solution, that same solution yielded crystals of $[ICl_2][SbF_6]$, as confirmed by X-ray analysis. The X-ray crystal structure of $[ICl_2][SbF_6]$ is the first example of a structure containing an iodine(III) cation in which the halogen ligands are not all the same and where a strong iodine-fluorine secondary interaction exists.

Aubke and co-workers have also reported the preparation of IBr_2SO_3F [26,127] and $[IBr_2][Sb_2F_{11}]$.[27] The former compound was prepared by the oxidative addition of bromine to iodine(I) fluorosulfate and was characterized on the basis of its vibrational spectra. The $[Sb_2F_{11}]^-$ salt of $[IBr_2]^+$ was prepared by the anion exchange of IBr_2SO_3F with a very large excess of SbF_5. This latter compound was subsequently characterized by elemental analysis, vibrational spectroscopy and u.v-visible absorption spectroscopy. $[IBr_2][Sb_2F_{11}]$ was prepared during the course of this work by the reaction of IBr with SbF_5. This reaction was initially designed to produce the $[IBr]^+$ cation but an X-ray structure analysis showed the compound to contain the $[IBr_2]^+$ cation. The geometry around the iodine atom in this compound is similar to that of $[ICl_2][SbF_6]$ in that there are bridging fluorine interactions to the $[Sb_2F_{11}]^-$ anions, which complete the square-planar geometry around iodine.

The asymmetric interhalogen cation $[BrICl]^+$ has also been reported and was characterized on the basis of its Raman spectrum. Aubke and co-workers [27] report the preparation of $BrIClSO_3F$ by the reaction of equimolar amounts of IBr_2SO_3F and ICl_2SO_3F. Shamir and Lustig [38] have

reported a much more novel preparation whereby an equimolar amount of chlorine was added to a 1:1 stoichiometric mixture of antimony pentachloride and iodine monobromide at -196°C. A similar reaction was carried out here using liquid SO_2 as solvent, and a very dark crystalline material was obtained. A single crystal X-ray study revealed the material to contain a disordered iodine(III) cation of approximate stoichiometry $[IBr_{0.75}Cl_{1.25}]^+$.

The X-ray crystal structure of $[I_3][AsF_6]$ has been reported [32] by Passmore et al. and once again the $[I_3]^+$ cation is similar to $[ICl_2]^+$ with the central iodine in a square-planar environment with bonds to two terminal iodines and weaker bridging interactions to two fluorines of two separate $[AsF_6]^-$ anions.

These well characterized compounds provide a series with iodine(III) in a square- or rectangular-planar environment having a range of interactions to fluorine, chlorine, bromine and iodine. Such a series is ideal for further testing the correlation of [127]I Mössbauer parameters with ligand electronegativity, and for calculating h_p and h_s values using the relationships described in Chapter 4. There are a number of other square-planar iodine compounds which will provide a useful comparison to the former compounds in terms of their Mössbauer spectra. $K[ICl_4]$ and I_2Cl_6 are ideal compounds to compare with the $[ICl_2]^+$ cation. Also Alcock and Countryman [128] have reported the X-ray crystal structures of a series of diphenyliodonium salts $[Ph_2IX]_2$ where X = Cl, Br and I. All three compounds are isomorphous showing the overall structure of centrosymmetric dimers held together by halogen bridges.

Since the dimers are precisely planar these compounds will provide a useful comparison to the square-planar cations mentioned previously. In this series of compounds the halogens occupy the bridging positions of the square-planar iodine geometry, rather than the terminal positions as in the $[IX_2]^+$ cations.

B. RESULTS AND DISCUSSION

(i) X-ray Crystallography

Crystal data for the three compounds, $[ICl_2][SbF_6]$, $[IBr_2][Sb_2F_{11}]$ and $[IBr_{0.75}Cl_{1.25}][SbCl_6]$ are found in Table 5.1. Intensity measurements were made on either a Syntex $P2_1$ or Nicolet P3 diffractometer. The details regarding data acquisition are also given in Table 5.1. Lorentz and polarization corrections were applied to all the data. The three structures were solved using conventional heavy-atom methods to locate the iodine and/or antimony atoms in Patterson maps. Subsequent Fourier maps revealed the positions of the remaining atoms and confirmed the positional assignments of the heavy atoms. The details concerning the final stages of refinement are also found in Table 5.1. The systematic absences for $[ICl_2][SbF_6]$ (Table 5.1) indicated the space groups Cmca (No. 64) or Cc2a (standard setting Aba2 (No. 41)). The structure was solved and refined in the space group Cmca and subsequent refinement in the space group Cc2a resulted in no improvement. Preliminary precession photographs of the disordered compound $[IBr_{0.75}Cl_{1.25}][SbCl_6]$ indicated that the unit cell was triclinic. The

Table 5.1.

Crystal, Acquisition and Refinement Data for $[ICl_2][SbF_6]$, $[IBr_2][Sb_2F_{11}]$ and $[IBr_{0.75}Cl_{1.25}][SbCl_6]$

Crystal Data

	$[ICl_2][SbF_6]$	$[IBr_2][Sb_2F_{11}]$	$[IBr_{0.75}Cl_{1.25}][SbCl_6]$
System	orthorhombic	orthorhombic	triclinic
a, Å	10.751(3)	14.445(3)	7.084(1)
b, Å	12.087(4)	14.034(5)	6.299(1)
c, Å	12.982(2)	12.725(3)	13.511(3)
α, deg.	90	90	94.50(2)
β, deg.	90	90	100.32(2)
γ, deg.	90	90	92.56(2)
U, Å^3	1687.0(8)	2580(1)	590.3(2)
D_{calcd}, gcm^{-3}	3.41	3.81	3.18
Reflections used in cell determination (No./2θ range)	$15/30° < 2\theta < 35°$	$15/18° < 2\theta < 28°$	$15/20° < 2\theta < 29°$
Z	8	8	2
fw	433.7	739.3	565.7
F(000)	1536	2592	506
μ(MoKα), cm^{-1}	76.8	123.2	88.5
space group	Cmca or Cc2a	Pbca	P$\bar{1}$ or P1
Systematic absences	hkℓ,h+k=2n; okℓ,k=2n; hoℓ,ℓ=2n; hko,h=2n	hkℓ,no conditions; okℓ,k=2n;hoℓ,ℓ=2n; hko,h=2n;hoo,(h=2n); oko,(k=2n); ooℓ,(ℓ=2n)	no conditions

Table 5.1. (contd.)

Data Collection

$$[ICl_2][SbF_6] \quad [IBr_2][Sb_2F_{11}] \quad [IBr_{0.75}Cl_{1.25}][SbCl_6]$$

	$[ICl_2][SbF_6]$	$[IBr_2][Sb_2F_{11}]$	$[IBr_{0.75}Cl_{1.25}][SbCl_6]$
mode		$\theta:2\theta$	
wavelength		MoKα radiation ($\lambda=0.71069$Å)	
stds.	3/67	2/18	2/48
No./interval [a]	$(4,-4,-1)$,	$(4,-1,-1)$ &	$(-1,1,3)$ &
	$(2,0-,2)$ &	$(4,-1,1)$	$(-1,-1,7)$
	$(-1,3,-1)$		
scan range, deg.	Kα_1 -0.9 to	Kα_1 -1.2 to	Kα_1 -1.2 to
	Kα_2 +0.9	Kα_2 +1.2	Kα_2 +1.2
scan speeds,[b] deg. min^{-1}	2.5 - 29.3	4.0 - 29.3	4.0 - 29.3
max 2θ deg., quadrant	55, hkℓ	45, hkℓ	55, h$\pm$k$\pm\ell$

Details of Refinements

	$[ICl_2][SbF_6]$	$[IBr_2][Sb_2F_{11}]$	$[IBr_{0.75}Cl_{1.25}][SbCl_6]$
absorption correction	spherical $\mu R = 1.19$ (R=0.016cm) A*: 3.47-5.29	spherical $\mu R = 1.90$ (R=0.015cm) A*: 5.25-12.50	none
No. of nonzero data	1037	1668	2738
No. of data with F>2.0σ(F)	941	1390	2360
No. of data with F>6.0σ(F)	788	1009	1917

Table 5.1.

Details of Refinement (contd.)

	$[ICl_2][SbF_6]$	$[IBr_2][Sb_2F_{11}]$	$[IBr_{0.75}Cl_{1.25}][SbCl_6]$
R factors			
$2\sigma:R_1{}^c$	0.040	0.065	0.061
$R_2{}^d$	0.045	0.064	0.075
$6\sigma:R_1$	0.031	0.042	0.048
R_2	0.039	0.050	0.063
max.shift/error	0.05	0.001	0.002
weighting scheme [e]	f	$w=1.0/(\sigma(F_0)^2 + 0.001F_0{}^2)$	$w=1.0/(\sigma(F_0)^2 + 0.0023F_0{}^2)$
highest peak in final diff.map,[g] e/A^3	+3.4	+1.3	+3.6
lowest valley in final diff.map, e/A^3	-1.2	-1.2	-1.1

[a] No systematic trends in the intensities of the standards were observed.

[b] Dependent on prescan.   [c] $R_1 = (\Sigma||F_0|-|F_c|/\Sigma|F_0|)$.

[d] $R_2 = [\Sigma w||F_0|-|F_c||^2/\Sigma w|F_0|^2]^{1/2}$

[e] In each case the final comparison of the average $w||F_0|-|F_c||^2$ as a function of F_0 and $\sin\theta$ after the use of these schemes showed no systematic trends.

[f] The weighting scheme used was w = XY, where: (1) X = $(\sin\theta)/0.37$ if $\sin\theta$ < 0.37 or X = $0.40/\sin\theta$ if $\sin\theta$ > 0.40, otherwise X = 1, and (2) Y = 70.0/F if F > 70.0 or Y = F/50.0 if F < 50.0, otherwise Y = 1.0.

[g] In all cases the final difference Fourier was featureless with the maximum peaks and minimum valleys found around heavy atoms.

structure was solved and refined in the centric space group P$\bar{1}$ and subsequent refinement in P1 did not improve the analysis. A complete listing of observed and calculated structure factor amplitudes of all crystal structures may be found by referring to reference 129.

a) Structure of [ICl$_2$][SbF$_6$]

The final atomic position coordinates and thermal parameters for [ICl$_2$][SbF$_6$] are found in Tables 5.2 and 5.3 respectively.

The bond lengths and bond angles of the molecule are given in Table 5.4. The crystal structure of [ICl$_2$][SbF$_6$] consists of infinite chains of [SbF$_6$]$^-$ anions cis-bridged through fluorine to [ICl$_2$]$^+$ cations. The atomic arrangement is illustrated in Figure 5.1 and a stereoscopic view of the packing in the unit cell along the c axis is shown in Figure 5.2. The structure then could be considered as consisting of bent [ICl$_2$]$^+$ cations and slightly distorted octahedral [SbF$_6$]$^-$ anions. The [SbF$_6$]$^-$ anion has crystallographic mirror symmetry since the antimony atom is located at the special position o,y,z. The anion is not unusual, with the terminal Sb-F distances averaging 1.858Å, while the bridging Sb-F distance is somewhat longer at 1.894(6)Å. As expected the Sb-F bond trans to the bridging fluorine is the shortest Sb-F distance in the molecule.

The environment about the iodine is similar to that found in both ISbCl$_8$ and IAlCl$_6$,[19] namely a nearly square-planar configuration, although in [ICl$_2$][SbF$_6$] the arrangement about iodine is comprised of two chlorines and two fluorines rather than four chlorines. The [ICl$_2$]$^+$ cation also possesses crystallographic symmetry in the form of a two-fold

Table 5.2.

Atomic Coordinates ($\times 10^4$) for $[ICl_2][SbF_6]$

	x/a	y/b	z/c
I(1)	2500	901(1)	2500
Sb(1)	0	2038(1)	-568(1)
Cl(1)	1650(2)	-340(2)	3606(2)
F(1)	0	698(6)	-1281(7)
F(2)	0	3429(6)	51(7)
F(3)	1251(6)	1567(6)	308(5)
F(4)	1224(6)	2566(5)	-1494(4)

Table 5.3.

Thermal Parameters[†] for $[ICl_2][SbF_6]$

	U_{11}	U_{22}	U_{33}	U_{12}	U_{13}	U_{23}
I(1)	447(4)	425(4)	309(3)	0	82(3)	0
Sb(1)	363(3)	347(3)	284(3)	0	0	26(3)
Cl(1)	591(12)	585(11)	501(10)	-63(9)	149(10)	112(9)
F(1)	824(54)	382(32)	735(51)	0	0	-159(36)
F(2)	781(52)	511(43)	673(48)	0	0	-243(36)
F(3)	599(34)	1051(49)	671(34)	105(33)	-235(29)	173(33)
F(4)	656(31)	637(29)	627(29)	-149(26)	247(27)	90(25)

[†] Temperature factors ($\times 10^4$) in the form $\exp\left(-2\pi^2 \sum_{ij} U_{ij} H_i H_j a_i^* a_j^*\right)$

Table 5.4.

Bond Lengths (Å) and Bond Angles (°) for $[ICl_2][SbF_6]$ [a]

Estimated Standard Deviations in Parentheses

(a) Bond lengths (Å)		(b) Bond angles (°)	
I(1) - Cl(1)	2.268(2)	Cl(1) - I(1) - Cl(1')	97.2(1)
I(1) - F(4)	2.650(6)	Cl(1) - I(1) - F(4)	86.7(1)
Sb(1) - F(1)	1.867(8)	F(4) - I(1) - F(4')	91.2(2)
Sb(1) - F(2)	1.863(8)	Cl(1) - I(1) - F(4')	169.4(1)
Sb(1) - F(3)	1.851(7)	F(1) - Sb(1) - F(2)	175.8(4)
Sb(1) - F(4)	1.894(6)	F(1) - Sb(1) - F(3)	92.2(3)
		F(1) - Sb(1) - F(4)	88.7(3)
		F(2) - Sb(1) - F(3)	90.7(3)
		F(2) - Sb(1) - F(4)	88.3(3)
		F(3) - Sb(1) - F(3")	93.2(3)
		F(3) - Sb(1) - F(4)	89.4(3)
		F(3) - Sb(1) - F(4')	177.3(3)
		F(4) - Sb(1) - F(4")	88.1(3)
		I(1) - F(4) - Sb(1)	155.3(3)

[a] Symmetry transformations are: (') 1/2-x,y,1/2-z; (") -x,y,z
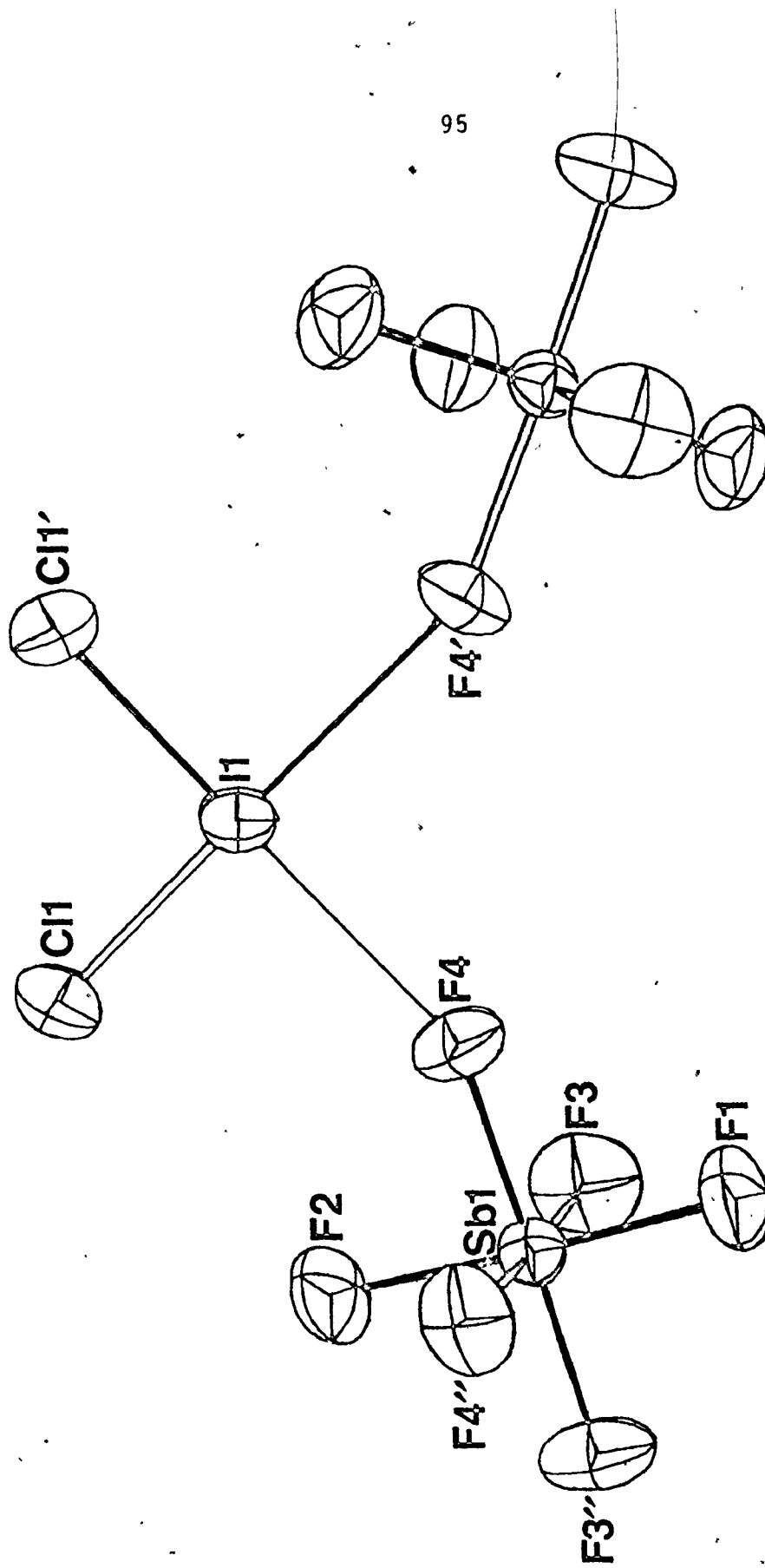
Figure 5.1.   Structure of [ICl₂][SbF₆] showing the coordination sphere around iodine including the [SbF₆]⁻ anions.   Symmetry transformations: ('), ½-x, y, ½-z; ("), -x, y, z.
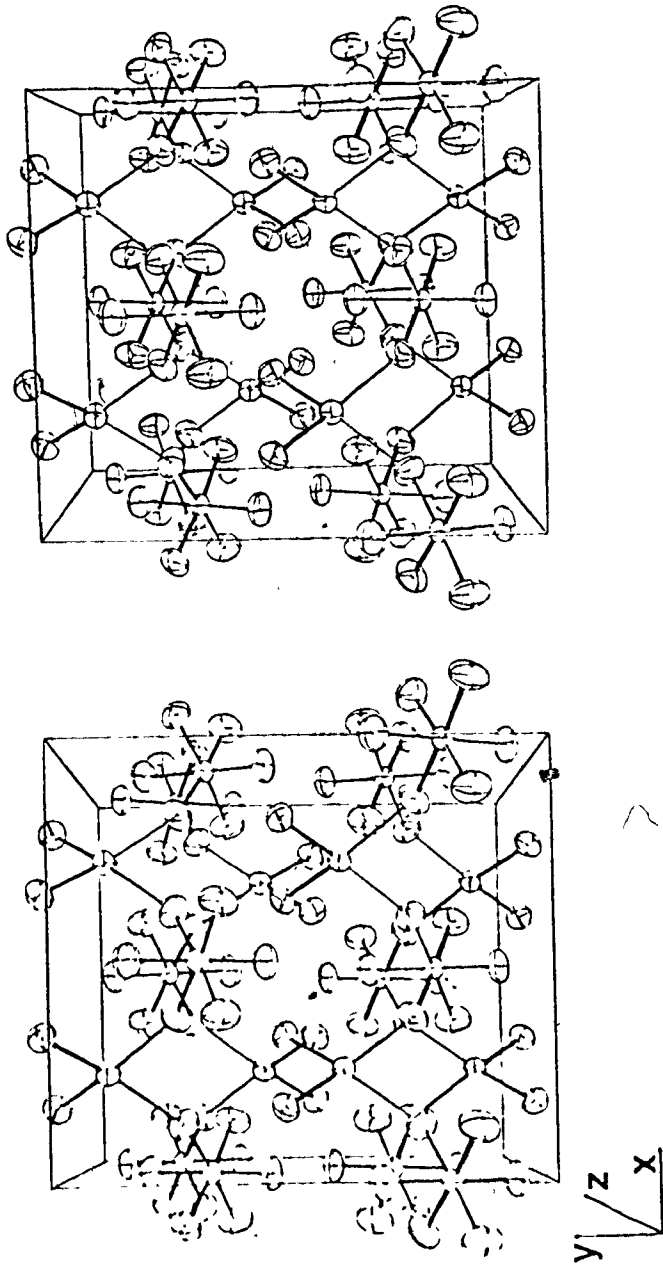
Figure 5.2.   Stereoscopic drawing of the unit cell of $[ICl_2][SbF_6]$ viewed down the c axis.

axis since the iodine atom is located at the special position

(1/4,y,1/4). The terminal I-Cl distance in the $[ICl_2]^+$ cation of

2.268(2)A may be compared to the corresponding bond lengths in the

$[AlCl_4]^-$ and $[SbCl_6]^-$ analogues, which range from 2.26(4) to 2.33(4)A.[19]

These distances are significantly shorter than the terminal I-Cl bonds

in the neutral I_2Cl_6 molecule [130] (2.38, 2.39A) or in the anions in

$K[ICl_4] \cdot H_2O$ [131] (2.42, 2.47A) and $[SCl_3][ICl_4]$ [132] (2.437(2), 2.469(3)A).

It is apparent that as the charge on the ion becomes more negative the

terminal I-Cl bond length increases, as one might have expected. As the

terminal I-Cl bonds become weaker there is a corresponding strengthening

of the I---Cl bridging, or secondary bonds until they become of similar

length to the terminal bonds. This situation is reached in $K[ICl_4] \cdot H_2O$

and $[SCl_3][ICl_4]$ where the bridging contacts from the $[ICl_4]^-$ anion are

rather weak. In $[ICl_2][SbF_6]$ the secondary contacts completing the

rectangular arrangement about the iodine are through fluorine so that a

direct comparison with the other molecules is not possible. However,

this kind of problem has been treated by Wiebenga and Kracht [133] who have

established a relationship between electrostatically corrected

experimental bond lengths and calculated bond orders for a series of

interhalogen compounds. Using their relationships the secondary or

bridging contacts (mean 2.90A) in $[ICl_2][SbCl_6]$ and $[ICl_2][AlCl_4]$ have a

bond order of 0.47 while in I_2Cl_6 the bridging bond is much shorter

(2.70A) and hence stronger, having a bond order of 0.58. The I---F

bridging contacts in $[ICl_2][SbF_6]$ are 2.650(6)A which correspond to a

bond order of 0.42. This is only slightly weaker than that found for the

secondary contacts in the hexachloroantimonate and tetrachloroaluminate complexes. This I---F distance (2.650Å) is quite short and may be compared to the covalent single bond distance of 1.92Å and the van der Waals contact distance of 3.45Å.[134] Direct comparisons with other I-F distances are difficult to make because of the paucity of structural data for other iodine-fluorine molecules (see later this Chapter). Iodine pentafluoride [135] has I-F bond lengths ranging from 1.6Å to 1.88Å with secondary I---F contacts greater than 2.91(1)Å, but no experimental value for an iodine(III)-fluorine covalent contact is known. Other iodine-fluorine contacts that have been reported are of the secondary or bridging type. In $[S_7I][SbF_6]$ [87] the I---F distance is 2.92(2)Å, while in $[I_2][Sb_2F_{11}]$ [17] the shortest secondary contact is 2.89(2)Å. Both of these distances are much longer than that reported here for $[ICl_2][SbF_6]$ and correspond to bond orders of < 0.3 as determined from the correlation of Wiebenga and Kracht.[133] The recent crystal structure of $[I_5][AsF_6]$ [32] however reports a very short I---F interaction (2.73(1)Å) between a terminal iodine of the cation and a fluorine of a neighbouring $[AsF_6]^-$ anion.

Alcock and Countryman [128] recently studied the crystal structures of a series of diphenyliodonium halides in order to examine secondary bonding effects. These compounds provide a useful comparison to the structure of $[ICl_2][SbF_6]$ because their structures are similar to that of I_2Cl_6. It was found that in dimeric $(C_6H_5)_2IX$ (X = Cl, Br, I) the mean bond lengths are I-C, 2.09; I-Cl, 3.09; I-Br, 3.25 and I-I, 3.44Å. The I-X bonds in each case are about 0.77Å longer than in the corresponding

IX gas, indicating bond orders of approximately 0.35. The iodine-fluorine interaction in $[ICl_2][SbF_6]$ (bond order 0.42) is much stronger than the secondary interactions which occur in the above series of compounds and this aspect will be discussed later in terms of their [127]I Mössbauer spectra.

Deviation of the Cl-I-Cl bond angles from 90° are found for all these $[ICl_2]^+$ compounds, the angles being 92.5(1.4), 96.7(1.4) and 97.2(1)° for the $[SbCl_6]^-$, $[AlCl_4]^-$ and $[SbF_6]^-$ compounds respectively, although that for $[ICl_2][SbCl_6]$ is not significantly different from 90°. The Cl-I-Cl angle opens up as the size of the anion decreases. However much more significant differences are found in the angle at the bridging halogen. In $[ICl_2][SbF_6]$ the I-F-Sb angle is 155.3(3)° which is much larger than the I-Cl-Sb and I-Cl-Al angles, 115.8° and 112° in $[ICl_2][SbCl_6]$ and $[ICl_2][AlCl_4]$ respectively. This is possibly because of the smaller size of fluorine compared to chlorine. One other notable difference between the three $[ICl_2]^+$ structures lies in the degree of deviation from planarity of the $[ICl_2X_2]$ rectangular unit. In the cases of the hexachloroantimonate and tetrachloroaluminate molecules the maximum deviation of any atom from the plane of the $[ICl_4]$ moiety is never more than 0.18Å and these are therefore similar to the $[ICl_4]^-$ ion in $K[ICl_4] \cdot H_2O$.[131] A least-squares mean planes analysis of the $[ICl_2F_2]$ fragment in $[ICl_2][SbF_6]$ shows that the two fluorine atoms lie 0.46 and -0.46Å out of the plane defined by the iodine and the two chlorine atoms. These distortions must arise as a result of constraints imposed on the structure by the cis-bridged arrangements at both the cation and anion. Such constraints are apparently not so critical in the $[SbCl_6]^-$ and

$[AlCl_4]^-$ cases, which are also <u>cis</u>-bridged structures, because of the larger size of the bridging halogen in these latter molecules.

It has been suggested [19] that these compounds containing the $[ICl_2]^+$ cation could be represented as resonance hybrids of the type

$$[ICl_2]^+[SbCl_6]^- \leftrightarrow [ICl_4]^-[SbCl_4]^+ \qquad (5.1)$$
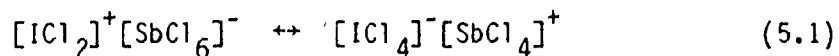
but since the $[SbCl_6]^-$ or $[SbF_6]^-$ anions are barely distorted from regular O_h geometry this does not appear reasonable. It is more reasonable to describe the structure of $[ICl_2][SbF_6]$ as a nearly covalent <u>cis</u>-bridged polymer.

The ^{19}F NMR spectrum of a solution of I_2Cl_6/SbF_5 in SO_2ClF which ultimately produced crystals of $[ICl_2][SbF_6]$ is shown in Figure 5.3. It is clear that in this solution, at low temperature, the $[Sb_2F_{11}]^-$ anion (I) predominates.

I
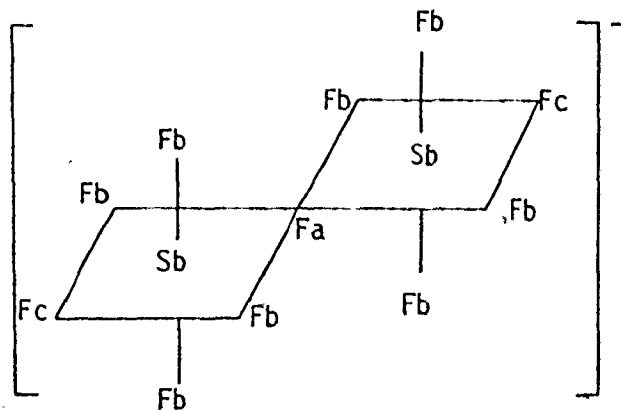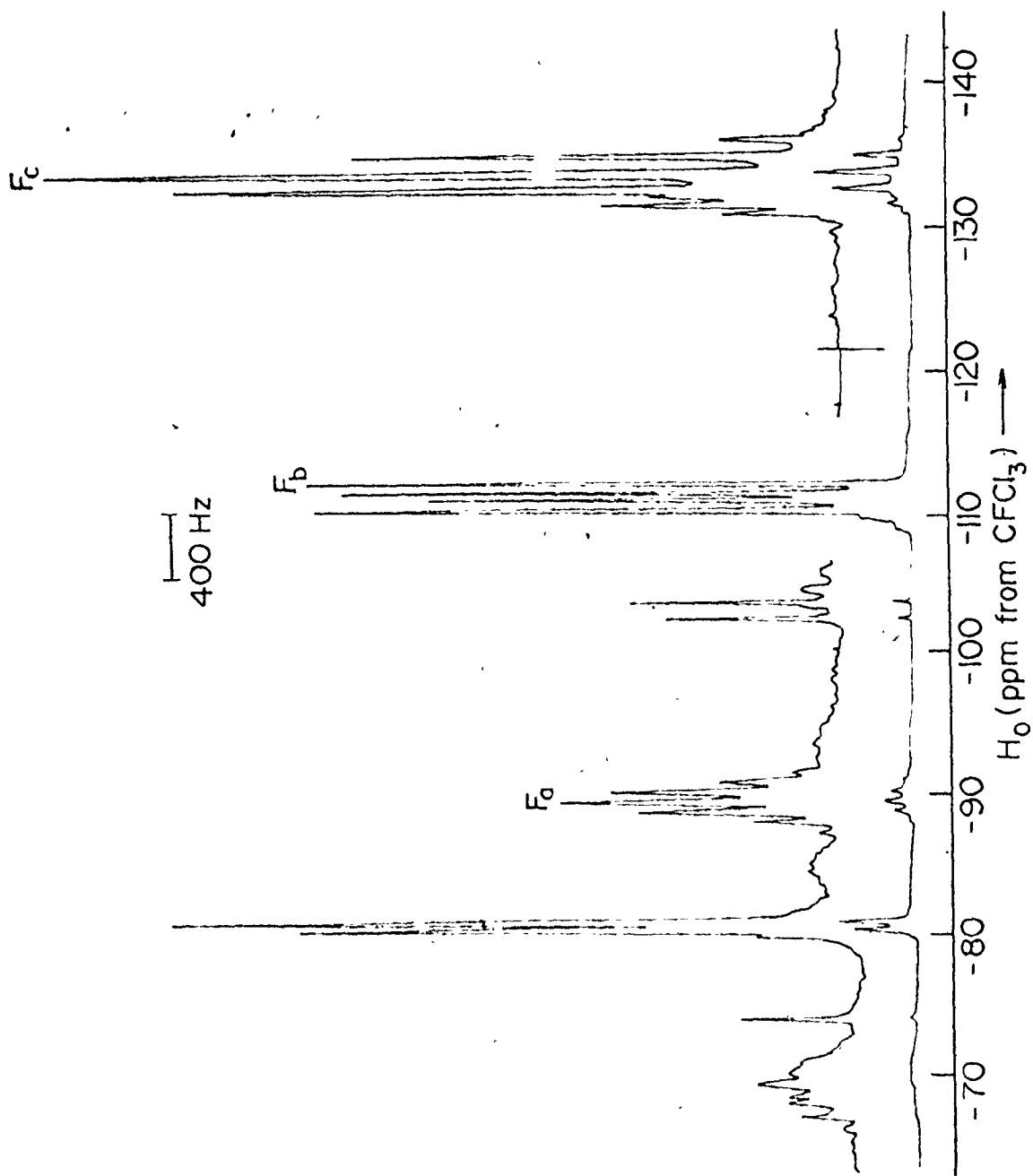
Figure 5.3. ^{19}F NMR spectrum of SO_2ClF solution of I_2Cl_6/SbF_5 recorded at $-120°C$.

The low field multiplet observed at -89.9 ppm (all shifts relative to external $CFCl_3$) is assigned to the bridging fluorine Fa which couples to Fb with J_{Fa-Fb} = 63 Hz. The doublet of doublets at -111.9 ppm is due to the eight equivalent fluorines Fb. Finally a high field quintet at -135.6 ppm is due to the two equivalent fluorines Fc such that J_{Fc-Fb} = 105 Hz. A partially resolved coupling of ca. 10 Hz to the bridging fluorine Fa is also observed. Two additional weak lines in the spectrum at -103.2 and -104.4 ppm are attributed to the presence of a small amount of SbF_5; the same lines are present in the ^{19}F NMR spectrum of SbF_5 in SO_2ClF. Multiplets found at ~ -70 and ~ -81 ppm are thought to be due to the presence of antimony chloride fluorides. Since no single sharp line is observed in the spectrum this indicates that there is no appreciable quantity of $[SbF_6]^-$ present in solution. Thus it appears that while the $[Sb_2F_{11}]^-$ anion is more stable in solution in the presence of excess SbF_5, the $[SbF_6]^-$ anion is able to stabilize the $[ICl_2]^+$ cation in the solid state. That Aubke and co-workers [27] were able to obtain a red solid analyzing as $[ICl_2][Sb_2F_{11}]$ by pumping under vacuum on a mixture of I_2Cl_6 and excess SbF_5 remains something of a mystery. Presumably the SbF_5 initially removes a chlorine from the I_2Cl_6 to produce an antimony chloride fluoride which undergoes exchange with SbF_5 to give a $[Sb_2F_{11}]^-$ salt according to equation (5.2).

$$I_2Cl_6 + 6SbF_5 \rightarrow 2[ICl_2][Sb_2F_{11}] + 2SbF_4Cl \qquad (5.2)$$
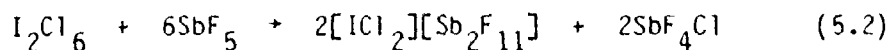
The molecule SbF_4Cl has never been isolated but presumably rearranges to produce other antimony(V) chloride fluorides all of which are quite volatile.[136-138] The lines at ~ -70 to -80 ppm in the ^{19}F NMR spectrum are thought to be due to these species. In the SO_2ClF solution an equilibrium between $[Sb_2F_{11}]^-$, $[SbF_6]^-$ and SbF_5 (5.3), probably exists with the equilibrium lying largely to the left-hand side.

$$[ICl_2][Sb_2F_{11}] \;\rightleftharpoons\; [ICl_2][SbF_6] \;+\; SbF_5 \qquad (5.3)$$
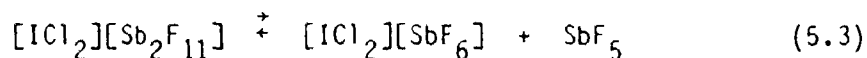
b) **Structure of $[IBr_2][Sb_2F_{11}]$**

The final atomic positional coordinates and the thermal parameters for $[IBr_2][Sb_2F_{11}]$ are given in Table 5.5 and 5.6 respectively. The bond lengths and bond angles of the molecule are given in Table 5.7. The atomic arrangement in the molecule is illustrated in Figure 5.4 and a stereoscopic view of the packing in the unit cell, along the c axis is shown in Figure 5.5.

The X-ray crystal structure of $[IBr_2][Sb_2F_{11}]$ consists of infinite chains of $[IBr_2]^+$ cations each of which has the square-planar geometry around iodine completed by bridging interactions to fluorine atoms of two separate $[Sb_2F_{11}]^-$ anions. These $[Sb_2F_{11}]^-$ anions have terminal Sb-F bonds averaging 1.84Å, while the cation bridging Sb-F distances are 1.868(12) and 1.862(12)Å respectively. The bridging Sb-F distances in the anion are 2.030(13) and 2.003(12)Å, and the Sb-F-Sb bond angle is 157.3(6)°. The geometry of the $[Sb_2F_{11}]^-$ anion in $[IBr_2][Sb_2F_{11}]$ is very similar to that which is found in $[I_2][Sb_2F_{11}]$.[17]

Table 5.5.

Atomic Coordinates ($\times 10^4$) for $[IBr_2][Sb_2F_{11}]$

	x/a	y/b	z/c
I(1)	3611(1)	7370(1)	955(1)
Br(1)	2680(2)	8213(2)	-329(2)
Br(2)	4526(2)	6375(2)	-203(2)
Sb(1)	-522(1)	10853(1)	3284(1)
Sb(2)	1640(1)	9162(1)	2883(1)
F(1)	-1195(8)	9880(9)	3875(10)
F(2)	-104(9)	11231(9)	4582(9)
F(3)	553(8)	9925(9)	3382(9)
F(4)	347(8)	11681(8)	2694(10)
F(5)	-1488(9)	11711(9)	3243(11)
F(6)	-734(11)	10362(12)	1960(9)
F(7)	2646(8)	8441(8)	2432(10)
F(8)	1093(9)	9125(13)	1592(10)
F(9)	2153(11)	10319(10)	2558(15)
F(10)	945(11)	8133(10)	3306(12)
F(11)	2101(10)	9250(12)	4218(10)

Table 5.6.

Thermal Parameters for $[IBr_2][Sb_2F_{11}]$ [a]

	U_{11}	U_{22}	U_{33}	U_{12}	U_{13}	U_{23}
I(1)	638(9)	537(9)	452(8)	94(8)	75(7)	5(7)
Br(1)	865(19)	687(17)	609(15)	95(15)	-140(14)	-1(14)
Br(2)	1195(24)	861(19)	646(16)	416(19)	185(18)	-86(15)
Sb(1)	481(9)	455(9)	465(8)	8(8)	34(7)	27(8)
Sb(2)	505(9)	473(9)	491(8)	32(8)	58(7)	84(7)
F(1)	624(79)	623(81)	816(84)	-42(74)	244(66)	203(71)
F(2)	862(94)	946(99)	536(78)	-191(85)	-122(76)	-199(74)
F(3)	683(85)	741(89)	3(76)	342(79)	137(72)	50(74)
F(4)	594(78)	699(86)	893(97)	-9(72)	153(74)	222(77)
F(5)	676(89)	644(87)	1149(111)	177(78)	-8(82)	362(80)
F(6)	1125(120)	1324(136)	490(74)	-261(108)	11(81)	-182(83)
F(7)	715(85)	653(85)	742(80)	105(72)	179(74)	-127(72)
F(8)	716(101)	1660(168)	662(83)	272(110)	-162(76)	-85(99)
F(9)	1080(120)	608(91)	1825(161)	-14(83)	763(124)	131(112)
F(10)	1348(147)	611(95)	1277(128)	-128(95)	589(111)	-255(92)
F(11)	963(107)	1334(131)	636(84)	303(113)	-171(80)	-440(93)

[a] Temperature factors ($\times 10^4$) in the form $\exp(-2\pi^2 \Sigma\Sigma_{ij} U_{ij} H_i H_j a_i^* a_j^*)$

Table 5.7.

Bond Lengths (Å) and Bond Angles (°) for $[IBr_2][Sb_2F_{11}]$

Estimated Standard Deviations in Parentheses

(a) Bond lengths (Å)

I(1) - Br(1)	2.424(3)		Sb(1) - F(5)	1.844(13)
I(1) - Br(2)	2.422(3)		Sb(1) - F(6)	1.846(13)
I(1) - F(4)	2.845(12)		Sb(2) - F(3)	2.003(12)
I(1) - F(7)	2.782(12)		Sb(2) - F(7)	1.862(12)
Sb(1) - F(1)	1.838(12)		Sb(2) - F(8)	1.823(13)
Sb(1) - F(2)	1.837(12)		Sb(2) - F(9)	1.832(14)
Sb(1) - F(3)	2.030(13)		Sb(2) - F(10)	1.840(15)
Sb(1) - F(4)	1.868(12)		Sb(2) - F(11)	1.829(13)

(b) Bond angles (°)

Br(1) - I(1) - Br(2)	100.0(1)	F(4) - Sb(1) - F(5)	92.2(5)
Br(1) - I(1) - F(7)	85.1(3)	F(4) - Sb(1) - F(6)	88.7(6)
Br(1) - I(1) - F(4)	169.5(3)	F(5) - Sb(1) - F(6)	95.3(7)
Br(1) - I(1) - F(5)	80.4(2)	F(3) - Sb(2) - F(7)	179.3(5)
Br(2) - I(1) - F(7)	174.9(3)	F(3) - Sb(2) - F(8)	87.8(6)
Br(2) - I(1) - F(4)	89.3(3)	F(3) - Sb(2) - F(9)	85.1(6)
F(7) - I(1) - F(4)	85.6(3)	F(3) - Sb(2) - F(10)	84.2(6)
F(1) - Sb(1) - F(2)	91.2(6)	F(3) - Sb(2) - F(11)	87.4(6)
I(1) - F(4) - Sb(1)	151.6(6)	F(7) - Sb(2) - F(8)	92.6(6)
I(1) - F(7) - Sb(2)	153.3(6)	F(7) - Sb(2) - F(9)	95.5(6)
F(1) - Sb(1) - F(3)	84.4(5)	F(7) - Sb(2) - F(10)	95.1(6)
F(1) - Sb(1) - F(4)	169.3(5)	F(7) - Sb(2) - F(11)	92.2(6)
F(1) - Sb(1) - F(5)	95.5(6)	F(8) - Sb(2) - F(9)	89.8(8)
F(1) - Sb(1) - F(6)	90.5(6)	F(8) - Sb(2) - F(10)	90.3(7)
F(2) - Sb(1) - F(3)	83.1(5)	F(8) - Sb(2) - F(11)	175.2(7)
F(2) - Sb(1) - F(4)	87.8(6)	F(9) - Sb(2) - F(10)	169.3(7)
F(2) - Sb(1) - F(5)	94.9(6)	F(9) - Sb(2) - F(11)	90.2(8)
F(2) - Sb(1) - F(6)	169.5(6)	F(10)- Sb(2) - F(11)	88.8(7)
F(3) - Sb(1) - F(4)	84.9(5)	Sb(1) - F(3) - Sb(2)	157.3(6)
F(3) - Sb(1) - F(5)	177.9(5)		
F(3) - Sb(1) - F(6)	36.8(6)		
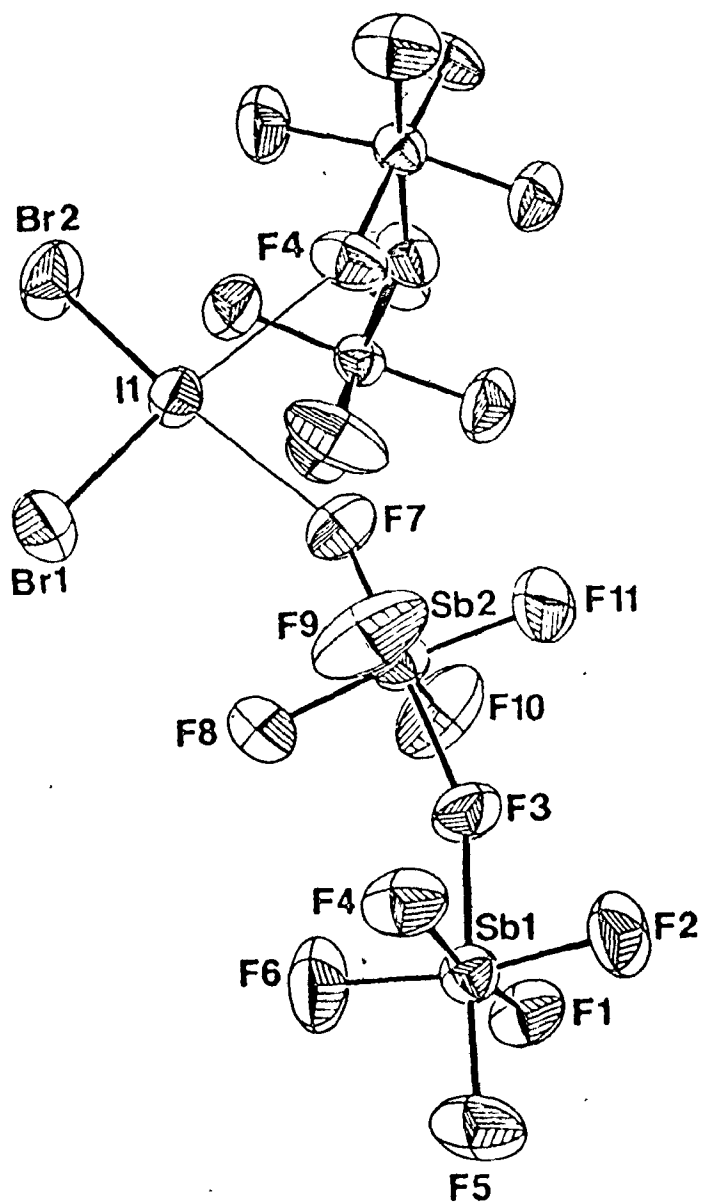
Figure 5.4.   Structure of [IBr$_2$][Sb$_2$F$_{11}$] showing the coordination sphere around iodine, including [Sb$_2$F$_{11}$]$^-$ anions.
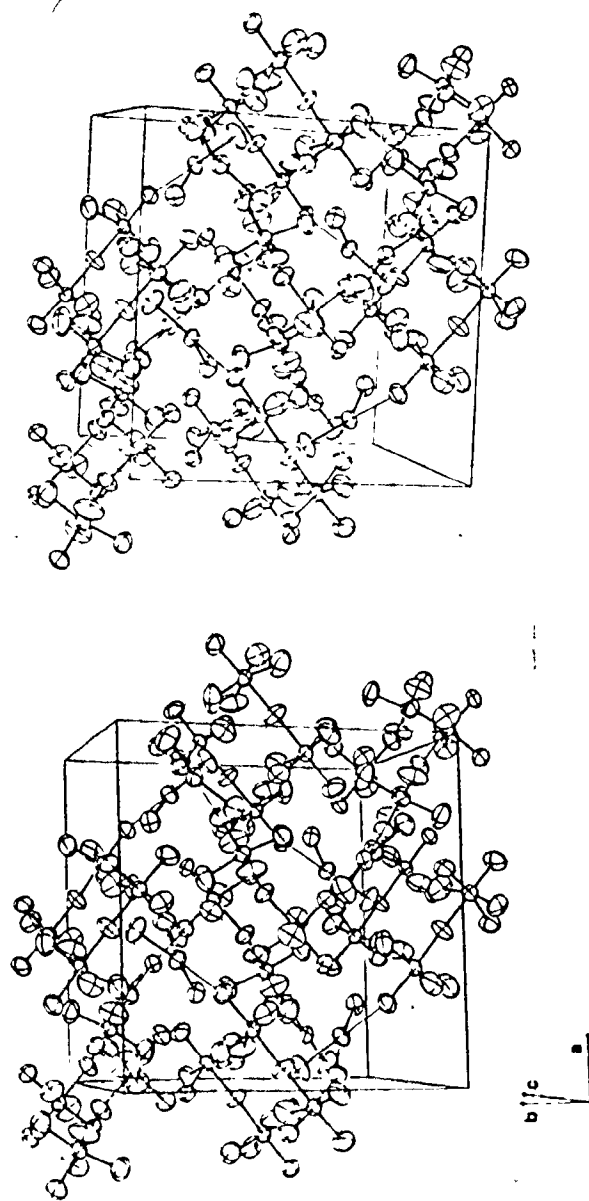
Figure 5.5.   Stereoscopic view of the packing in the unit cell of $[IBr_2][Sb_2F_{11}]$, along the c axis.

The environment about the iodine atom, like the previous $[IX_2]^+$ cations discussed, is essentially square planar with two terminal I-Br bonds and two bridging I---F interactions. This is the first X-ray crystal structure reported for a compound containing the $[IBr_2]^+$ cation and the I-Br bond distances are 2.424(3) and 2.422(3)Å. These distances compare to the I-Br distance in gaseous IBr (as determined by vibrational spectroscopy) which is 2.470(5)Å [139] and the sum of the covalent radii of bromine and iodine which is 2.48Å.[133] The bridging I---Br interactions in diphenyliodonium bromide [128] are substantially longer and average 3.250Å. The I---F secondary interactions in $[IBr_2][Sb_2F_{11}]$ are 2.845(12) and 2.782(12)Å, both of which are significantly longer than the same interaction in $[ICl_2][SbF_6]$ (2.650(6)Å, present work) but similar to other I---F secondary interactions which have been reported.[17,87,135] Using the relationship of Wiebenga and Kracht,[133] these bridging I---F interactions in $[IBr_2][Sb_2F_{11}]$ have bond orders of ca. 0.35.

As is the case of the compounds which contain the $[ICl_2]^+$ cation,[19] there is significant deviation of the X-I-X bond angle from 90° in $[IBr_2][Sb_2F_{11}]$. In the former compounds the Cl-I-Cl angle was found to open up as the size of the anion decreased. However in the case of $[IBr_2][Sb_2F_{11}]$ the larger size of bromine compared to chlorine seems to be the most important factor, and coupled with the longer secondary contacts, the Br-I-Br bond angle has opened up to 100.0(1)°. The I-F-Sb bridging bond angles in $[IBr_2][Sb_2F_{11}]$ are 153.3(6) and 151.6(6)°. $[IBr_2][Sb_2F_{11}]$ is very similar to both $[ICl_2][SbCl_6]$ and $[ICl_2][AlCl_4]$ in terms of the degree of deviation from planarity of the $[IX_2Y_2]$

rectangular unit. A least-squares mean plane analysis of the $[IBr_2F_2]$ fragment in $[IBr_2][Sb_2F_{11}]$ shows that one fluorine atom lies +0.23Å out of the plane defined by the iodine and two chlorine atoms, while the other fluorine atom remains in the $[ICl_2]$ plane. The angle between the two planes defined by Br(1)-I(1)-Br(2) and F(4)-I(1)-F(7) is 4.7°. The analogous two planes in $[ICl_2][SbF_6]$ have an angle between them of 13.9°. Thus in $[ICl_2][SbF_6]$ where the secondary interactions between cation and anion are strong, the $[IX_2Y_2]$ rectangular unit is distorted from planarity more severely than in $[ICl_2][SbCl_6]$,[19] $[ICl_2][AlCl_4]$ [19] and $[IBr_2][Sb_2F_{11}]$ where the longer, weaker, secondary interactions allow the $[IX_2Y_2]$ moiety to be less distorted.

As was previously mentioned $[IBr_2][Sb_2F_{11}]$ was prepared by reacting SbF_5 with IBr in a 2.5:1 ratio, a reaction initially designed to prepare the $[IBr]^+$ cation, according to (5.4). Several subsequent attempts to prepare the $[IBr]^+$ cation were also unsuccessful, suggesting

$$2IBr + 5SbF_5 \xrightarrow{\quad\times\quad} 2[IBr][Sb_2F_{11}] + SbF_3 \qquad (5.4)$$
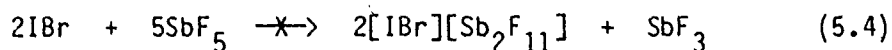
that it is not possible to prepare this species, at least by this method. Since the $[I_2]^+$ [17] and $[Br_2]^+$ [140] cations have been identified by X-ray crystallography it seemed reasonable that $[IBr]^+$ should also exist. This particular aspect will be discussed at greater length in the following Chapter. If there had been excess Br_2 present in the reaction mixture which produced $[IBr_2]^+$ the following equation (5.5) could account for the observed products. However the reaction was carefully repeated with the

$$2IBr + Br_2 + 5SbF_5 \rightarrow 2[IBr_2][Sb_2F_{11}] + SbF_3 \qquad (5.5)$$
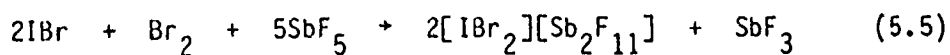
IBr first being prepared in situ and the same result was obtained. Thus the $[IBr_2]^+$ cation is the product of a complex reaction.

The visible absorption spectrum of a very dilute solution of $[IBr_2][Sb_2F_{11}]$ in SO_2 was recorded and found to have a band maximum at 360 nm, with a very weak shoulder at ca. 470 nm. These values agree quite well with the absorption bands reported for $[IBr_2]^+$ in other solvents.[26,141]

c) Structure of $[IBr_{0.7}Cl_{1.25}][SbCl_6]$

The X-ray structure analysis of this material revealed chlorine/bromine disorder in the cation, which has the approximate stoichiometry $[IBr_{0.75}Cl_{1.25}]^+$. In the early stages of the structure determination the atoms which were later designated as XA and XB were refined as bromines. However the isotropic temperature factors for these two atoms were 0.080(14) and 0.092(18), both of which are much too high for bromine, thereby indicating that there is less electron density at these positions than had been assigned. At the same stage of refinement the isotropic thermal parameter for the iodine atom was 0.0288(4). Varying the temperature factors of all the atoms in the structure anisotropically, resulted in R_1 refining to 0.075. The population parameters of the two atoms initially assigned as bromines were then varied and these refined to 0.70 and 0.60 for the disordered atoms XA and XB respectively, and gave an improved $R_1 = 0.049$. A similar result was obtained when the two atoms were initially assigned as chlorines; the

population parameters refining to 1.54 and 1.38 for the disordered atoms

XA and XB, respectively. Thus if atom XA is assigned as a bromine the

population parameter refines to 0.70, corresponding to a 24 electron

scatterer; while if it is assigned as chlorine the population parameter

refines to 1.54, corresponding to a 26 electron scatterer. Atom XA then

behaves, on average as a 25 electron scatterer, consistent with a

composition comprised of about 0.45 Br and 0.55 Cl. Assignment of the

disordered atom XB as bromine results in a population parameter of 0.60

(ca. 21 electrons) while refinement as chlorine results in a population

parameter of 1.38 (ca. 23 electrons). Thus an average 22 electron

scatterer would be comprised of about 0.30 Br and 0.70 Cl. These values

result in a cation with an overall stoichiometry which is approximately

$[IBr_{0.75}Cl_{1.25}]^+$. In the subsequent stages of the refinement the

scattering factor curves for atoms XA and XB were calculated using the

curves for chlorine and bromine [142] and the above ratios for each atom.

The scattering factor curve for XA as a function of $sin\theta/\lambda$ was

constructed by taking 0.45 $sfac_{Br}$ + 0.55 $sfac_{Cl}$ for each of the given

values for $sin\theta/\lambda$. The resultant scattering factor curve for atom XA as

well as, the curves for Cl and Br are shown in Figure 5.6. An alternative

method for calculating the scattering factor curve for atom XA would be

to take the value the population parameter refined to when XA was

initially assigned as Cl and scale the scattering factor curve for Cl by

this number. The same calculation could be done by assuming it to be Br.

But, as Figure 5.6 illustrates, the first method of calculating a

composite curve using both the Cl and Br scattering curves gives better
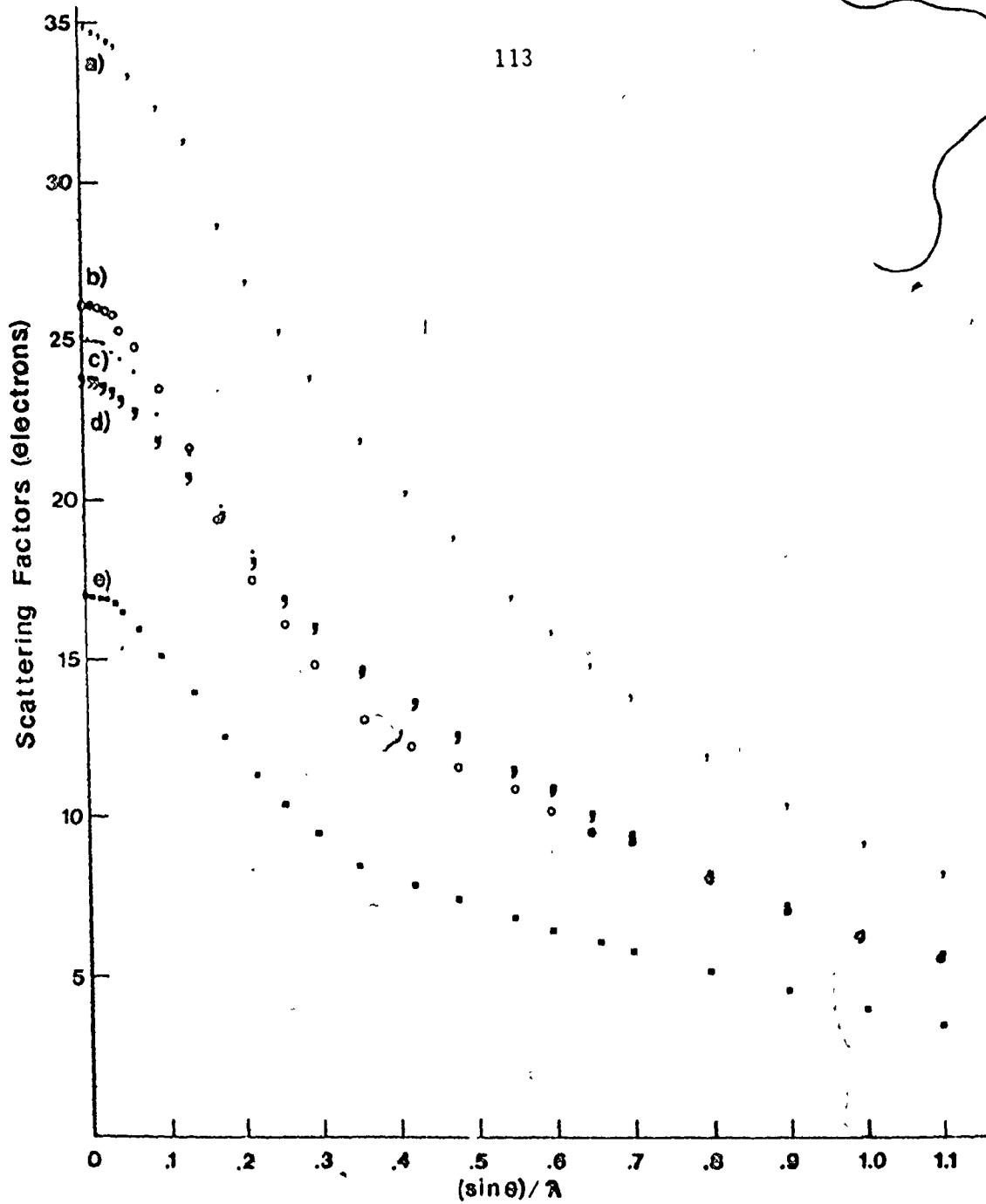
Figure 5.6.   Calculated scattering factor curve as a function of sinθ/λ
              for disordered atom XA; a) scattering curve for Br (sfac$_{Br}$),
              b) 0.70 (sfac$_{Br}$), c) 0.45 (sfac$_{Br}$) + 0.55 (sfac$_{Cl}$),
              d) 1.54 (sfac$_{Cl}$), e) sfac$_{Cl}$.

average values for the scattering factors of atom XA as a function of sinθ/λ, particularly at small sinθ/λ. A similar scattering curve for XB was constructed by this method. In the final stages of the least-squares refinement the population parameters of XA and XB were varied and both refined to one, and the thermal parameters for these disordered atoms were reasonable, indicating that the calculated scattering factor curves for the disordered atoms XA and XB are good models of their scattering power.

A structure solution was also attempted in the acentric space group P1 to test whether the observed disorder in space group P$\bar{1}$ was due to a crystallographically imposed center of symmetry. Refinement in space group P1 did not remove the disorder problem and the overall agreement was not improved despite the fact that the number of refined parameters was nearly doubled.

The chemical significance of the disordered cation $[IBr_{0.75}Cl_{1.25}]^+$ will be discussed later in terms of its Raman and Mössbauer spectra. Since the population parameters for the disordered atoms XA and XB refined to different values, thereby indicating different amounts of chlorine and bromine at these two crystallographic positions, there could be some $[IBrCl]^+$ cations present in the crystal structure. It is difficult to say how reliable the individual population parameters are for these disordered atoms and although the observed disorder is likely $[ICl_2]^+/[IBr_2]^+$ disorder it is also possible that the $[BrICl]^+$ cation is present.

The final atomic position coordinates and the thermal parameters for $[IBr_{0.75}Cl_{1.25}][SbCl_6]$ are given in Tables 5.8 and 5.9 respectively. The bond lengths and bond angles of the molecule are found in Table 5.10. The atomic arrangement in the molecule is illustrated in Figure 5.7 and a stereoscopic view of the packing in the unit cell along the b axis is shown in Figure 5.8.

The crystal structure of $[IBr_{0.75}Cl_{1.25}][SbCl_6]$ is similar to the structures of those compounds already discussed, and consists of infinite chains of two crystallographically unique alternating $[SbCl_6]^-$ anions trans-bridged through chlorine to he disordered cations. The two crystallographically discreet $[SbCl_6]^-$ anions are similar to each other and not unusual in their geometries. Each $[SbCl_6]^-$ anion possesses crystallographic symmetry in the form of an inversion centre since Sb(1) is found at the special position (0,0,0) and Sb(2) is located at the special position (0,1/2,1/2). As a result of the trans-bridged chlorine interaction to the cations, the anions are distorted from regular O_h symmetry to D_{4h} symmetry. In the Sb(1) octahedron the average Sb-Cl terminal bond distance is 2.338Å while in the Sb(2) octahedron the terminal Sb-Cl distances average 2.344Å. The Sb-Cl bridging bond lengths are elongated in these two octahedra to 2.416(3) and 2.422(3)Å respectively. The Cl-Sb-Cl bond angles in both $[SbCl_6]^-$ anions remain close to the values expected for a regular octahedron.

The disordered cation has the same square-planar geometry which is found in other iodine(III) interhalogen cations and the relevant parameters are summarized in Table 5.11. The I(1)-XA and I(1)-XB bond

Table 5.8.

Atomic Coordinates ($\times 10^4$) for $[IBr_{0.75}Cl_{1.25}][SbCl_6]$

	x/a	y/b	z/c
I(1)	3088(1)	5347(1)	3485(1)
Sb(1)	0	0	0
Sb(2)	0	5000	5000
XA	4913(3)	8618(3)	3223(2)
XB	5441(3)	3886(4)	1627(2)
Cl(1)	1391(5)	2008(5)	4379(2)
Cl(2)	3077(4)	6714(5)	5539(2)
Cl(3)	-208(4)	6530(5)	3398(2)
Cl(4)	6984(4)	1452(5)	9689(2)
Cl(5)	8572(5)	6971(4)	515(2)
Cl(6)	478(5)	1502(5)	1734(2)

Table 5.9.

Thermal Parameters for $[IBr_{0.75}Cl_{1.25}][SbCl_6]$ [a]

	U_{11}	U_{22}	U_{33}	U_{12}	U_{13}	U_{23}
I(1)	364(4)	367(4)	243(3)	28(2)	53(2)	32(2)
Sb(1)	325(5)	216(4)	203(4)	-14(3)	61(3)	9(3)
Sb(2)	302(5)	250(4)	202(4)	18(3)	52(3)	-2(3)
XA	514(13)	454(12)	542(13)	21(8)	43(9)	18(8)
XB	456(14)	668(17)	505(14)	-10(10)	174(10)	-44(11)
Cl(1)	662(20)	341(14)	366(14)	164(13)	198(13)	10(11)
Cl(2)	382(15)	505(17)	461(17)	-90(13)	-21(13)	64(13)
Cl(3)	424(15)	430(15)	256(12)	91(11)	82(10)	106(10)
Cl(4)	383(15)	416(15)	491(16)	86(11)	126(12)	92(12)
Cl(5)	507(17)	310(13)	491(16)	-56(11)	132(13)	129(12)
Cl(6)	582(18)	512(17)	263(13)	-120(14)	131(12)	-110(11)

[a] Temperature factors ($\times 10^4$) in the form $\exp(-2\pi^2 \sum_i \sum_j U_{ij} H_i H_j a_i^* a_j^*)$

Table 5.10.

Bond Lengths (Å) and Bond Angles (°) for $[IBr_{0.75}Cl_{1.25}][SbCl_6]$ [a]

Estimated Standard Deviations in Parentheses

(a) Bond lengths (Å)

I(1) - XA	2.427(2)		Sb(1) - Cl(5)	2.332(3)
I(1) - XB	2.373(3)		Sb(1) - Cl(6)	2.416(3)
I(1) - Cl(3)	2.927(3)		Sb(2) - Cl(1)	2.333(3)
I(1) - Cl(6)	2.976(3)		Sb(2) - Cl(2)	2.354(3)
Sb(1) - Cl(4)	2.343(3)		Sb(2) - Cl(3)	2.422(3)

(b) Bond angles (°)

XA - I(1) - XB	97.67(9)	Cl(4) - Sb(1) - Cl(4")	180.00(10)
Cl(6) - I(1) - Cl(3)	81.11(9)	Cl(5) - Sb(1) - Cl(5')	180.00(10)
XA - I(1) - Cl(6)	172.71(9)	Cl(1) - Sb(2) - Cl(2)	89.84(11)
XA - I(1) - Cl(3)	91.66(8)	Cl(1) - Sb(2) - Cl(3)	90.98(10)
XB - I(1) - Cl(6)	89.57(9)	Cl(1) - Sb(2) - Cl(1)	180.00(10)
XB - I(1) - Cl(3)	170.67(8)	Cl(1) - Sb(2) - Cl(2^{IV})	90.16(11)
Cl(4) - Sb(1) - Cl(6)	89.82(11)	Cl(1) - Sb(2) - Cl(3^{IV})	89.02(10)
Cl(5) - Sb(1) - Cl(6)	87.61(11)	Cl(2) - Sb(2) - Cl(3)	89.51(10)
Cl(5')- Sb(1) - Cl(6)	92.40(11)	Cl(2) - Sb(2) - Cl(2^{IV})	180.00(11)
Cl(6) - Sb(1) - Cl(4")	90.18(11)	Cl(2) - Sb(2) - Cl(3^{IV})	90.49(10)
Cl(6) - Sb(1) - Cl(6'")	180.00(11)	Cl(3) - Sb(2) - Cl(3)	180.00(9)
Cl(5) - Sb(1) - Cl(4)	89.39(11)	Sb(2) - Cl(3) - I(1)	109.29(10)
Cl(4) - Sb(1) - Cl(5')	90.62(11)	Sb(1) - Cl(6) - I(1)	122.11(13)

[a] Symmetry transformations are: (') 1-x,1-y,-z; (") 1-x,-y,1-z;

(''') -x,-y,-z;   (IV) -x,1-y,1-z.
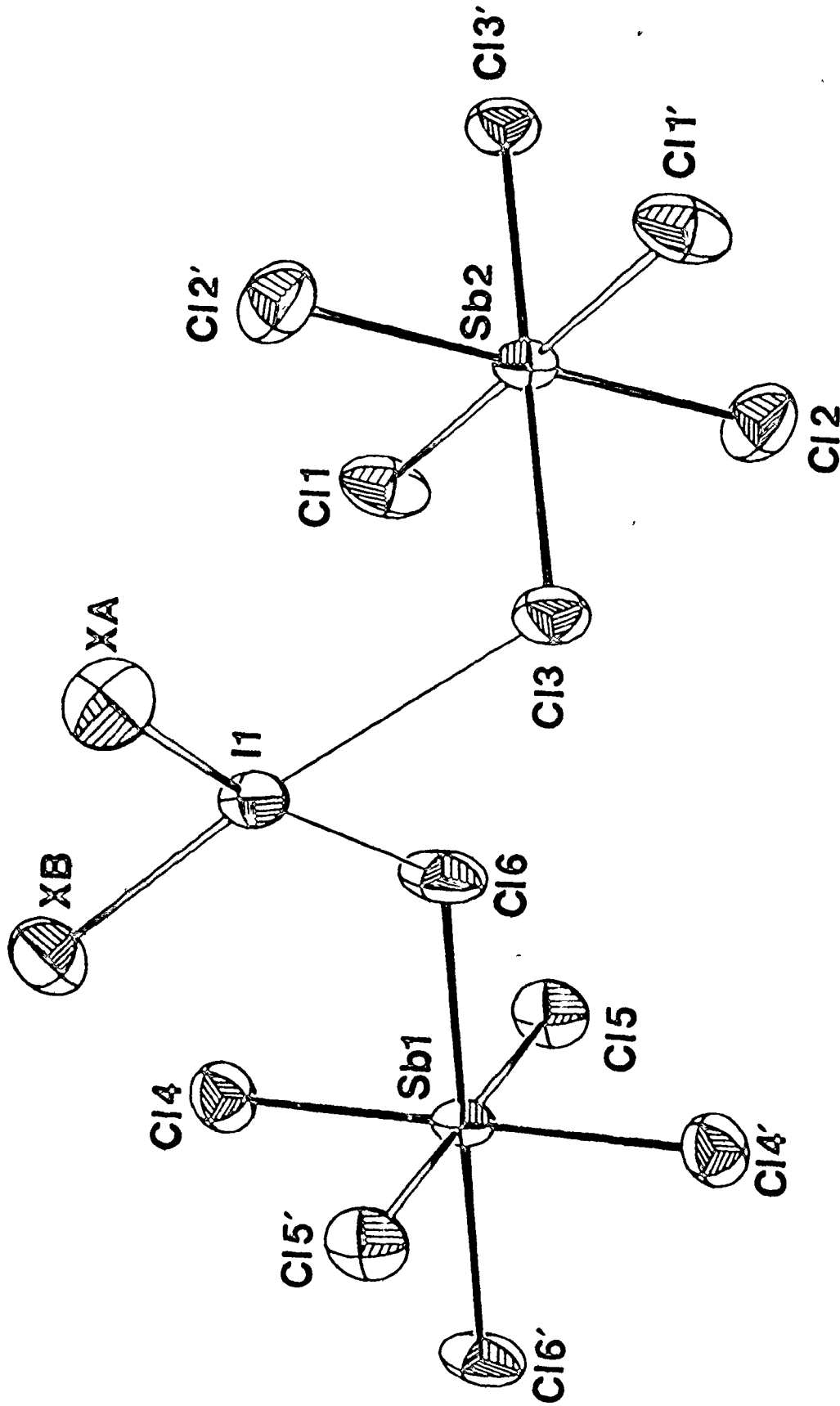
Figure 5.7.   Atomic arrangement of $[IBr_{0.75}Cl_{1.25}][SbCl_6]$.
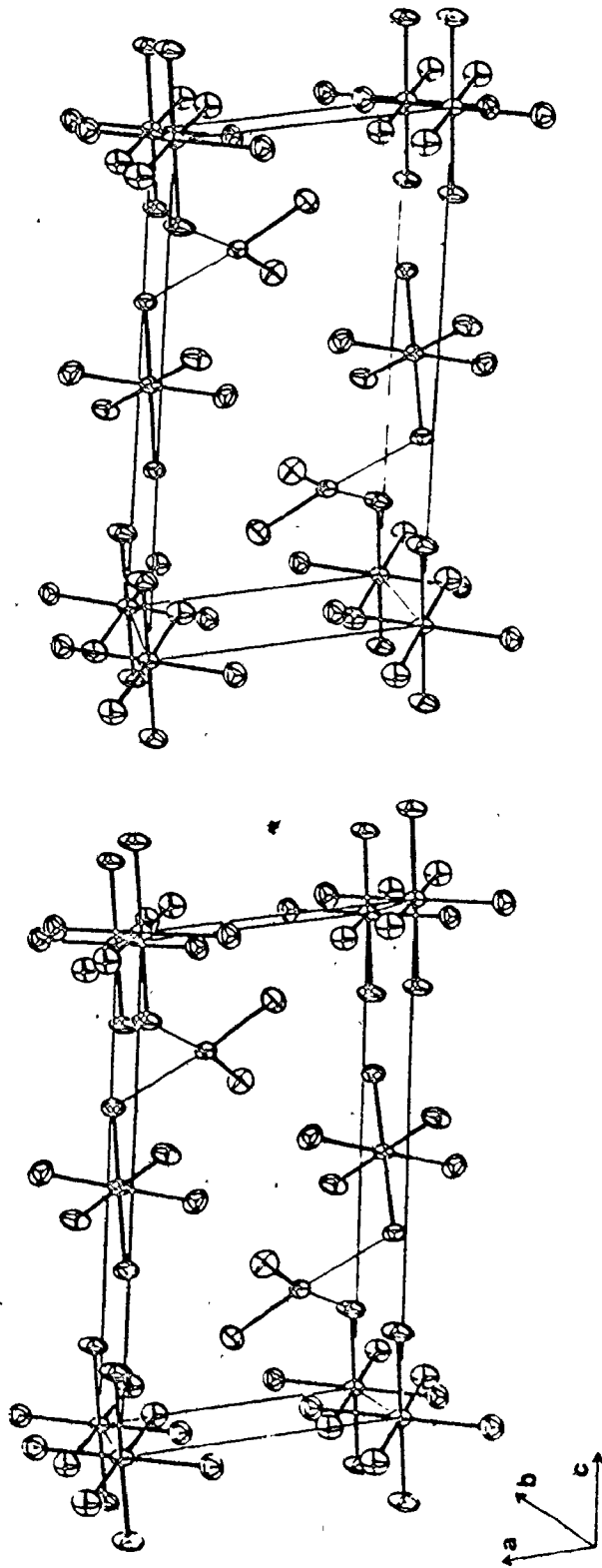
Figure 5.8.   Stereoscopic drawing of the unit cell of $[IBr_{0.75}Cl_{1.25}][SbCl_6]$ viewed along the b axis.

Table 5.11.

Geometry Around Iodine in $[IX_2][SbY_6]$ and Related Compounds
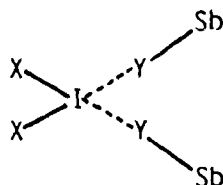
	I-X (Å)	I---Y (Å)	X-I-X (°)	Y---I---Y (°)	I-Y-Sb (°)	$[IX_2Y_2]$[a]
$[ICl_2][SbF_6]$	2.268(2)	2.650(6)	97.2(1)	91.2(2)	155.3(3)	13.9
$[ICl_2][SbCl_6]$ [19]	2.33(4)	2.85(4)	92.5(14)	85.0(14)	116.8	7.9 [b]
	2.29(4)	3.00(4)			114.8	
$[ICl_2][AlCl_4]$ [19]	2.29(4)	2.86(4)	96.7(14)	85.3(14)	116	4.1 [b]
	2.26(4)	2.88(4)			108	
I_2Cl_6 [130]	2.38(3)	2.72(3)	94(1)	86(1)		0
	2.39(3)	2.68(3)				
$[IBr_2][Sb_2F_{11}]$	2.424(3)	2.845(12)	100.0(1)	85.6(3)	151.6(6)	4.7
	2.422(3)	2.782(12)			153.3(6)	
$[IBr_{0.75}Cl_{1.25}][SbCl_6]$	2.427(2)	2.927(3)	97.67(9)	81.11(9)	109.3(1)	0.9
	2.373(3)	2.976(3)			122.1(1)	
$[I_3][AsF_6]$	2.660(2)	3.01(1)	101.75(6)	101.58 [c]	124.42 [c]	11.1 [c]
	2.669(2)	3.07(1)			118.94 [c]	

[a] $[IX_2Y_2]$ represents the angle in degrees between the two planes defined by IX_2 and IY_2.

[b] Calculated here from atomic positions in reference 19.

[c] Calculated here from atomic positions in reference 32.

lengths are 2.427(2) and 2.373(3)Å, respectively. These bond distances may be compared to the I-Cl terminal bond distances found in the $[SbCl_6]^-$,[19] $[AlCl_4]^-$ [19] and $[SbF_6]^-$ (section (a)) analogues of $[ICl_2]^+$ and the I-Br terminal bond distances found in $[IBr_2][Sb_2F_{11}]$ (section (b)). The I-Cl bond distances in the $[ICl_2]^+$ cations average 2.29Å while the I-Br bond distances in $[IBr_2][Sb_2F_{11}]$ average 2.423Å. The I(1)-XA(XB) bond lengths are consistent with the previous discussion whereby the disordered atom XA was found to have a higher percentage of bromine than disordered atom XB. The I(1)-XA distance is the same as the I-Br distance in $[IBr_2]^+$ whereas the I(1)-XB bond distance is roughly midway between the I-Cl and I-Br average terminal bond lengths found above. These distances are consistent with a formulation for the cation which would include some $[BrICl]^+$. It must be kept in mind that the final bond distance between the I(1) atom and one of the disordered atoms, say XA is the average distance between all pairs of these two atoms found at these particular positions in the crystal structure.

The bridging contacts from the cation to the anion are through chlorine rather than through fluorine as in the previous two structures; these distances are I(1)---Cl(3), 2.927(3)Å and I(1)---Cl(6) 2.976(3)Å. The corresponding secondary interactions in $[ICl_2][SbCl_6]$ [19] and $[ICl_2][AlCl_4]$ [19] average 2.90Å while in I_2Cl_6,[130] a more covalent type of compound, the bridging bond is much shorter at 2.70Å. From the relationship of Wiebenga and Kracht,[133] these bridging I---Cl interactions have a bond order of ca. 0.45, similar to that which is found for the bridging I---F interaction in $[ICl_2][SbF_6]$ (this Chapter, section (a)).

The XA-I(1)-XB bond angle in the disordered cation is 97.67(9)°, a value which is similar to that found in the other cations so far discussed. Whereas the I-X-Sb bridging bond angles in $[ICl_2][SbF_6]$ and $[IBr_2][Sb_2F_{11}]$ (section (a) and (b)) are large, 155.3(3)° and 151.6(6)° respectively, the angles at the bridging halogens in $[IBr_{0.75}Cl_{1.25}][SbCl_6]$ are 109.29(10)°, (I(1)-Cl(3)-Sb(2)) and 122.11(13)°, (I(1)-Cl(6)-Sb(1)), similar to the analogous angles found in $[ICl_2][SbCl_6]$ [19] and $[ICl_2][AlCl_4]$.[19] The trend observed here seems to be that for a small bridging atom like fluorine, the angle at the bridging atom needs to be quite large, whereas for a larger bridging atom such as chlorine this constraint is not as critical and the angle can be smaller.

A least-squares mean planes analysis of the $[IXAXBCl_2]$ fragment of $[IBr_{0.75}Cl_{1.25}][SbCl_6]$ has shown that Cl(3) and Cl(6) lie -0.02 and +0.04Å respectively out of the plane defined by XA-I(1)-XB and that the angle between the planes XA-I(1)-XB and Cl(3)-I(1)-Cl(6) is 0.9°. This cation is the most planar of the cations which have been discussed so far. The long secondary interactions from cation to anion coupled with the large bridging halogen (chlorine) allow the cation to adopt a nearly perfectly planar arrangement.

d) Summary of Crystal Structures

The discussion in this Chapter has dealt with the X-ray crystal structures of three new compounds $[ICl_2][SbF_6]$, $[IBr_2][Sb_2F_{11}]$ and $[IBr_{0.75}Cl_{1.25}][SbCl_6]$. The main structural features of interest in these compounds have been concerned with the geometry around the iodine

atom in the cations, i.e. the strength of the primary and secondary bonds to iodine, and the various angles in the cation, particularly at the bridging halogen atom. Table 5.11 summarizes these data for the above compounds as well as for some related compounds which have also been discussed.

(ii) Mössbauer Spectroscopy

The iodine-127 Mössbauer data for the iodine(III) interhalogen cations, whose structures have been determined, and several related compounds are presented in Table 5.12; the ^{129}I literature data have been converted to their ^{127}I equivalents by multiplying the ^{129}I isomer shifts by -0.345.[113] The spectra were fitted as previously described (Chapter 2) and the absorber line widths which were allowed to vary in the transmission integral fitting are greater than the natural line width of 1.27 mms^{-1}. Figure 5.9 shows the ^{127}I Mössbauer spectrum of $[(C_6H_5)_2ICl]_2$ measured at 4.2° K, which resembles that of the $[ICl_4]^-$ anion in that transition no. 2 is well resolved at high negative velocity.[47] This means that the quadrupole coupling constant $e^2q^{127}Q_g/h$ is large and positive for this and for all of these square-planar compounds. Since $e^{127}Q_g$ is negative, the sign of the electric field gradient must therefore also be negative and hence the values are those expected for a central iodine bonded to four ligands in the xy plane, with the non-bonded electron pairs along the z axis. Examination of Table 5.12 reveals that within experimental error these interhalogen cations with the same terminal I-X interactions, i.e. $[ICl_2][SbCl_6]$,

-Table 5.12.

^{127}I Mössbauer Data for Square Planar Iodine(III) Cations and Related Species

Compound	Isomer Shift (mms^{-1})	$e^2q^{127}Q_g/h$ (MHz)	n	Γ (mms^{-1})	Γ_A	χ^2/deg. of freedom	U_p	h_p ($h_s=0$)	h_s ($h_p=2U_p$)
[ICl$_2$][SbCl$_6$]	-1.28(5)	3066(30)	0.08(6)	2.02(18)	1.47(10)	0.83	1.34	1.90	0.13
[ICl$_2$][SbF$_6$]	-1.27(5)	3066(30)	0.25(2)	1.59(14)	0.85(8)	0.96	1.34	1.89	0.13
[IBr$_2$][Sb$_2$F$_{11}$]	-1.26(8)	2676(13)	0.36(1)	2.39(8)	0.92(2)	1.64	1.17	1.87	0.08
[IBr$_{0.75}$Cl$_{1.25}$][SbCl$_6$]	-1.35(1)	2806(9)	0.26(1)	1.88(5)	1.35(2)	1.93	1.22	2.02	0.07
[I$_3$][AsF$_6$]	-0.87(5)	-2880(26)		2.31(18)	1.53(11)	1.03	1.26	1.23	0.00
	-0.59(11)	2267(54)					0.99	0.77	0.20
I$_2$Cl$_6$	-1.58(3)	2973(19)	0.09(3)	2.91(15)	0.42(1)	1.38	1.30	2.39	0.03
	-1.39(2) a	3060(10)	0.06(2)				1.33		

Table 5.12. (Contd.)

Compound	Isomer Shift (mms^{-1})	$e^2q^{127}Q_g/h$ (MHz)	n	Γ (mms^{-1})	T_A	χ^2/deg. of freedom	U_p	h_p $(h_s=0)$	h_s $(h_p=2U_p)$
$K[ICl_4]\cdot H_2O$	-1.53 [b]	$3094(20)$							
$[(C_6H_5)_2ICl]_2$	-0.54	$2044(19)$	$0.31(2)$	$2.13(13)$	$0.32(1)$	0.98	0.89	0.69	0.18
$[(C_6H_5)_2IBr]_2$	$-0.68(2)$	$1970(13)$	$0.36(1)$	$1.81(8)$	$0.81(3)$	1.15	0.86	0.92	0.13
$[(C_6H_5)_2II]_2$	$-0.71(5)$	$1951(33)$		$2.08(13)$	$0.51(2)$	1.60	0.85	0.97	0.12
	$0.04(4)$	$-780(33)$					0.34	-0.26	0.10
KI	$0 \ (-0.14(2))$ [c]								

a Reference 61 (converted from ^{129}I data).   b Reference 14.

c Isomer shift of KI relative to ZnTe source.
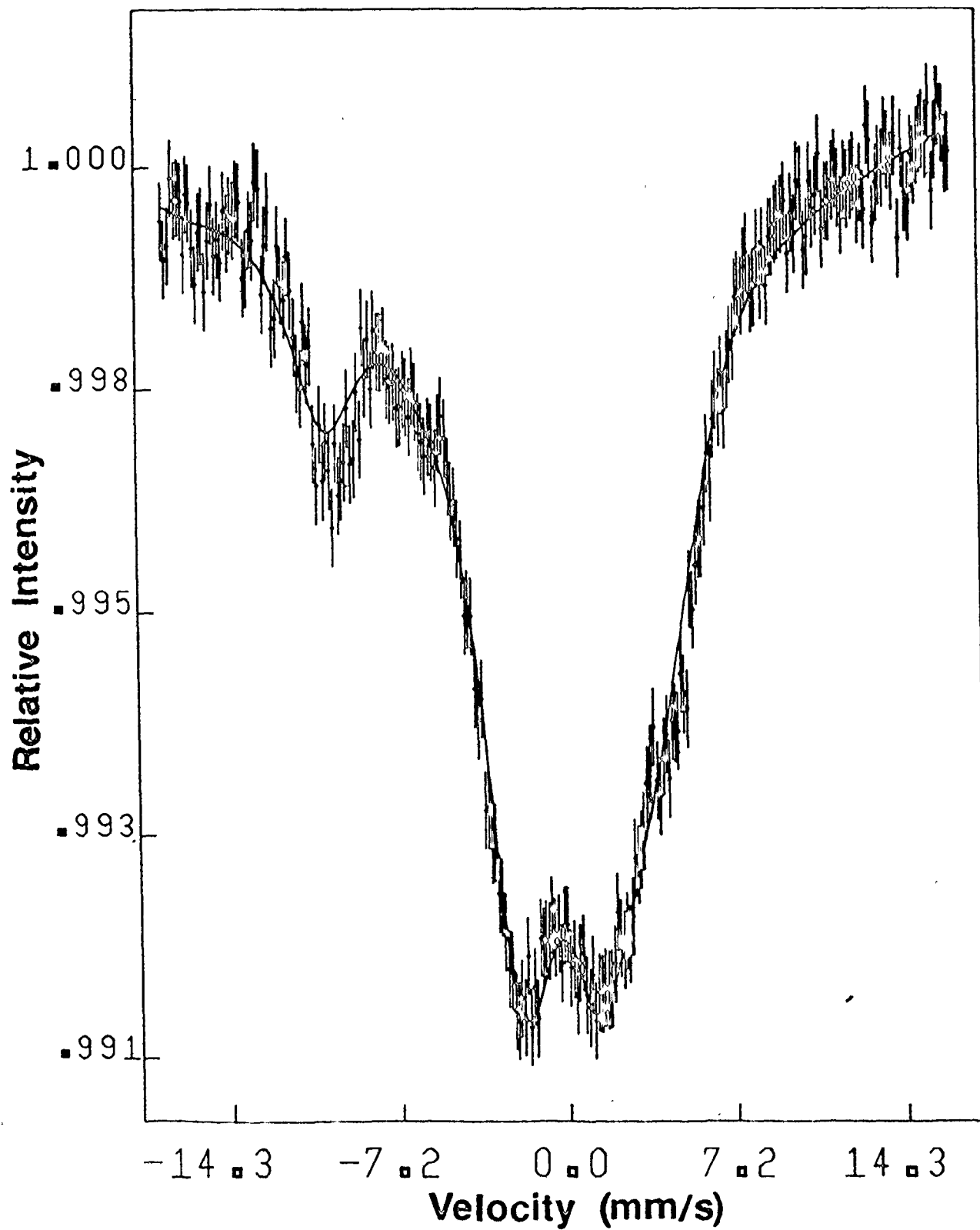
Figure 5.9. ^{127}I Mössbauer spectrum of $[(C_6H_5)_2ICl]_2$ measured at 4.2°K.
The solid line represents the best fit to the data.

$[ICl_2][SbF_6]$, I_2Cl_6 and $K[ICl_4] \cdot H_2O$ have nearly the same quadrupole

coupling constants despite the fact that the bridging I---Y interactions

are not the same, i.e. I---Cl in $[ICl_2][SbCl_6]$ and I---F in $[ICl_2][SbF_6]$.

$K[ICl_4] \cdot H_2O$, the only compound with the iodine in an anionic species, has

the largest quadrupole coupling constant of this series. The constancy

in these coupling constants is at first somewhat surprising since in

Chapter 4 it was found that for a series of linear $[X-I-Y]^-$ (X,Y = F, Cl,

Br, I) anions the quadrupole coupling constant increased as the

electronegativity of both X and Y ligands increased. Apparently this

behaviour does not seem to carry over to bridging or secondary

interactions and indeed the previous crystallographic discussion found

that the secondary I---Cl interactions in $[ICl_2][SbCl_6]$ were of roughly

the same strength as the secondary I---F interactions in $[ICl_2][SbF_6]$, as

judged by their very similar bond orders. The implication is that the

total electron density in the xy plane does not change significantly in

these two compounds. It seems then that in these interhalogen cations it

is mainly the primary bonding interactions to the central iodine atom

which determine the magnitude of the quadrupole coupling constant.

Further evidence for this is found by examining the diphenyliodonium

halides. In these compounds the halogens form bridging bonds to the

iodine and the quadrupole coupling constants are at least 30% smaller

than in the analogous interhalogen cations.

There is however a correlation between ligand electronegativity

and quadrupole coupling constant similar to that found for the linear

$[X-I-Y]^-$ anions. As the terminal halogen bonded to the central iodine of

the cation is varied the magnitude of the quadrupole coupling constant

changes and $e^2q^{127}Q_g/h$ for $[ICl_2]^+ > [IBr_{0.75}Cl_{1.25}]^+ > [IBr_2]^+ > [I_3]^+$,

which follows the order of decreasing halogen electronegativity. Since

the disordered cation $[IBr_{0.75}Cl_{1.25}]^+$ has both chlorine and bromine

bonded to the central iodine $e^2q^{127}Q_g/h$ lies between that for the $[IBr_2]^+$

and $[ICl_2]^+$ cations. The ^{127}I Mössbauer spectrum of $[IBr_{0.75}Cl_{1.25}]$-

$[SbCl_6]$ was computed incorporating only one iodine site. It was not

possible to resolve the spectrum into two sites which might arise from

say a mixture of $[ICl_2]^+$ and $[IBr_2]^+$ species since the isomer shifts and

quadrupole coupling constants of these individual compounds are not

drastically different. Hence on the basis of Mössbauer spectroscopy it

is not possible to ascertain whether the disordered cation

$[IBr_{0.75}Cl_{1.25}]^+$ contains any discreet $[BrICl]^+$ cations or whether it is

a mixture of the $[ICl_2]^+$ and $[IBr_2]^+$ cations.

As was previously mentioned the quadrupole coupling constants

found for the diphenyliodonium halides $[Ph_2IX]_2$ (X = Cl, Br, I) are

significantly smaller than those of the $[IX_2]^+$ (X = Cl, Br, I) cations

because in the latter compounds the quadrupole coupling constants are

mainly influenced by the strong primary iodine-halogen bonds, whereas in

the $[Ph_2IX]_2$ series [128] the primary bond is from iodine to carbon. The

iodine-halogen bonds are less significant in determining the magnitude of

the quadrupole coupling constant since they are now long, bridging

interactions. For example the bridging I---Cl interactions in $[Ph_2ICl]_2$

average 3.085Å, a distance which is similar to the bridging I---Cl

interactions in $[ICl_2][SbCl_6]$ [19] and $[ICl_2][AlCl_4]$,[19] which average

2.90Å. It is once again noted that the quadrupole coupling constants in these diphenyliodonium halides decrease with the decreasing electronegativity of the bridging halogen. However changing the bridging halogens in these compounds does not have as dramatic an effect on the quadrupole coupling constant as varying the terminal halogens in the $[IX_2]^+$ cations because it is the primary bonds to iodine which mainly determine the magnitude of the quadrupole splitting. Thus in the $[IX_2]^+$ cations, although the bridging or secondary contacts to the halogen atom in the anion are important in determining the sign of $e^2q^{127}Q_g/h$ their contribution to the magnitude of $e^2q^{127}Q_g/h$ is small.

It is interesting to compare the quadrupole coupling constants of the $[IX_2]^+$ cations with the analogous $[IX_2]^-$ anions. Although the geometry around the iodine atom in these two classes of compounds is drastically different (bent in the former if secondary interactions are ignored and linear in the latter) these $[IX_2]$ pairs have remarkably similar coupling constants. Hence the p-electron imbalance in these two classes of compounds is nearly the same and this is reflected by their respective U_p values (Tables 4.1 and 5.12).

The isomer shifts of the $[IX_2]^+$ cations are all quite negative with respect to the KI reference and also significantly more negative than the corresponding $[IX_2]^-$ anions. The main contributor to this large negative shift in the cations is the positive charge which causes the s-orbitals to contract, resulting in a higher s-electron density at the iodine nucleus. In addition, the I-X bonds in the anions, for example

(I-Cl, 2.55(2)Å;[143] I-Br, 2.695(2)Å;[9] I-I, 2.90(2)Å [144]) are generally
significantly longer than the corresponding I-X bonds in the cations and
hence the s-electrons are not deshielded to the same extent in the
anions. The existing crystallographic data for the $[IX_2]^+$ cations is
consistent with a valence bond description comprised of sp^3 and sp^3d^2
contributions. However the Mössbauer data suggest that the s-character
of the bonds is low, which is indicative of a formulation for these
compounds where localized p-orbitals form principally p-σ bonds. The
isomer shifts of the various $[IX_2]^+$ cations do not change very much from
one compound to another. The first four compounds in Table 5.12 have
isomer shifts which are the same within experimental error. The isomer
shift for the central iodine atom in the $[I_3]^+$ cation is however
significantly more positive than these former four compounds where iodine
is bonded to chlorine and/or bromine. Presumably the iodine-iodine bonds
in the $[I_3]^+$ cations are not as effective in removing p-electron density
from the central iodine atom. Perhaps also the positive charge is more
evenly spread over all these iodine atoms rather than being localized on
the central iodine as in $[ICl_2]^+$. Since the isomer shifts in [127]I
Mössbauer spectra are generally very small it is difficult to place any
significance on the shifts of the first four compounds in Table 5.12.
I_2Cl_6 and $K[ICl_4] \cdot H_2O$ have the most negative isomer shifts and this is
probably because these two compounds are approaching the situation where
the central iodine atom is bonded strongly to four atoms in a square-
planar geometry. The isomer shifts for the diphenyliodonium halides are
much less negative than the shifts of the $[IX_2]^+$ cations, as would be

expected for this type of compound which contains iodine-carbon bonds as the primary interaction. The s-electrons are not deshielded to the same extent as in the cations as a result of this, and also there is no formal positive charge on the iodine atom in the $[Ph_2IX]_2$ series. There is perhaps also more participation of the s-electrons in the bonds to carbon. The variation in shifts within the group of diphenyliodonium halides, as in the cations, is rather small.

Table 5.12 also gives the values of U_p calculated for all these compounds as well as the value of h_p and h_s calculated using equation (4.6). Following the notation of Perlow and Perlow,[14] in the case of the $[X-I-Y]^-$ anions where the bond axis is the molecular symmetry axis, $h_p = |U_p|$ while for the square-planar compounds $h_p = 2U_p$. It is immediately evident that the agreement between $2U_p$ and h_p is not good especially for the diphenyliodonium halides. The values for h_s calculated for the $[IX_2]^+$ cations are all positive and indicate that a small amount of s-electron density has been removed. The values of h_s for the diphenyliodonium halides however are somewhat high and perhaps reflect some s-electron participation in the bonding scheme. However agreement between U_p and h_p is not very good and therefore as was alluded to in the previous Chapter, equation (4.6), which was calculated from the Mössbauer data of the linear $[X-I-Y]^-$ anions may not have general applicability. Indeed the isomer shifts and quadrupole coupling constants for a series of compounds are as informative if not more meaningful than the numbers which are calculated from these semi-

empirical relationships. In essence the above data seems to imply that the isomer shift and quadrupole coupling constant are not always strictly proportional as has been suggested.

Most of the compounds found in Table 5.12 have a significant eta value so that although the principal axis of the electric field gradient is along the direction of the non-bonded electron pairs there is some degree of asymmetry in the x and y directions. In I_2Cl_6[133] and $[ICl_2][SbCl_6]$ [19] where all the halogen ligands are the same and the $[ICl_4]$ rectangular unit is nearly planar, the value of n is small. But in $[ICl_2][SbF_6]$ where the bridging chlorines of the previous compounds have been replaced by bridging fluorines, and the $[ICl_2F_2]$ rectangular unit is no longer planar, n = 0.25. Similarly in the remaining compounds, if X and Y in the $[IX_2Y_2]$ rectangular unit are not the same the value of eta ranges from 0.25-0.36.

(iii) Raman Spectroscopy

Many of the interhalogen cations of iodine have been identified and characterized on the basis of their Raman spectra. The $[ICl_2]^+$ cation has been identified by Raman spectroscopy in the $[SbCl_6]^-$,[37,145] $[AlCl_4]^-$,[37,145] $[SO_3F]^-$ [26] and $[SO_3Cl]^-$ [37] salts. The bent $[ICl_2]^+$ cation has C_{2v} symmetry and thus three Raman active modes of vibration. These are $v_1(A_1)$, the symmetric I-Cl bond stretch; $v_2(A_1)$, the Cl-I-Cl angle deformation mode; $v_3(B_1)$ the antisymmetric I-Cl bond stretch. The frequencies of these vibrations for the $[SbCl_6]^-$ [145] and $[AlCl_4]^-$ [145]

salts of $[ICl_2]^+$ are found in Table 5.13. Also presented in this Table are the frequencies of vibration for $[ICl_2][SbF_6]$, $[IBr_2][Sb_2F_{11}]$ and $[IBr_{0.75}Cl_{1.25}][SbCl_6]$.

The Raman spectrum of $[ICl_2][SbF_6]$ was measured during the course of this work and is similar to the spectra of the above compounds with respect to the number of bands found. The deformation mode, ν_2 is found at 142 cm^{-1}. The symmetric and antisymmetric stretching modes have been assigned to the bands found at 393 and 387 cm^{-1} respectively. These values are substantially higher than those which have been reported for other compounds containing the $[ICl_2]^+$ cation but there is no other assignment which is reasonable. The ν_2 and ν_3 vibrations in the $[IX_2]^+$ cations are usually found at a lower frequency than that of the parent interhalogen; for example the I-Cl stretch in ICl occurs at 381 cm^{-1}. The I-Cl bond distance in ICl has been determined spectroscopically [147] and is 2.321Å, while an X-ray crystal structure determination [119] has found the I-Cl distance to be 2.351Å in β-ICl. The I-Cl bond distance in $[ICl_2][SbF_6]$ is 2.268(2)Å which is somewhat shorter than that found in ICl itself. This shorter, stronger bond in $[ICl_2][SbF_6]$ could account for the unusually high I-Cl stretching frequency. In addition to the above bands, a fairly intense lattice vibration occurs at 55 cm^{-1} and a weak peak at 291 cm^{-1} has been assigned to ν_5 of the $[SbF_6]$ anion. [148]

The Raman spectrum of the $[IBr_2]^+$ cation has been reported and like all $[IX_2]^+$ cations should exhibit three Raman active modes of vibration. The reported frequencies are, ν_1 at 256 cm^{-1}, ν_2 at 124 cm^{-1} and ν_3 at 256 cm^{-1}. [37] The authors suggest that the observation of only

Table 5.13.

Raman Frequencies of Square Planar Iodine(III) Cations, $\Delta\nu$ (cm^{-1})

$[ICl_2][SbCl_6]^a$	$[ICl_2][AlCl_4]^a$	$[ICl_2][SbF_6]$	$[IBr_2][Sb_2F_{11}]$	$[IBr_{0.75}Cl_{1.25}][SbCl_6]$	Assignment for anion	Assignment for cation
371(100)	366(100)	393(100)		362(62)		$\nu_1(A_1)$ } I-Cl st.
364(66)	350(66)	387(45)		356(58)		$\nu_3(B_1)$ }
				336(60)	$\nu_1(A_{1g})$	
				296(13)	$\nu_2(E_g)$	
				258(13)		
			257(63)	250(62)		$\nu_3(B_1)$ } I-Br st.
			232(100)	242(100)		$\nu_1(A_1)$ }
			197(34)	174(13)	$\nu_5(T_{2g})$	
		291(9)				
147(10)	143(9)	142(35)	123(12)	129(33)		$\nu_2(A_1)$ bend
		55(57)				lattice

^{a} Reference 145.

one stretching mode is due to the accidental coincidence of the two allowed stretching modes. The Raman spectrum of a solid sample of $[IBr_2][Sb_2F_{11}]$ was recorded and is comparable to that obtained in SO_2 solvent. A very weak line at 123 cm^{-1} has been assigned as the Br-I-Br deformation mode. A broad band centred at about 197 cm^{-1} is probably due to a vibrational mode of the $[Sb_2F_{11}]^-$ anion. Peaks at 257 and 232 cm^{-1} have been assigned to the antisymmetric and symmetric I-Br stretching modes respectively of the $[IBr_2]^+$ cation. These assignments are found in Table 5.13.

The assignment of the Raman spectra of the $[ICl_2]^+$ and $[IBr_2]^+$ cations is very useful in the interpretation of the rather complex Raman spectrum of $[IBr_{0.75}Cl_{1.25}][SbCl_6]$. The Raman spectrum of the $[BrICl]^+$ cation has previously been reported by two groups. Aubke et al.[27] have reported the Raman spectrum $IBrClSO_3F$ while Shamir and Lustig [38] have reported the Raman spectrum of $[IBrCl][SbCl_6]$. The disordered compound $[IBr_{0.75}Cl_{1.25}][SbCl_6]$ was prepared during the course of this work by using a method very similar to that used by Shamir and Lustig [38] to prepare $[IBrCl][SbCl_6]$. This is a very complex reaction whereby an equimolar mixture of IBr and $SbCl_5$ is treated with an equivalent amount of liquid Cl_2 and allowed to warm up to room temperature over a period of several hours. Aubke et al.[27] prepared $IBrClSO_3F$ by melting an intimate, equimolar mixture of IBr_2SO_3F and ICl_2SO_3F.

On the basis of X-ray crystallographic data alone it was not possible to discern conclusively whether $[IBr_{0.75}Cl_{1.25}]^+$ is comprised of a mixture of $[ICl_2]^+$ and $[IBr_2]^+$ cations or whether there are discreet $[IBrCl]^+$ cations present. The Raman spectrum of $[IBr_{0.75}Cl_{1.25}][SbCl_6]$ is shown in Figure 5.10 and is much more complicated than would be expected from a single species such as $[IBrCl][SbCl_6]$. As was previously mentioned the bent $[IX_2]^+$ cations have three Raman active fundamentals, hence a mixture of $[IBr_2]^+$ and $[ICl_2]^+$ cations should exhibit a total of six Raman active modes of vibration. If the $[BrICl]^+$ cation (C_s symmetry) was present exclusively there would be only three modes of vibration due to the cation. A mixture of $[ICl_2]^+$, $[IBr_2]^+$ and $[BrICl]^+$ cations would show a very complex Raman since the I-Cl(Br) stretches of the $[ICl_2]^+$ and $[IBr_2]^+$ cations would not be very different in energy from the I-Cl(Br) stretches of $[BrICl]^+$. The Raman spectrum of $[IBr_{0.75}Cl_{1.25}][SbCl_6]$ has been assigned as follows. Peaks found at 174, 258, 296 and 336 cm^{-1} are assigned as $[SbCl_6]^-$ anion vibrations according to the designations of Table 5.13. Additional peaks at 162, 187, 266 and 307 cm^{-1} could also be $[SbCl_6]^-$ anion peaks since there are two crystallographically discreet anions present in the compound, and likely two chemically different anions present since one would be bridged to $[ICl_2]^+$ and the other to $[IBr_2]^+$. The symmetric and antisymmetric I-Cl stretches of the $[ICl_2]^+$ cation occur at 362 and 356 cm^{-1} respectively and are close to those reported for the $[ICl_2]^+$ cation in $[ICl_2][SbCl_6]$ and $[ICl_2][AlCl_4]$ (Table 5.13). The peak at 129 cm^{-1} is the deformation mode of either $[ICl_2]^+$ or $[IBr_2]^+$ and is probably the latter. The
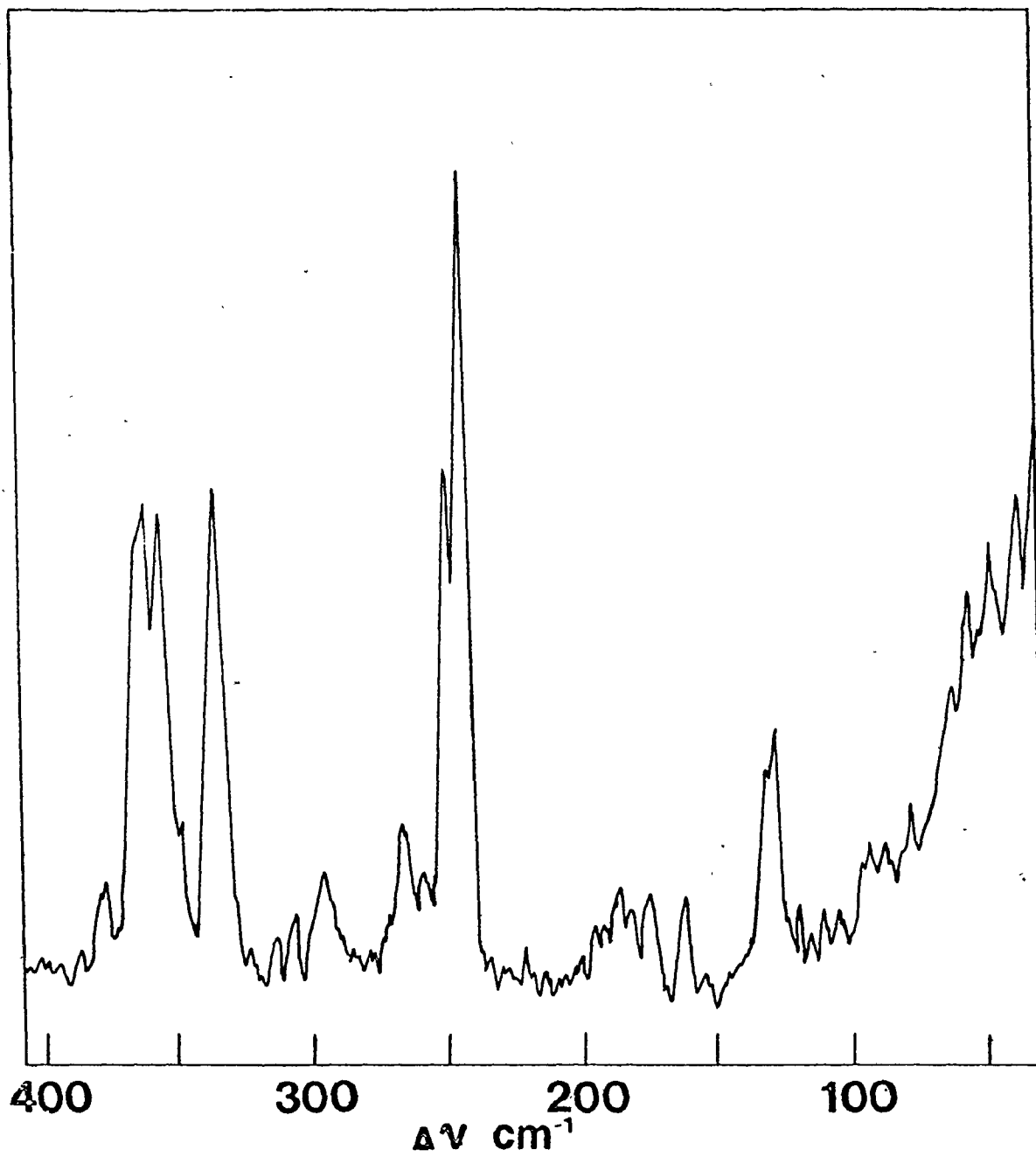
Figure 5.10.   Raman spectrum of $[IBr_{0.75}Cl_{1.25}][SbCl_6]$ at $-196°C$ using 5145 Å excitation.

symmetric and antisymmetric bond stretches of $[IBr_2]^+$ are at 250 and 242 cm^{-1}, again in good agreement with those previously reported (Table 5.13). Thus while Shamir and Lustig [38] and others [27] have interpreted their Raman data as being consistent with the $[BrICl]^+$ formulation exclusively, in view of the inconclusive X-ray crystallographic data, Mössbauer spectrocopy and the Raman data obtained here, it is concluded that $[IBr_{0.75}Cl_{1.25}][SbCl_6]$ is primarily a crystallographic mixture of $[ICl_2][SbCl_6]$ and $[IBr_2][SbCl_6]$ although it is not possible to eliminate the possibility that small quantities of the $[IBrCl]^+$ cation may be present.

CHAPTER 6

The Preparation and Characterization of $[I_3Cl_2][SbCl_6]$

A. Introduction

The reactions of I_2Cl_6 with a number of Lewis acids, such as $SbCl_5$,[75] $AlCl_3$,[75] SbF_5 [27](present work) and SO_3 [126] have been thoroughly studied. The hexachloroantimonate,[75] tetrachloroaluminate,[75] and more recently the hexafluoroantimonate (present work) salts of $[ICl_2]^+$ have all been well established by X-ray crystallographic studies.

In an effort to further the studies of the reactions of I_2Cl_6 with potential Lewis acid acceptors and synthesize new polyhalogen cations of iodine the reaction of I_2Cl_6 with antimony(III) chloride was investigated. This reaction produced a highly crystalline material whose [121]Sb Mössbauer spectrum indicated the presence of Sb(V) rather than Sb(III).

It had been reported [33-35] that under suitable conditions iodine monochloride combines with antimony pentachloride to produce compounds with the general formulae $I[SbCl_6] \cdot nICl$ (n = 2-4), i.e., containing the cations $[I_3Cl_2]^+$, $[I_4Cl_3]^+$ and $[I_5Cl_4]^+$. The existence of any of these higher polyatomic cations of iodine has not been verified conclusively until now.

In this Chapter the X-ray crystal structure of $[I_3Cl_2][SbCl_6]$, the first structure of an interhalogen compound of iodine containing a cation of the general type $[I_nCl_{n-1}]^+$ is presented. The laser Raman

spectrum and visible absorption spectrum of $[I_3Cl_2][SbCl_6]$ are very similar to the corresponding spectra which have previously been reported for $[I_2Cl][SbCl_6]$.[37,38] A single crystal, sublimed from the product of the reaction reported to produce $[I_2Cl][SbCl_6]$ was found to have the same unit cell parameters as $[I_3Cl_2][SbCl_6]$.

Subsequent to the completion of this work Pohl and Saak [149] have reported the X-ray crystal structures of the $[SbCl_6]^-$ and $[AlCl_4]^-$ salts of $[I_3Cl_2]^+$ as well as that of $[I_3Br_2][SbCl_6]$. Their crystal structure determination of $[I_3Cl_2][SbCl_6]$ confirms the findings of this work. These workers prepared their compound according to equation (6.1) More

$$3ICl + SbCl_5 \rightarrow [I_3Cl_2][SbCl_6] \qquad (6.1)$$
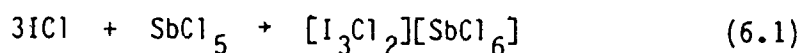
recently still, Shamir and Thorup [150] have also reported the X-ray crystal structure of $[I_3Cl_2][SbCl_6]$.

B. Results and Discussion

   (i) Structure of $[I_3Cl_2][SbCl_6]$

Crystal data for $[I_3Cl_2][SbCl_6]$ are found in Table 6.1. Intensity measurements were made on a Syntex $P2_1$ diffractometer. The details regarding data acquisition are also given in Table 6.1. Lorentz and polarization corrections were applied to the data and the structure was solved using coventional heavy atom methods. The iodine and antimony atoms were located using a Patterson map, and subsequent Fourier maps revealed the positions of the remaining atoms and confirmed the

Table 6.1. Crystal data for $[I_3Cl_2][SbCl_6]$

Crystal Data

system	triclinic [a]
a	7.090(1) Å
b	11.591(2) Å
c	7.126(1) Å
α	122.29(1)°
β	98.85(1)°
γ	115.86(1)°
U	383.5(1) Å³
D_{calcd}	3.404 g cm⁻¹
Ref'ns used in cell determination (No./2θ range)	10/17°<2θ<31°
Z	1
f_w	786.4
F(000)	346
μ(MoKα)	92.6 cm⁻¹
space group	P1̄ or P1
systematic absences	No conditions

Data Collection

mode	θ:2θ	
wavelength	MoKα radiation ($\lambda = 0.71069$Å)	
stds.	2/48	
No./interval	(-1,3,-4) and (0,-2,1)	
scan range	K_{α_1} -1.0° to K_{α_2} +1.0°	
scan speeds	4.0°-29.3°/min	
max 2θ quadrant	55°, h±k±l	

Details of Refinement

absorption correction	none	
secondary extinction b	$g = 2.44 \times 10^{-3}$	
No. of nonzero data	1711	
No. of data with F > 2.0σ(F)	1667	
No. of data with F > 6.0σ(F)	1545	
R factors 2σ:	R_1	0.034
	R_2	0.042
6σ:	R_1	0.032
	R_2	0.040
Max. shift/error	0.09	
Weighting scheme	$w=1.0(\sigma(F_0)^2 + 1.1\times10^{-5}F_0^3+0.5\sin\theta)$	
Highest peak in final difference map	+4.1 e/Å³	
Lowest valley in final difference map	-2.0 e/Å³	

Table 6.1: (contd.)

a The Delauney reduced primitive triclinic cell for this compound has
$a' = 9.842$, $b' = 7.126$, $c' = 7.739Å$, $\alpha' = 91.17$, $\beta' = 134.35$, $\gamma' = 95.44°$. It is related to the above cell by the transformation
$(011)/(00\bar{1})/(\bar{1}\bar{1}\bar{1})$.

b The extinction correction used followed the method of Larson
(A. C. Larson, Acta Cryst., 23, 664 (1967)).

positional assignments of the heavy atoms. The structure was solved and refined in the triclinic space group $P\bar{1}$ and there was no improvement in P1. A complete listing of observed and calculated structure factor amplitudes may be found by consulting reference 129. The final atomic positional coordinates are given in Table 6.2 and the anisotropic thermal parameters are found in Table 6.3. The bond lengths and bond angles of the molecule are given in Table 6.4.

The crystal structure consists of $[I_3Cl_2]^+$ cations and $[SbCl_6]^-$ anions which form infinite zig-zag chains as a result of a secondary cation-anion interaction which occurs via a bridging chlorine atom. The atomic arrangement is illustrated in Figure 6.1 and a stereoscopic view of the packing in the unit cell is shown in Figure 6.2. The central iodine atom of the $[I_3Cl_2]^+$ cation lies on a crystallographic centre of symmetry such that the cation is planar, and possesses C_{2h} symmetry. The $[SbCl_6]^-$ anion is a slightly distorted octahedron with the terminal Sb-Cl distances averaging 2.348Å, while the bridging Sb---Cl(1) distance is somewhat longer at 2.416(2)Å. The I(1)-I(2) bond distance in $[I_3Cl_2][SbCl_6]$ is 2.9057(6)Å. This may be compared to the analogous I-I bond distance found in the structurally related $[I_5]^+$ cation,[151] (2.896(2)-2.920(2)Å) and the average I-I distance observed in various symmetric and asymmetric $[I_3]^-$ ions.[152] The terminal I(1)-Cl(3) bond distance in the $[I_3Cl_2]^+$ cation is 2.333(1)Å as compared to the I-Cl bond distance [119] in β-ICl which is 2.351(14)Å. In β-ICl, in addition to the short I-Cl bond (2.351Å) there is another longer I---Cl interaction at 2.939(12)Å which is almost colinear (175°) with the primary bond. A

Table 6.2. Atomic Positional Coordinates of $[I_3Cl_2][SbCl_6] \times 10^4$

	x/a	y/b	z/c
I(1)	1765.8(6)	8336.3(5)	682.0(7)
I(2)	0	0	0
Sb(1)	5000	5000	0
Cl(1)	3269(3)	4901(2)	2627(3)
Cl(2)	6918(3)	7979(2)	2661(3)
Cl(3)	5817(3)	833(2)	3254(3)
Cl(4)	8420(3)	5637(2)	2661(3)

Table 6.3. Thermal parameters [a] for $[I_3Cl_2][SbCl_6]$

	U_{11}	U_{22}	U_{33}	U_{12}	U_{13}	U_{23}
I(1)	317(2)	311(2)	397(2)	191(2)	182(2)	268(2)
I(2)	298(3)	314(3)	360(3)	175(2)	159(2)	249(2)
Sb(1)	223(2)	187(2)	299(3)	99(2)	109(2)	155(2)
Cl(1)	411(8)	341(7)	390(7)	158(6)	229(7)	226(6)
Cl(2)	476(8)	209(6)	475(8)	164(6)	254(7)	194(6)
Cl(3)	333(7)	402(8)	478(8)	173(6)	174(6)	302(7)
Cl(4)	341(7)	517(9)	561(9)	241(7)	120(7)	363(8)

[a] Temperature factors ($\times 10^4$) in the form $\exp(-2\pi^2 \sum_i \sum_j U_{ij} H_i H_j a_i^* a_j^*)$

Table 6.4. Bond Lengths (Å) and Bond Angles (°) for $[I_3Cl_2][SbCl_6]$ [a]

Estimated Standard Deviations in Parentheses

Bond Lengths (Å)

I(1) - I(2)	2.9057(6)	Sb(1) - Cl(1)	2.416(2)
I(1) - Cl(3)	2.333(1)	Sb(1) - Cl(2)	2.341(2)
I(1) - Cl(1)	2.941(1)	Sb(1) - Cl(4)	2.355(2)

Bond Angles (°)

I(1) - I(2) - I(1')	180.000(7)	Cl(1) - Sb(1) - Cl(4)	89.56(8)
Cl(3) - I(1) - I(2)	92.62(7)	Cl(1")- Sb(1) - Cl(4)	90.44(8)
Cl(3) - I(1) - Cl(1)	177.56(8)	Cl(2) - Sb(1) - Cl(4)	89.98(8)
Cl(1) - I(1) - I(2)	89.55(5)	Cl(2")- Sb(1) - Cl(4)	90.02(8)
I(1) - Cl(1) - Sb(1)	109.75(5)	Cl(1) - Sb(1) - Cl(1")	180.00(4)
Cl(1) - Sb(1) - Cl(2)	89.71(7)	Cl(2) - Sb(1) - Cl(2")	180.00(7)
Cl(1) - Sb(1) - Cl(2")	90.29(7)	Cl(4) - Sb(1) - Cl(4")	180.00(8)

[a] Symmetry transformations are: (') -x,-y,-z; (") 1-x,1-y,-z.
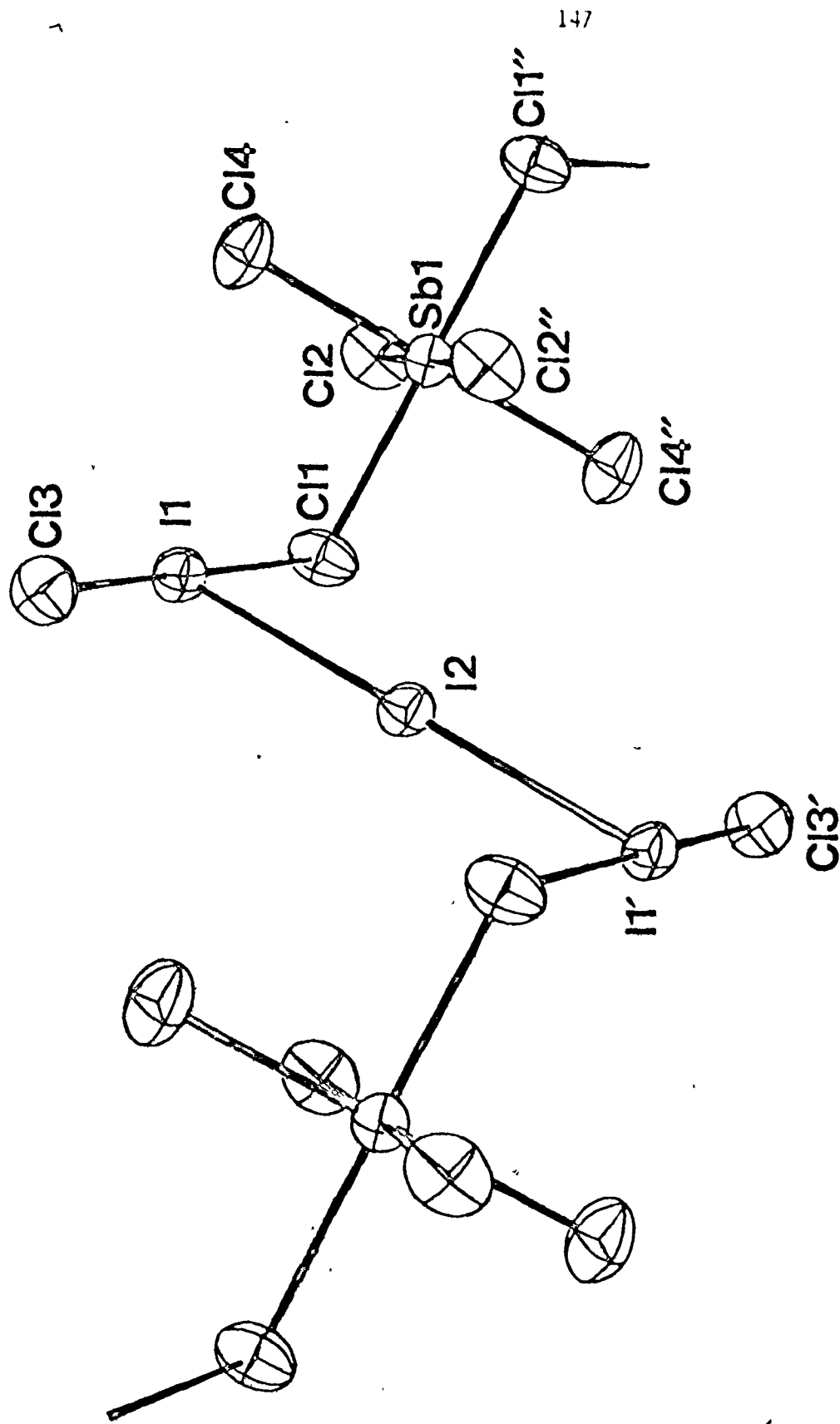
Figure 6.1. Molecular geometry of [I₃Cl₂][SbCl₆] showing the trans-bridged configuration of cation and anion. Symmetry transformations are: ('), -x, -y, -z; (") 1-x, 1-y, -z.

148
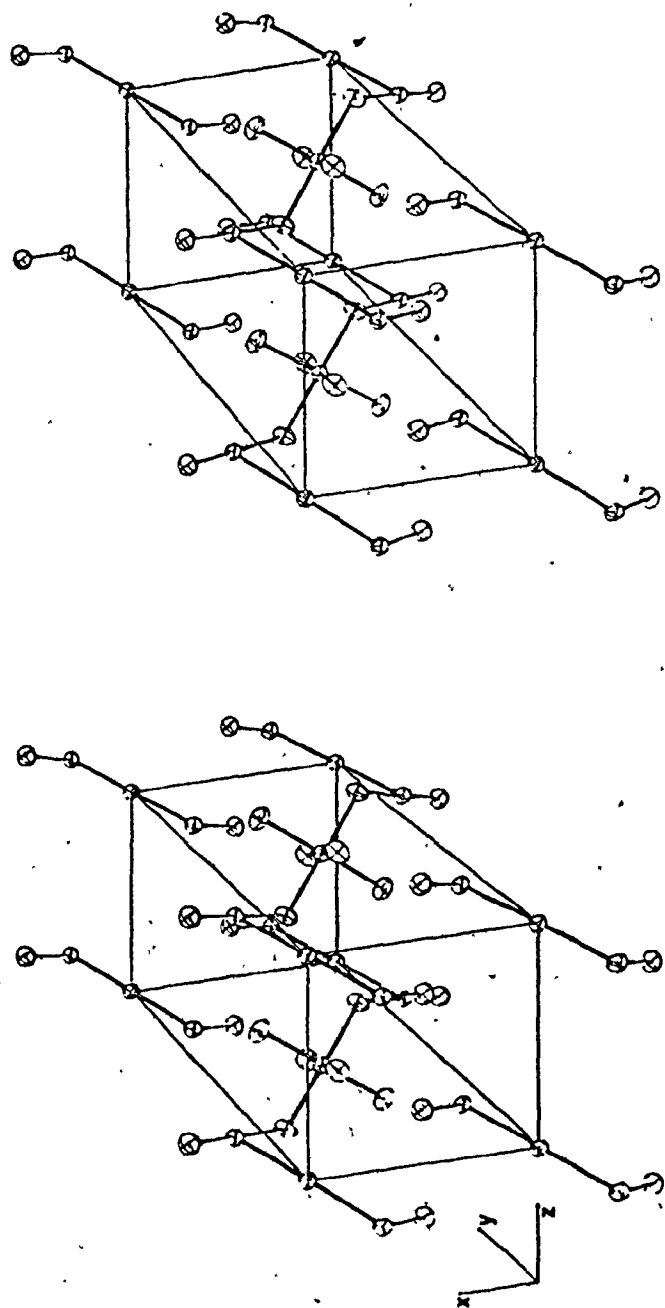
Figure 6.2.   Stereoscopic drawing of the unit cell of $[I_3Cl_2][SbCl_6]$ viewed along the y axis.

similar interaction is present in $[I_3Cl_2]^+$ in the form of a secondary or bridging $I(1)---Cl(1)$ contact at $2.941(1)Å$ so that the $Cl(3)-I(1)---Cl(1)$ angle is $177.56(8)°$. These terminal and bridging iodine-chlorine interactions are similar to those which occur in salts of $[ICl_2]^+$.[19]

The $Cl(3)-I(1)-I(2)$ and $Cl(1)---I(1)-I(2)$ bond angles found in $[I_3Cl_2][SbCl_6]$ are $92.62(7)$ and $89.55(5)°$ respectively. These values are very similar to those found for the analogous angles in $[I_5][SbF_6]$.

The bond orders of the strong bonding interactions found in $[I_3Cl_2][SbCl_6]$ may be estimated by using the relationship between electrostatically corrected experimental bond lengths and calculated bond orders established for a series of interhalogen compounds by Wiebenga and Kracht.[133] According to this method the $I(1)-I(2)$ bond distance found in $[I_3Cl_2][SbCl_6]$ corresponds to a bond order of ca. 0.6. The terminal $I(1)-Cl(3)$ bond has an estimated bond order of 0.9. The analogous terminal I-I distances in the $[I_{15}]^{3+}$ cation [151] have an average bond order of 0.85. It appears then that the $I(1)-Cl(3)$ interaction in $[I_3Cl_2][SbCl_6]$ is of comparable strength to the corresponding I-I interactions in $[I_{15}]^{3+}$.

The variation in bond lengths present in the $[I_3Cl_2]^+$ cation from the expected values for bonds of bond order one suggests that it may be described by the valence bond structures I-III.

$$
\begin{array}{ccc}
\overset{\displaystyle Cl}{\underset{}{|}} & \overset{\displaystyle Cl}{\underset{}{|}} & \overset{\displaystyle Cl}{\underset{}{|}} \\
{}^+I - I \quad I & I \quad I - I^+ & I \quad {}^+I \quad I \\
\underset{Cl}{|} & \underset{Cl}{|} & \underset{Cl}{|} \\
(I) & (II) & (III)
\end{array}
$$
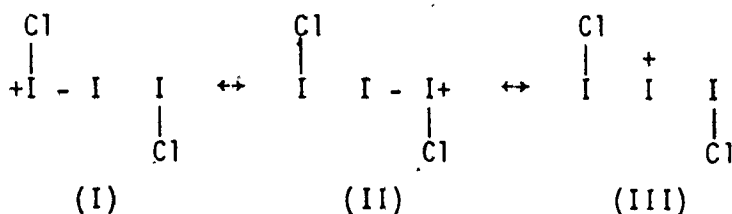
Structures I and II imply formal bond orders of 1.0 and 0.5 for terminal and central bonds respectively, while structure III, a minor contributor to the bonding description, would have a formal bond order of 1.0 for terminal bonds and 0 for the central bonds. An alternative charge distribution in $[I_3Cl_2]^+$ may be obtained by using the above bond orders and a bond valence type formalism similar to that of Brown.[153] According to this method the sum of the bond orders to a particular atom must be equal to the sum of that atom's valency plus its charge. Since in $[I_3Cl_2]^+$, the I(1)-I(2) bond has an estimated bond order of 0.6 and the I(1)-Cl(3) estimated bond order is 0.9, the central I(2) atom must have a charge of +0.2, while the I(1) atoms much each have a charge of +0.5. This is shown in structure IV.
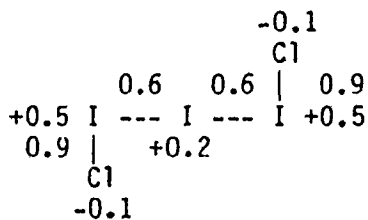
```
                          -0.1
                           Cl
                0.6    0.6 |  0.9
        +0.5 I --- I --- I +0.5
         0.9 |      +0.2
             Cl
            -0.1

                     (IV)
```

Since the bond order of the terminal Cl(3) atoms is 0.9 they must bear a charge of -0.1 each so that the net charge on the $[I_3Cl_2]$ moiety is +1.0. Considering this charge distribution it is reasonable that there is a secondary interaction between the I(1) atoms of the cation which possess the highest formal positive charge, and the Cl(1) atoms of the $[SbCl_6]^-$ anions, whereas the less positive, central I(2) atom shows no such

interaction. The formalism employed above to arrive at this model is of course semi-empirical, depending to a large extent on the method used to obtain bond orders, and in neglecting the I(1)---Cl(1) secondary interaction assumes that the molecule is ionic.

(ii) Raman Spectroscopy

The laser Raman spectrum of a large crystal of $[I_3Cl_2][SbCl_6]$ obtained at liquid nitrogen temperature using 6328Å excitation is shown in Figure 6.3; the observed frequencies and their relative intensities are given in Table 6.5. The spectrum shows the three characteristic Raman active fundamentals (one of which is split) of the $[SbCl_6]^-$ anion. The measured frequencies are 334 (ν_1, A_{1g}), 296, 259 (ν_2, E_g), and 174 cm^{-1} (ν_5, T_{2g}), and are in good agreement with those of other salts containing the hexachloroantimonate anion.[154] The splitting of ν_2 is consistent with an effective lowering of symmetry in the anion, from O_h to D_{4h} ($E_g + A_{1g} + B_{1g}$) due to the interaction of the anion with the cation via the bridging Cl(1) atom, which distorts the Sb-Cl(1) bond. This effect has also been observed in the Raman spectra of hexafluoroantimonate and hexafluoroarsenate salts.[148] The remaining lines in the spectrum apart from the low frequency lattice modes are due to the vibrations of the cation. There are 3n-6 = 9 vibrational modes expected and since $[I_3Cl_2]^+$ is centrosymmetric, (C_{2h} symmetry) six are infrared active, and three modes of A_g symmetry are Raman active. The band at 354 cm^{-1} with a shoulder at 348 cm^{-1} is assigned to the I-Cl stretching mode of $[I_3Cl_2]^+$. This splitting results from the isotope
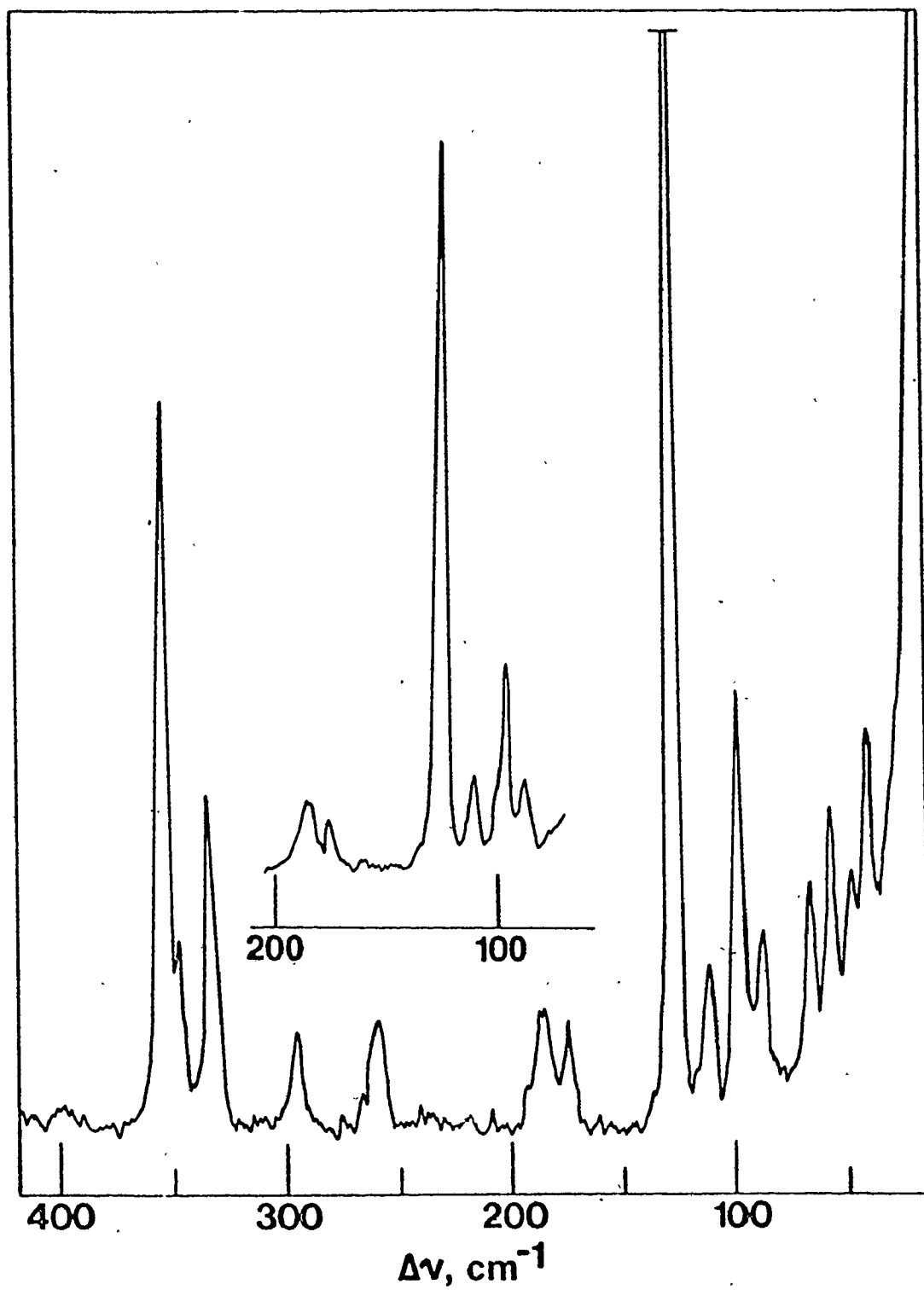
Figure 6.3.   Raman spectrum of $[I_3Cl_2][SbCl_6]$ at -196°C using 6328.Å excitation.

Table 6.5. Raman Frequencies and Assignments for $[I_3Cl_2][SbCl_6]$

Relative intensity	Frequency shift (cm^{-1})	Assignments	
		$[I_3Cl_2^+$ (C_{2h})	$[SbCl_6]^-$ (O_h)
	40		
	48		
	57		
	66	lattice	
	88		
	97		
	112		
100	126	$\nu_3(A_g)$ I-I-Cl bend	
6	174		ν_5 (T_{2g})
9	184	$\nu_2(A_g)$ I-I st.	
8	259		ν_2 ($E_g + A_{1g} + B_{1g}$)
10	296		
25	334		ν_1 (A_{1g})
16	348	$\nu_1(A_g)$ I-^{37}Cl st.	
52	354	$\nu_1(A_g)$ I-^{35}Cl st.	

effect of ^{35}Cl and ^{37}Cl, and the intensities of the peaks are in the expected 3:1 ratio. The most intense band at 126 cm^{-1} is the I(2)-I(1)-Cl(3) bend, while the remaining line at 184 cm^{-1} is assigned to the I-I stretch. Both stretching modes of $[I_3Cl_2]^+$ occur at a frequency lower than that which is observed for free ICl and I_2 molecules (381 and 213 cm^{-1} respectively [146]) due to a weakening of the bond as a result of additional interactions.

The Raman spectrum of $[I_2Cl][SbCl_6]$ has been reported [37,38] and although the relative intensities of the lines vary, the frequency shifts are nearly the same as those reported here for $[I_3Cl_2][SbCl_6]$. It has been proposed that the structure of $[I_2Cl]^+$ is that of a bent, asymmetric $[I_2X]^+$ cation which would have C_s symmetry and therefore exhibit three Raman active modes of vibration, as does $[I_3Cl_2]^+$. However, as previously mentioned $[I_3Cl_2]^+$ would have six infrared active modes while $[I_2Cl]^+$ would have only three infrared active modes whose frequencies would be coincident with those observed in the Raman. While these authors [38] report a satisfactory chemical analysis for $[I_2Cl][SbCl_6]$ they do not provide any infrared data, which is critical to an unambiguous structural assignment based upon vibrational spectroscopy. Unfortunately this is not a trivial matter and attempts to do this have so far been unsuccessful for several reasons. In spite of the availability of Fourier Transform (FT) infrared spectrometers equipped with far infrared capabilities, the efficiency and quality of the experiment decreases rapidly at low energies, usually resulting in very broad lines compared to those observed in the Raman. $[I_3Cl_2][SbCl_6]$ and $[I_2Cl][SbCl_6]$ as

prepared by Shamir and Lustig [38] are both very moisture sensitive and strong oxidants, reacting very quickly with hydrocarbon mulling agents such as nujol, and with polyethylene when the latter material is used as a sample holder for neat solids. The fluorine containing polymer FEP (copolymer of perfluoropolypropylene and perfluoropolyethylene) is inert to the above compounds, however it transmits the light poorly, absorbing strongly from about 1600 to 450 cm^{-1}, and exhibits a broad band at about 205 cm^{-1}.

In view of the difficulties encountered with the infrared experiment the procedure of Shamir and Lustig was repeated in an attempt to prepare $[I_2Cl][SbCl_6]$ and crystals were sublimed into quartz capillaries by the method described for $[I_3Cl_2][SbCl_6]$. A single crystal suitable for diffractometer measurements was obtained and it was found to have the same unit cell parameters [155] as $[I_3Cl_2][SbCl_6]$ and a quick structure solution revealed that it was indeed $[I_3Cl_2][SbCl_6]$. This was verified by examining a number of crystals. A large crystal of this material exhibited a Raman spectrum identical to that of $[I_3Cl_2][SbCl_6]$.

The preparation of $[I_3Cl_2][SbCl_6]$ was effected by the reaction of I_2Cl_6 with $SbCl_3$ in SO_2 solvent. Thus the antimony(III) undergoes oxidation to antimony(V), while iodine(III) has formally been reduced to iodine(I) according to equation (6.2).

$$I_2Cl_6 + 2SbCl_3 \rightarrow 2ICl + 2SbCl_5 \qquad (6.2)$$
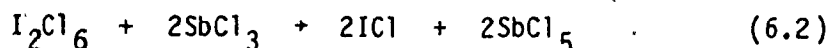
Subsequent to this, chloride is removed from ICl by $SbCl_5$ to produce $[I]^+$ and $[SbCl_6]^-$. The $[I]^+$ cation is an extremely strong Lewis acid and requires stabilization by two moles of ICl, thereby producing $[I_3Cl_2][SbCl_6]$; equations (6.3) and (6.4).

$$3ICl + SbCl_5 \rightarrow [I]^+ \cdot 2ICl[SbCl_6]^- \qquad (6.3)$$

$$[I]^+ \cdot 2ICl[SbCl_6]^- \rightarrow [I_3Cl_2][SbCl_6] \qquad (6.4)$$
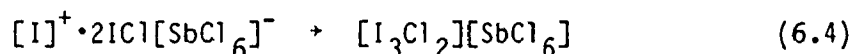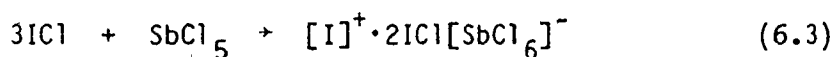
Since the preparation was initially carried out using the stoichiometry shown in equation (6.2), there is only one mole of ICl available per mole of $SbCl_5$, and not three moles, as the stoichiometry of equation (6.3) requires. Thus the $[I_3Cl_2]^+$ cation forms despite a shortage of ICl. These are just the conditions under which the $[I_2Cl]^+$ cation might have been expected to have been produced. It therefore seems unlikely that the formation of $[I_2Cl][SbCl_6]$ would result from the reaction of ICl with an excess of $SbCl_5$, as has been reported.[37] It is interesting to note that the Raman spectrum of the material produced from the reaction of ICl with excess $SbCl_5$ is the same as that reported here for $[I_3Cl_2][SbCl_6]$. In a separate experiment it was also shown that the reaction of ICl with $SbCl_5$ in a 3:1 ratio also produces $[I_3Cl_2][SbCl_6]$ and this has been confirmed subsequently by Pohl and Saak [149] who determined the crystal structure of $[I_3Cl_2][SbCl_6]$ which was prepared using this method.

The reaction of I_2 with $SbCl_5$ in excess Cl_2 at $-78°C$ reported by Shamir and Lustig [38] to produce $[I_2Cl][SbCl_6]$ is very complex. In view of the information obtained from single crystal X-ray measurements here it appears that this material is in fact $[I_3Cl_2][SbCl_6]$, and this has recently been acknowledged by the original authors.[150] When this particular reaction was repeated it was noted that a yellow solid remained behind when the excess liquid Cl_2 was removed at $-78°C$. After warming to room temperature this solid quickly turned black. Also, while it was reported that the reaction was nearly quantitative it was found in this work that the $I_2/SbCl_5$ mixture had to be treated with liquid Cl_2 at least three times in order to ensure complete reaction. In order to identify this yellow solid which is formed initially at low temperature the Raman spectrum of the reaction mixture was measured at $-196°C$, immediately after the Cl_2 had been removed at $-78°C$. This is shown in Figure 6.4. There is evidence for the presence of I_2Cl_6 since the lines at 342, 312 and 197 cm^{-1} are very close to the frequencies of the three most intense bands of I_2Cl_6 [156] (344, 314 and 198 cm^{-1}). The lines at 367, 360, 266 and 170 cm^{-1} are also observed in the Raman spectrum of $SbCl_5$ at $-196°C$.[157] Thus at low temperature the sample appears essentially to be a mixture of I_2Cl_6 and $SbCl_5$. If a small amount of $[I_3Cl_2][SbCl_6]$ has formed, the lines of its spectrum are masked by those of the former two constituents. After warming to room temperature for a few hours the same sample exhibits a Raman spectrum identical to that of $[I_3Cl_2][SbCl_6]$. There is no evidence for the formation of $[ICl_2][SbCl_6]$ which is usually produced by the reaction of I_2Cl_6 with excess $SbCl_5$.[75]
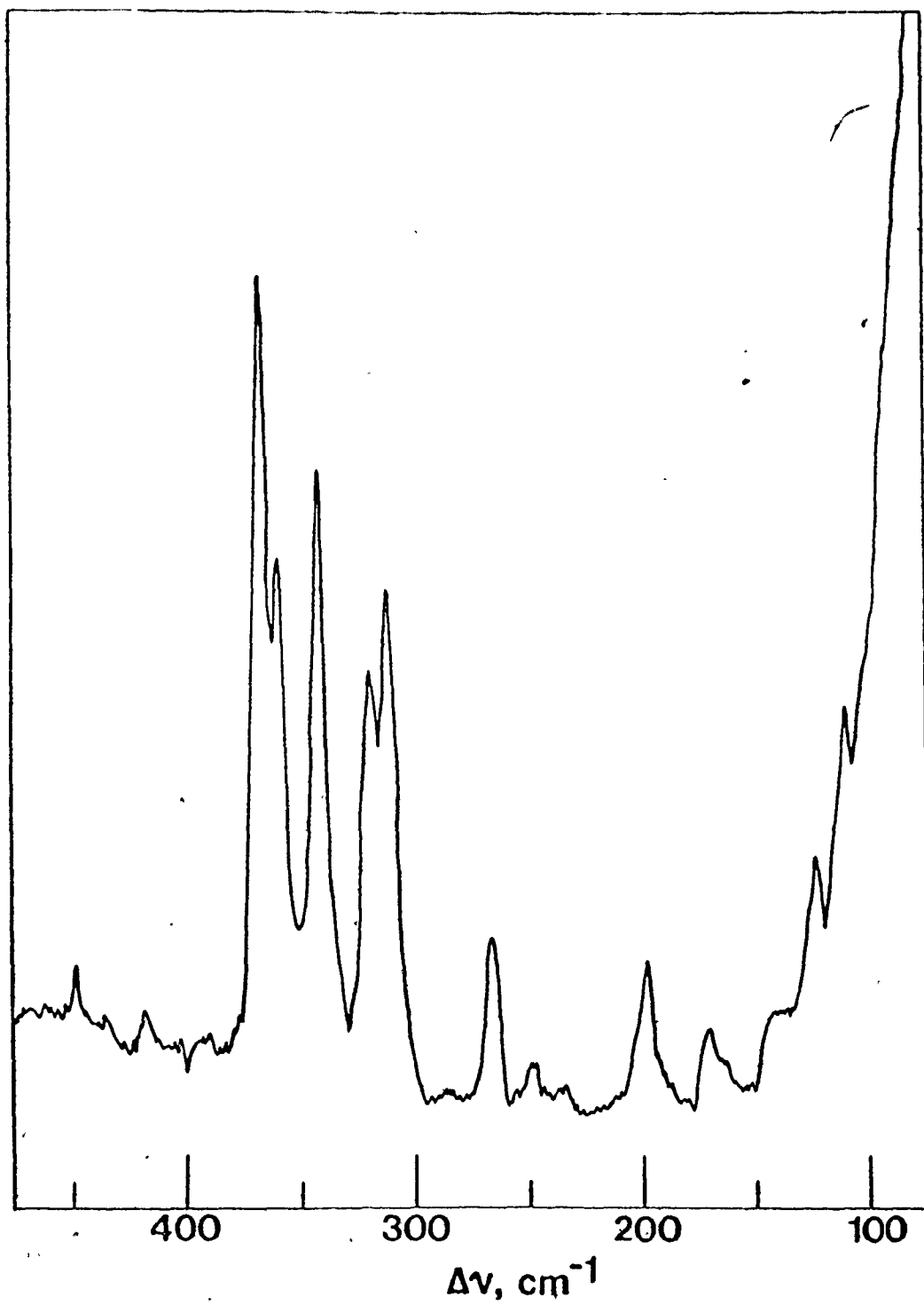
Figure 6.4.   Raman spectrum of I_2 + $SbCl_5$ + Cl_2 (after removing excess liquid Cl_2) at -196°C using 5145 Å excitation.

Had there been evidence in the Raman spectrum of the reaction mixture for the formation of ICl (ν I-Cl, 384 cm^{-1}), the subsequent formation of $[I_3Cl_2][SbCl_6]$ could be envisioned to occur by the same mechanism as suggested previously. Also, since there is no $[ICl_2][SbCl_6]$ formed, one possible explanation for the formation of the observed product is that as the reaction mixture begins to warm, the I_2Cl_6 formed at low temperature dissociates. The I_2 and Cl_2 may recombine to form ICl, ultimately producing $[I_3Cl_2]^+$ by interacting with $SbCl_5$ as discussed above.

In addition to the crystallographic and Raman evidence presented above it was found that the visible absorption spectrum of $[I_3Cl_2][SbCl_6]$ in SO_2 has a band maximum at 440 nm. This is very close to the band maximum of 450 nm which has been previously reported for $[I_2Cl][SbCl_6]$.[38]

The preparation of $[I_2Cl][SbCl_6]$ has also been reported by several other authors. Corbett et al.[39,40,158,159] have reported the results of phase studies on $I_2/ICl/SbCl_5$ mixtures which indicate the presence of $[I_2Cl][SbCl_6]$. They also interpret their [35]Cl and [127]I NQR measurements as being consistent with this formulation. The work described in this Chapter has however cast considerable doubt on the existence of $[I_2Cl][SbCl_6]$, at least in so far as it was reported by other workers.[37,38] There is still no X-ray crystallographic evidence for the existence of any asymmetric $[I_2X]^+$ or $[XIY]^+$ interhalogen cation of iodine. In Chapter 5 the X-ray crystal structure of $[IBr_2][Sb_2F_{11}]$ was described. It was the product of a reaction initially designed to prepare $[IBr]^+$, another asymmetric cation, whose existence still has not been established. Also the X-ray crystal structure of

$[IBr_{0.75}Cl_{1.25}][SbCl_6]$ was described and it was concluded to be primarily a crystallographic mixture of the symmetric $[IBr_2]^+$ and $[ICl_2]^+$ cations although the presence of some $[BrICl]^+$ could not be ruled out. In this Chapter it has been suggested that the $[I]^+$ initially formed during a chemical reaction (equation (6.3)) is stabilized by two moles of ICl to produce $[I_3Cl_2]^+$, rather than by one mole to produce $[I_2Cl]^+$. It is difficult to determine whether the driving force behind this behaviour is the preference of iodine to maintain some degree of symmetry in the cation, e.g. $[IX_2]^+$, $[I_2]^+$, $[I_3Cl_2]^+$, etc., or that being the least electronegative halogen iodine wants to form bonds to as many other atoms as is possible. This would make the central positions in these cations more desirable than terminal positions. This observation seems to be contrary to the conclusions of Aubke and co-workers [27] and others [38,158] who suggest that asymmetric interhalogen cations are thermodynamically more stable than are the symmetric cations. It is possible that these asymmetric cations do exist in solution and in the molten state where they can be stabilized by additional interactions with solvent or neighbouring molecules, however conclusive proof in the solid state can only be provided by an X-ray crystal structure determination.

(iii) Mössbauer Spectroscopy

The ^{127}I Mössbauer spectrum of $[I_3Cl_2][SbCl_6]$ is shown in Figure 6.5 and the Mössbauer parameters are, for the central iodine site: $e^2q^{127}Q_g/h = -2917(50)$ MHz, isomer shift $= -0.96(9)$ mms^{-1} (relative to KI); and for the outer two iodine atoms $e^2q^{127}Q_g/h = -2490(22)$ MHz,

isomer shift = -0.85(4) mms^{-1} (relative to KI), and eta = 0.69(2). The value of χ^2/degree of freedom was 1.18, T_A = 0.54(2) and the absorber line width was 1.73 mms^{-1} for both sites. In the initial stages of the fitting procedure the contributions of the two different iodine sites were fixed at their respective molar compositions. In the final stages of the fitting procedure this constraint was removed and the relative contribution refined to 0.30, which compares to the value of 0.33 expected from the formula.

The quadrupole coupling constant for the central iodine site in $[I_3Cl_2][SbCl_6]$ is significantly larger than that which has been measured for the central iodine site in $Cs[I_3]$, which is -2515 MHz.[61] The average I-I bond distance [4] in $Cs[I_3]$ is 2.93A while the analogous distance in $[I_3Cl_2]^+$ is 2.9057(6)A. The shorter bond distance in the latter compound probably contributes to the larger quadrupole coupling constant observed, however as was discussed previously the central iodine atom in the $[I_3Cl_2]^+$ cation bears a net charge of about +0.2. This would cause a larger p-electron imbalance and hence coupling constant than is found for the $[I_3]^-$ anion. Presumably this factor also contributes to the rather negative isomer shift of -0.96 mms^{-1} measured for the central iodine site.

The other iodine site in $[I_3Cl_2]^+$ consists of the two outer iodine atoms which have a very unusual geometry. The geometry around these two iodine atoms may be viewed according to VSEPR [18] as a very distorted trigonal bipyramid such that there is one fairly strong I-I interaction in the equatorial plane along with two lone pairs of
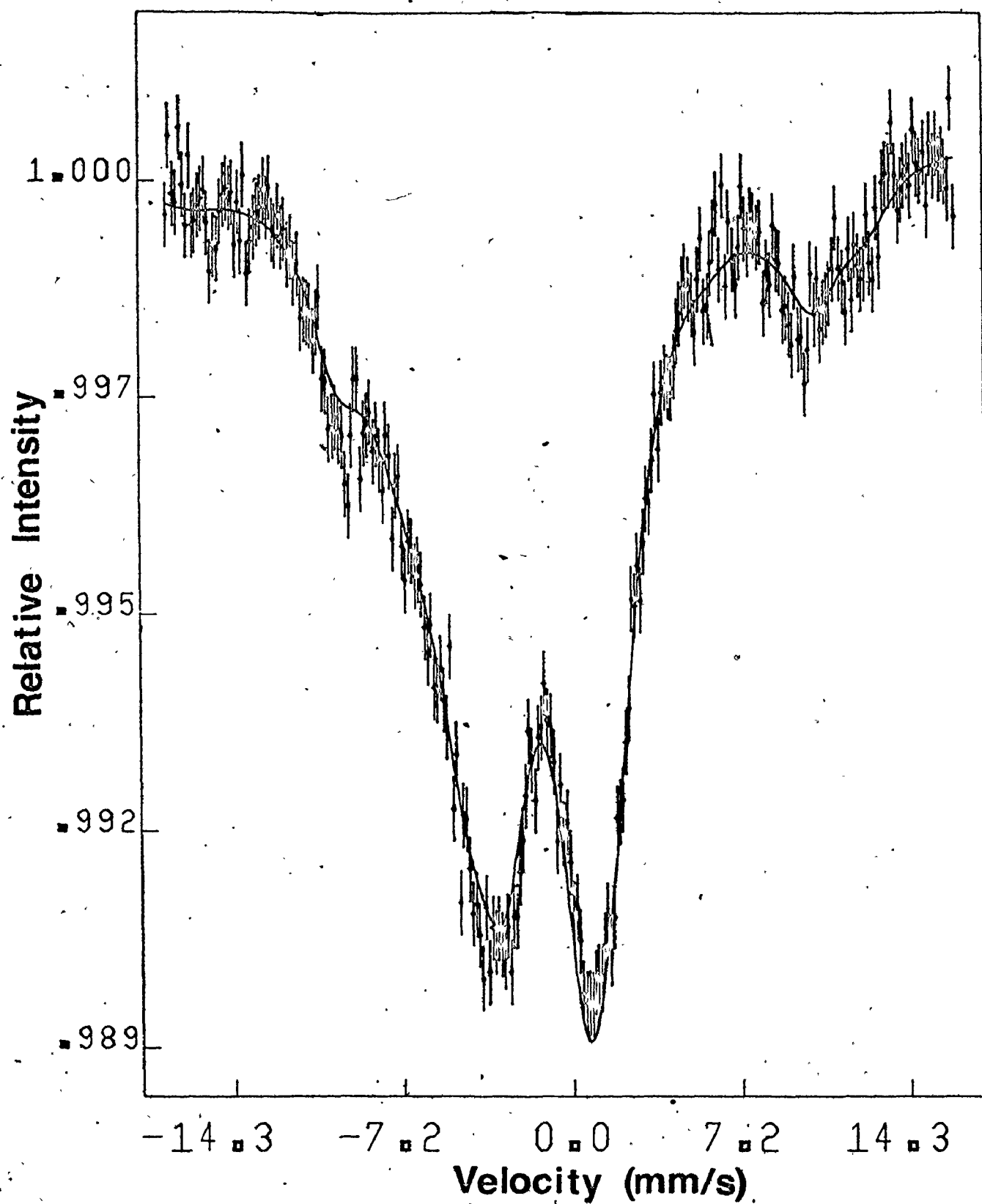
Figure 6.5. ^{127}I Mössbauer spectrum of $[I_3Cl_2][SbCl_6]$ measured at 4.2° K. The solid line represents the best fit to the experimental data.

electrons, and one strong and one weak axial I-Cl interaction. This distorted geometry accounts for the large eta value of 0.69 measured for this site. An eta value this large leads to some ambiguity in the sign of $e^2q^{127}Q_g/h$ but the choice of a negative coupling constant resulted in the best computer fit to the spectrum. The quadrupole coupling constant for this site was -2490 MHz which is significantly smaller than that measured for the central iodine site. This at first glance seems unusual since the central iodine site has only two I-I interactions while the other two iodine atoms have one each of an I-Cl and an I-I interaction as well as an additional weak I---Cl interaction. However in VSEPR terminology [18] the central iodine site has two axial bonding electron pairs and three equatorial non-bonded electron pairs which create a large positive electric field gradient. The other iodine site has a geometry consisting of two axial bonding electron pairs (although one is weak), two equatorial non-bonded pairs, and one equatorial bonding pair. This geometry presumably does not create as large an electric field gradient as that of the central site since the bridging I---Cl bond does not remove a significant amount of p-electron density from the iodine atom. Also the principal axis of the electric field gradient is not as clearly defined as in the central site, hence the large eta value. The central iodine atom in $[I_3][AsF_6]$ has a similar geometrical arrangement to the two outer iodine atoms in $[I_3Cl_2]^+$, at least in terms of the strong interactions, and the quadrupole coupling constants can be compared. The sign of $e^2q^{127}Q_g/h$ is positive in the former compound, however the ·

magnitude of $e^2q^{127}Q_g/h$ is similar (2267 MHz compared to -2490 MHz). The isomer shift for the outer two iodine atoms in $[I_3Cl_2]^+$ is -0.85 mms^{-1}, which is reasonable since the s-electron density should be fairly high, and is comparable to that for the central iodine in $[I_3]^+$ which is -0.59 mms^{-1}.

CHAPTER 7

^{127}I Mössbauer Studies of Some Chalcogen-Iodine Cations

A. Introduction

Compounds between sulfur and iodine were for a long time thought not to exist.[161] However Passmore and co-workers [87-90] and others [162-165] have recently been successful in isolating compounds containing sulfur-iodine bonds. Many of these novel compounds have been characterized by X-ray crystallography, but hitherto very little spectroscopic information on these interesting compounds has appeared. The iodine-sulfur system has also been extended further down group(VI) and there are now also examples of cationic species in which iodine is bonded to selenium [91] and tellurium.[93]

The iodine-chalcogen cations provide a nice series of well characterized compounds whose ^{127}I Mössbauer spectra may provide more detailed information about the nature of the bonding at the iodine atom. This is the first series of compounds in this thesis where iodine is not bonded to other halogen atoms and hence it will be interesting to compare the Mössbauer parameters with those obtained previously for the other compounds. The electrons in the bonds of these chalocogen-iodine compounds should be less polarized than in the interhalogen compounds since the electronegativities of iodine and the chalcogens are similar.

The Mössbauer parameters obtained for $[I_2][Sb_2F_{11}]$ will also provide a useful comparison to some of these compounds in terms of the structures involved. Finally the Mössbauer parameters of these compounds will be compared to those for an organo-sulfur iodide whose iodine-129 Mössbauer spectrum has been measured.[119]

B. Results and Discussion

The ^{127}I Mössbauer parameters for the compounds studied are summarized in Table 7.1 and the corresponding spectrum of $[S_7I][SbF_6]$ is shown in Figure 7.1. The isomer shifts of all these compounds are negative with respect to the reference compound KI and since $\delta R/R$ is negative for ^{127}I this means that the s-electron density at the iodine nucleus is higher in the former compounds than in KI. This could be achieved by the removal of p-electrons from the iodine atom as a result of bonding to the chalcogen atom, and since p-electrons shield the s-electrons, their removal would cause an increase in the effective s-electron density. Also if the positive charge of these cations resides to any extent on the iodine atom then the s-electrons will be contracted more strongly than the p-electrons, also resulting in a higher s-electron density at the iodine nucleus. Both of these effects could be operating simultaneously. The range of isomer shifts observed here are very similar to those which were measured for the linear iodine compounds in Chapter 4.   What appears clear here is that the bonding to iodine in the chalcogen-iodine cations is principally of p-character and that there is little involvement of the iodine 5s-electrons in the bonding to the

Table 7.1.

127-Iodine Mössbauer Data for Some Chalcogen Cations of Iodine

Compound	Isomer shift (mms^{-1})	$e^2q^{127}Q_g/h$ (MHz)	Γ (mms^{-1})	η	T_A	χ^2/degree of freedom	U_p	h_s $(h_p=U_p)$	h_p $(h_s=0)$
$[S_7I][AsF_6]$	-0.70(3)	-2453(19)	1.64(10)	-	1.27(8)	0.92	1.07	0.02	0.95
$[S_7I][SbF_6]$	-0.63(2)	-2453(11)	1.45(7)	-	0.85(3)	1.04	1.07	0.04	0.84
$[(S_7I)_4S_4][AsF_6]_6$	-0.68(2)	-2490(11)	1.25(6)	-	3.66(23)	3.29	1.09	0.03	0.92
$[(S_7I)_2][SbF_6]_3 \cdot 2AsF_3$	-0.69(8)	-2453(56)	1.78(18)	-	0.14(1)	1.00	1.07	0.02	0.93
	-0.60(16)	-2490(91)					1.09	0.05	0.79
$[S_2I_4][AsF_6]_2$	-0.80(3)	-2193(19)	2.65(13)	0.70(2)	1.16(4)	1.45	0.96	-0.03	1.11
$[Se_2I_4][AsF_6]_2$	-0.53(6)	-2360(37)	1.68(21)	0.19(4)	0.66(8)	0.83	1.03	0.06	0.67
	-0.53(6)	-2360(35)	1.77(22)	-	0.62(7)	0.85			
$[SeI_3][SbF_6]$	-0.54(8)	-2509(50)	2.00(30)	-	0.55(7)	0.77	1.09	0.07	0.67
$[TeI_3][AsF_6]$	-0.51(4)	-2026(19)	1.73(13)	-	0.76(5)	1.08	0.88	0.04	0.64
I_2	-0.49(2)	-2137(11)	1.99(7)	0.22(1)	0.84(2)	1.22	0.93	0.05	0.61
$[I_2][Sb_2F_{11}]$	-0.68(1)	-1951(11)	1.72(7)	0.19(2)	0.72(2)	1.03	0.85	0.01	0.92
KI	0	0	-	-	-	-	-	-	-
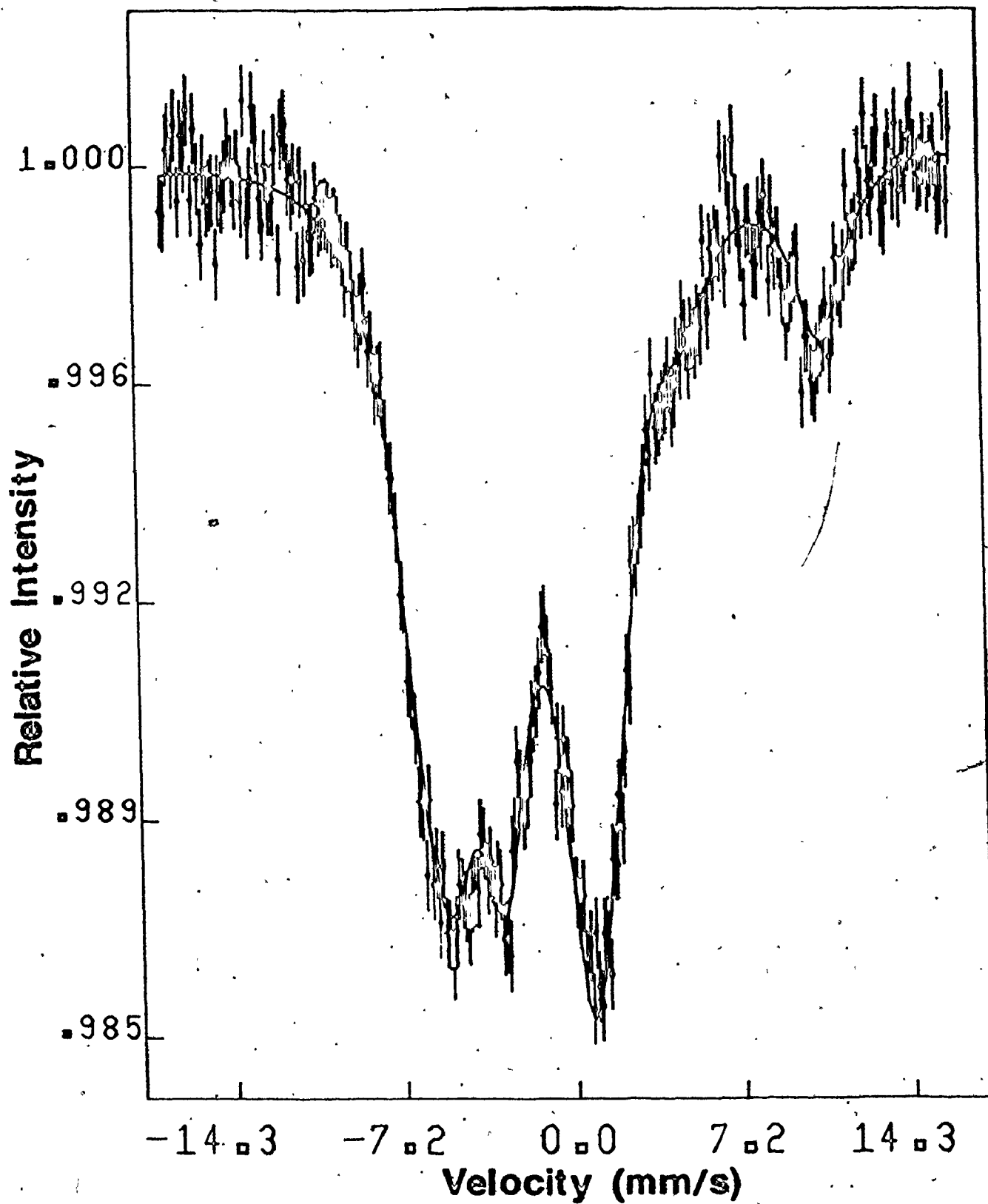
Figure 7.1. ^{127}I Mössbauer spectrum of $[S_7I][SbF_6]$ measured at 4.2°K. The solid line represents the best fit to the data.

chalcogen atom. If the s-electrons were involved to any extent in the bonding, a more positive isomer shift with respect to KI would be expected, as in say KIO_4 where the s-electrons are clearly involved in the bonding.

The compounds which contain the $[S_7I]$ unit (Table 7.1) have structures in which the exocyclic S-I distances are nearly constant at 2.347(6) to 2.355(7)Å. Secondary I---F contacts which range from 2.926(9) to 2.99(3)Å in these compounds complete an essentially linear S-I---F arrangement. The Mössbauer parameters for the exocyclic iodine atom in these compounds are essentially the same. The isomer shift of the iodine atom in these $[S_7I]^+$ compounds is more negative than that found for the iodide anion and could be the result of the different charges on the iodine; positive in the former and negative in the latter case. The $[S_7I]^+$ cations all have large negative quadrupole coupling constants, indicating a non-spherical distribution of electrons about the iodine, whereas the iodide anion has a spherical distribution of electrons and hence there is no electric field gradient. The quadrupole coupling constants measured for these compounds are up to 20% smaller than those of the linear $[X-I-Y]^-$ anions. This is mainly because in the $[X-I-Y]^-$ anions the iodine atom is bonded to electronegative halogen atoms while in the sulfur-iodine compounds the primary bond is to an atom of similar electronegativity. Since the quadrupole coupling constants are negative for the sulfur-iodine compounds there is an excess of electron density in the xy plane about the iodine atom compared to the z direction which is taken to be along the S-I---F internuclear axis. From

the measured values of $e^2q^{127}Q_g/h$, U_p, the p-electron imbalance can be

calculated using equation (1.25) and these values are found in Table 7.1.

For the $[S_7I]^+$ compounds $U_p > 1$ indicating that the iodine has had

slightly more than one p-electron removed from the noble gas electron

configuration of I^-. This removal of p-electrons from the iodine is

consistent with the observed increase in s-electron density compared to

the iodide anion as reflected by the more negative isomer shifts. If the

assumption is made that $U_p = h_p$ then one can calculate h_s from expression

(4.6) which leads to small positive values for h_s in all cases but one.

An alternative approach is to assume that there is no s-electron

contribution to the bond between iodine and sulfur and one can then use

the measured isomer shift to calculate h_p from expression (4.6). These

values are also found in Table 7.1 and although the agreement between h_p

calculated from expression (4.6) and U_p calculated from the quadrupole

coupling constants is reasonable in a few cases, there are large

discrepancies in a number of cases. Thus as was concluded in previous

Chapters these semi-empirical correlations do not have the general

applicability that has hitherto been assumed.

The quadrupole coupling constants are also much more negative

than those measured for molecular species such as CH_3I and CF_3I [55] and

are more like the value found for the central iodine in $[I_3]^-$.[61] The

secondary I---F interaction in these $[S_7I]^+$ cations is rather long at

2.96Å (cf. I---F in $[ICl_2][SbF_6]$, 2.650Å) but plays a significant part in

influencing the distribution of electrons about the iodine, keeping it in

an essentially linear arrangement. Potasek [119] has measured the 129-

iodine Mössbauer spectrum of $RS^{129}I$ (R = N-p-chlorophenyl-2-(benzyl-oxycarbonamide)-3-methylbutanamide) and found $^{129}\delta_{ZnTe}$ = -0.41 mms^{-1} and $e^2q^{129}Q_g/h$ = -1510 MHz. After conversion [113] to their 127-iodine equivalents ($^{127}\delta_{ZnTe}$ = -0.14 mms^{-1} and $e^2q^{127}Q_g/h$ = -2153 MHz) their values resemble those found for the RI (R = CH_3, CF_3, etc.) compounds [55] rather than the cations reported here. This is consistent with the molecular nature of the RI and RSI compounds compared to the charged species discussed here where strong cation-anion interactions occur.

The second iodine site in the compound $[(S_7I)_2I][SbF_6]_3 \cdot 2AsF_3$ has a slightly less negative isomer shift but similar quadrupole coupling constant compared to the values found for exocyclic iodine atom in the $[S_7I]^+$ cations. This indicates that there is a somewhat lower s-electron density at the central iodine in $[(S_7I)-I-(S_7I)]$ than for the S_7-I---F iodine. This perhaps indicates that there is less positive charge on this central, bridging iodine than on the exocyclic iodine, since the degree of p-character in the bonding of these iodines is approximately the same.

X-ray crystallography has shown that $[S_2I_4][AsF_6]_2$ has the novel distorted right triangular prismatic structure with one S_2 unit asymmetrically bonded to two I_2 units: S-S, 1.828(11)Å; I_1-I_2, 2.597(2)Å; S-I_1, 2.858(6)Å; S-I_2, 3.195(6)Å.[88] Preliminary X-ray data indicates that $[Se_2I_4]^{2+}$ has a similar structure.[91] An attempt was made to fit the spectra of these compounds to two unique iodine sites, but with little success; the Mössbauer fitting program diverges after only a few cycles. Suitable refinement of the spectra occurred when only one

site was incorporated in the fitting procedure, and when the value of the asymmetry parameter, η was allowed to vary in the case of $[S_2I_4]^{2+}$. The x^2 value for the latter refinement is somewhat high, although not unusual, perhaps suggesting that the bulk sample contained a small amount of impurity or decomposition product which of course would not be present in the single crystal selected from the bulk material and used for the X-ray structure analysis. The selenium analog gave a much better spectrum and a good fit to the data was obtained; when the value of eta was allowed to vary a marginally improved fit was obtained. This may be because the asymmetry parameter is compensating for the presence of two slightly different iodine environments which are probably present in the compound. The isomer shifts of the $[S_2I_4]^{2+}$ and $[Se_2I_4]^{2+}$ cations are similar to those found for the exocyclic site in the $[S_7I]^{+}$ containing species, but in view of the structures of these cations the $[I_2]^{+}$ cation provides a better comparison.

The discussion will therefore digress at this point to interpret the Mössbauer parameters of $[I_2][Sb_2F_{11}]$. Oxidation of iodine with antimony pentafluoride produces $[I_2][Sb_2F_{11}]$ whose vibrational spectra and crystal structure have been reported.[17] Analysis of the Mössbauer spectrum of this compound gives an isomer shift which is more negative and a quadrupole coupling constant which is smaller than in molecular iodine (Table 7.1). The more negative isomer shift in $[I_2]^{+}$ means that the s-electron density at iodine has increased. The most reasonable interpretation of the changes which occur on oxidation is based upon a molecular orbital description. The M.O. description for I_2 is such that

there is one net $\sigma(p_z)$ bond, i.e., $\sigma g^2(p_z)\pi_u^2(p_x)\pi_u^2(p_y)\pi_g^{*2}(p_x)\pi_g^{*2}(p_y)$. Oxidation results in the removal of a π_g^* electron from a p-π orbital and the I-I distance shortens from 2.66 to 2.55A.[17] This removal of a p-π electron deshields the 5s-electrons, increases the s-electron density, and the isomer shift becomes more negative. The net positive charge of the $[I_2]$ unit also causes the s-electrons to contract more relative to the p-electrons resulting in an effectively higher s-electron density. Removal of this antibonding π electron means that the I-I bond has acquired π character. The p-electron imbalance U_p is related to the electron occupation numbers U_x, U_y and U_z of the p_x, p_y and p_z orbitals by equation (1.26), i.e. $U_p = -U_z + 1/2(U_x + U_y)$. For each iodine in the iodine molecule then U_p becomes equal to $-U_z + 2$ while for $[I_2]^+$, $U_p = -U_z + 1.75$. Since n is small, $U_x = U_y = 1.75$. U_p is therefore reduced and a decrease in $e^2q^{127}Q_g/h$ to -1951 MHz for $[I_2]^+$ is observed. This gives a value of U_p of 0.85 (Table 7.1) and U_z is therefore 1.75 - 0.85 = 0.90. Using these values for U_x, U_y and U_p, the value for h_p, the number of p-electron holes can be calculated from equation (1.28), i.e. $h_p = 6 - (U_x + U_y + U_z) = 1.60$. Calculation of h_p using equation (4.6) gives a value of 0.92 which is not in very good agreement with the h_p value estimated above.

Passmore and co-workers [90] have estimated that each $[I_2]$ unit in $[S_2I_4]^{2+}$ has a charge of +2/3 and hence the Mössbauer parameters for $[S_2I_4]^{2+}$ and presumably $[Se_2I_4]^{2+}$ would be expected to lie between those of I_2 and $[I_2]^+$. In fact the isomer shift for the iodine atoms in $[S_2I_4]^{2+}$, assuming one site only, is more negative than that of $[I_2]^+$.

This suggests that the charge on each of the $[I_2]$ units in $[S_2I_4]^{2+}$ is greater than +2/3. $[Se_2I_4]^{2+}$ however has an isomer shift between that of I_2 and $[I_2]^+$ indicating a higher s-electron density than in I_2 but lower than in $[I_2]^+$. The quadrupole coupling constant of $[S_2I_4]^+$ is nearly the same as that found for iodine suggesting that the degree of p-electron participation in the bonding is the same. For the selenium analog the quadrupole coupling constant is much larger, indicating a greater p-electron imbalance at iodine and this is consistent with the more positive isomer shift also observed. Presumably there is better orbital overlap between the orbitals of selenium and iodine than sulfur and iodine, thereby allowing the charge on $[Se_2I_4]^{2+}$ to be more delocalized.

The remaining two cations $[SeI_3]^+$ and $[TeI_3]^+$ may be compared to the isoelectronic group (V) tri-iodides, AsI_3, SbI_3 and BiI_3 whose 129-iodine Mössbauer spectra have been measured.[166] In the trigonal pyramidal $[TeI_3]^+$ cation the average Te-I bond is 2.667(1)A and the I-Te-I bond angle is 99.90(3)°.[93] Secondary contacts between tellurium and fluorine atoms of the anion are also present at 2.88(1)A completing a pseudo-octahedral geometry around tellurium. $[SeI_3][AsF_6]$ [92] is isomorphous and probably isostructural with $[TeI_3][AsF_6]$. The structures of the neutral group (V) tri-iodides, AsI_3,[167] SbI_3,[168] and BiI_3 [168] are similar to that of $[TeI_3][AsF_6]$ where secondary contacts from tellurium to fluorine atoms of the anions have been replaced by long interactions from the central metal atom to iodine atoms of adjacent molecules. In AsI_3 and SbI_3 the arsenic and antimony atoms are significantly displaced from the centres of the iodine octahedra and have three short contacts to

iodine at 2.556(4) and 2.68(10)Å respectively. The octahedra are completed by secondary contacts to iodine at 3.50 and 3.316Å respectively. In BiI_3 however, the bismuth atom is situated at the centre of the iodine octahedron (Bi-I, 3.1Å) so that the lone pair of electrons is stereochemically inactive in this compound. One might then expect similar Mössbauer parameters for these two series of compounds since the same gross structure is observed by both systems and any differences could perhaps be attributed to the difference in charge and/or to the nature of the secondary contacts to iodine. Since the iodine atoms in $[TeI_3]^+$, and presumably also in $[SeI_3]^+$, are nearly the same distance from the central element the spectra were fitted assuming only one iodine environment. The isomer shifts are similar to those of the other cations reported in Table 7.1, but are more negative than the shifts [166] for AsI_3, SbI_3 and BiI_3 (mean -0.34 mms^{-1}), after these have been converted from their ^{129}I values.[113] This is probably due to the charge on the cation which contracts the s-orbitals, thereby increasing the effective s-electron density.

Okuda et al. [169] have reported ^{127}I NQR data for TeI_4 while Jones and Mauguin [170] have recently reported the ^{129}I Mössbauer spectrum of TeI_4 as well as of several other tellurium-iodides. The latter workers were able to resolve three independent iodine sites a result which is consistent with the X-ray crystal structure of TeI_4.[171] The terminal iodine atom in TeI_4 was found to have a quadrupole coupling constant of 1190 MHz and an isomer shift with respect to the ZnTe source of 0.70 mms^{-1}. The second site which was assigned to the iodine which

bridges two tellurium atoms had $e^2q^{129}Q_g/h$ = 600 MHz, n = 1.0 and the isomer shift was 0.30 mms^{-1}. The final site which corresponds to the iodine atom which bridges three tellurium atoms showed no quadrupole coupling and the isomer shift was 0.40 mms^{-1}. The first site in TeI$_4$, i.e. the terminal iodine atoms provide the best comparison with [TeI$_3$]$^+$ and after conversion [113] to their 127-iodine equivalents $e^2q^{127}Q_g/h$ = 1700 MHz and the isomer shift with respect to KI is -0.10 mms^{-1}. The isomer shift of the [TeI$_3$]$^+$ cation is more negative than the neutral compound and as was mentioned earlier the s-orbitals of the iodine atom are contracted in the cation causing a higher effective s-electron density and hence a more negative isomer shift. The quadrupole coupling constant of iodine in [TeI$_3$]$^+$ is somewhat larger than the converted coupling constant of TeI$_4$. This indicates a larger p-electron imbalance in the former compound and is caused by the removal of more p-electron density in [TeI$_3$]$^+$ because of the shorter Te-I bond. The Te-I bond distances in [TeI$_3$]$^+$ average 2.667Å [93] while in TeI$_4$ [171] the average terminal Te-I bond distance is 2.768Å.

The quadrupole coupling constant of [SeI$_3$]$^+$ is substantially more negative, than that of [TeI$_3$]$^+$, which is consistent with the higher electronegativity of the central atom in the former compound. However, both compounds have quadrupole coupling constants which are significantly larger than those found for the neutral group (V) tri-iodides. Since the iodine environments are essentially the same in both the neutral and charged species the larger quadrupole coupling constant in the latter compounds must be a consequence of the positive charge and smaller size

of the group (VI) cation compared to the isoelectronic group (V) neutral species. Both of these factors contribute to the shorter M-I bond observed in the cationic species creating a larger electric field gradient and hence a more negative quadrupole coupling constant in the cations. The Mössbauer parameters of $[TeI_3]^+$ and $[SeI_3]^+$ clearly indicate that there is considerable p-character in the M-I bonds.

CHAPTER 8

Application of ^{127}I Mössbauer Spectroscopy to Chemical Problems

A. Introduction

The previous Chapters in this thesis have dealt with the examination of the Mössbauer parameters of some series of iodine compounds in order to try and understand the factors which affect these parameters and also to determine the type of bonding which takes place in the various compounds. Several new interhalogen cations of iodine were prepared and characterized and their Mössbauer spectra were measured. During the course of this work it also became possible to utilize ^{127}I Mössbauer spectroscopy to help sort out some interesting chemical problems and this Chapter will present these results.

The nature of the colour change which occurs on cooling solutions of the $[I_2]^+$ cation in various solvents has puzzled chemists for some time. Measurements of the ^{127}I Mössbauer spectrum of frozen solutions of $[I_2][Sb_2F_{11}]$ in HSO_3F together with some recent work of Gillespie and Kapoor have elucidated the nature of the species formed at low temperature.

The relative electronegativity of the $-OTeF_5$ ligand with respect to fluorine has been speculated upon a number of times recently and because of the extensive chemistry which is developing with this $-OTeF_5$ ligand it is important that its electronegativity be established. ^{127}I

Mössbauer spectroscopy in conjunction with ^{129}Xe Mössbauer and ^{125}Te and ^{129}Xe NMR spectroscopy have conclusively established the electronegativity of the -OTeF$_5$ group.

(i) The $[I_4]^{2+}$ Cation

Iodine has been known for many years to produce deep blue solutions in 65% oleum and it was initially thought that the blue colour was due to the I^+ cation.[95] However it was firmly established in 1966 that the species in solution is in fact $[I_2]^+$. Since then the $[I_2]^+$ cation has been characterized by X-ray crystallography [17] in the $[Sb_2F_{11}]^-$ salt, by its characteristic resonance Raman spectrum [172] and by magnetic susceptibility measurements, [29,173] which have established its paramagnetism. Aubke and co-workers [173] have recently developed an improved synthesis for $[I_2][Sb_2F_{11}]$ and re-affirmed the existing magnetic susceptibility data. It was noticed early on that as solutions of $[I_2]^+$ were cooled, the colour changed from an intense blue to a deep red-brown near the freezing point of the solution and this colour change was monitored by uv-visible absorption spectroscopy.[174] Aubke and co-workers [173] have re-examined the susceptibility data of $[I_2][Sb_2F_{11}]$ and observed a drop in the susceptibility with temperature which was too large to be attributed to a temperature independent contribution (TIP) and which they have accounted for by suggesting that there is an interaction of an antiferromagnetic nature between contiguous $[I_2]^+$ cations in the solid lattice. The crystal structure of $[I_2][Sb_2F_{11}]$ [17] is consistent with this interpretation since the $[I_2]^+$ cations are not insulated by

intervening diamagnetic atoms, and are aligned in chains along the c axis of the monoclinic crystals so that the closest intermolecular distance is 4.29Å. Also, while the magnetic moment of solid $[I_2][Sb_2F_{11}]$ is 2.0 ± 0.1 BM [29] which indicates the presence of one unpaired electron, the magnetic susceptibility of an $I_2/S_2O_6F_2$ solution [174] was found to decrease with decreasing temperature until the species formed at low temperature becomes diamagnetic. Thus in the solid state where the ions are not free to move there seems to be an antiferromagnetic.ordering of the electron spins while in solution, where the ions are mobile, a significant interaction between pairs of $[I_2]^+$ cations occurs with a concomitant pairing of electrons. It is the structure of this species formed in solution at low temperature which has been the subject of controversy for some time. It has been suggested that the $[I_2]^+$ cation dimerizes extensively at low temperature to produce a diamagnetic $[I_4]^{2+}$ cation. There are at least three possible structures which the $[I_4]^{2+}$ cation could adopt: a tetrahedral structure, a rectangular-planar structure, and an acyclic chain structure might be reasonable. Since the sign of $e^2q^{127}Q_g/h$ and η can be determined from ^{127}I Mössbauer spectra, the principal axis of the electric field gradient and hence the geometry around the iodine atom may also be determined. The possible structures suggested above for the dimer would be expected to give rise to quite different ^{127}I Mössbauer spectra.

B. Results and Discussion

(i) The $[I_4]^{2+}$ Cation

The ^{127}I Mössbauer parameters of $[I_2][Sb_2F_{11}]$ and a frozen solution of $[I_2][Sb_2F_{11}]$ in HSO_3F are found in Table 8.1. The corresponding spectra are shown in Figures 8.1 and 8.2 respectively. The Mössbauer spectrum of the solid $[I_2][Sb_2F_{11}]$ was measured using approximately 400 mg of sample which was thoroughly mixed with dried teflon powder. The solution sample was prepared by dissolving $[I_2][Sb_2F_{11}]$ in HSO_3F and syringing it into the Kel-F sample holder. The holder was then cooled slowly to ensure that the blue solution turned completely red, and then it was frozen in liquid nitrogen. This procedure was repeated on a second sample to ensure that the Mössbauer parameters obtained were reproducible and that maximum conversion from monomer to dimer had been achieved.

The $[I_2][Sb_2F_{11}]$ was prepared [17] by the reaction of I_2 with SbF_5 in SO_2 solvent according to equation (8.1).

$$2I_2 + 5SbF_5 \rightarrow 2[I_2][Sb_2F_{11}] + SbF_3 \qquad (8.1)$$
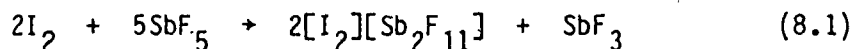
It was found however that in order to produce pure $[I_2][Sb_2F_{11}]$, as shown by its Raman spectrum, at least a 10-15% excess of SbF_5 over the 2.5:1 ratio of $SbF_5:I_2$ is required and furthermore the mother liquor should be decanted from the first crop of crystalline material obtained.

The Mössbauer parameters obtained for $[I_2][Sb_2F_{11}]$ were discussed in Chapter 7. As Figure 8.1 shows, transition no. 2 is well resolved at positive velocity indicating that $e^2Q^{127}Q_g/h$ is negative

Table 8.1.

^{127}I Mössbauer Parameters of $[I_2][Sb_2F_{11}]$ and Related Species

Compound	Isomer shift (mms^{-1})	$e^2q^{127}Q_g/h$ (MHz)	Γ (mms^{-1})	η	T_A	χ_2/degree of freedom
$[I_2][Sb_2F_{11}]$	-0.68(1)	-1951(11)	1.72(7)	0.19(2)	0.72(2)	1.02
$[I_2][Sb_2F_{11}]/HSO_3F$	-0.73(2)	1969(17)	1.99(9)	0.88(2)	0.58(2)	1.38
$[I_4][AsF_6]_2$	-0.81(2)	2007(15)	1.78(8)	0.85(2)	0.74(2)	2.39
$[I_4][AsF_6]_2$ [a] (amorphous)	-0.71(1)	1933(20)	1.43(5)	0.84(1)	2.52(5)	2.88
$[I_4][SbF_6]_2$ [b]	-0.84(2)	1951(13)	2.01(5)	0.91(1)	1.20(2)	5.58

[a] The reaction of I_2 with AsF_5 in SO_2 solvent produced crystalline $[I_4][AsF_6]_2$ while the same reaction in SO_2ClF resulted in immediate precipitation of an amorphous powder whose Mössbauer spectrum is consistent with $[I_4]^{2+}$.

[b] The reaction of I_2 with SbF_5 in the appropriate ratio produced a crystalline solid whose Mössbauer spectrum is also consistent with the presence of $[I_4]^{2+}$.
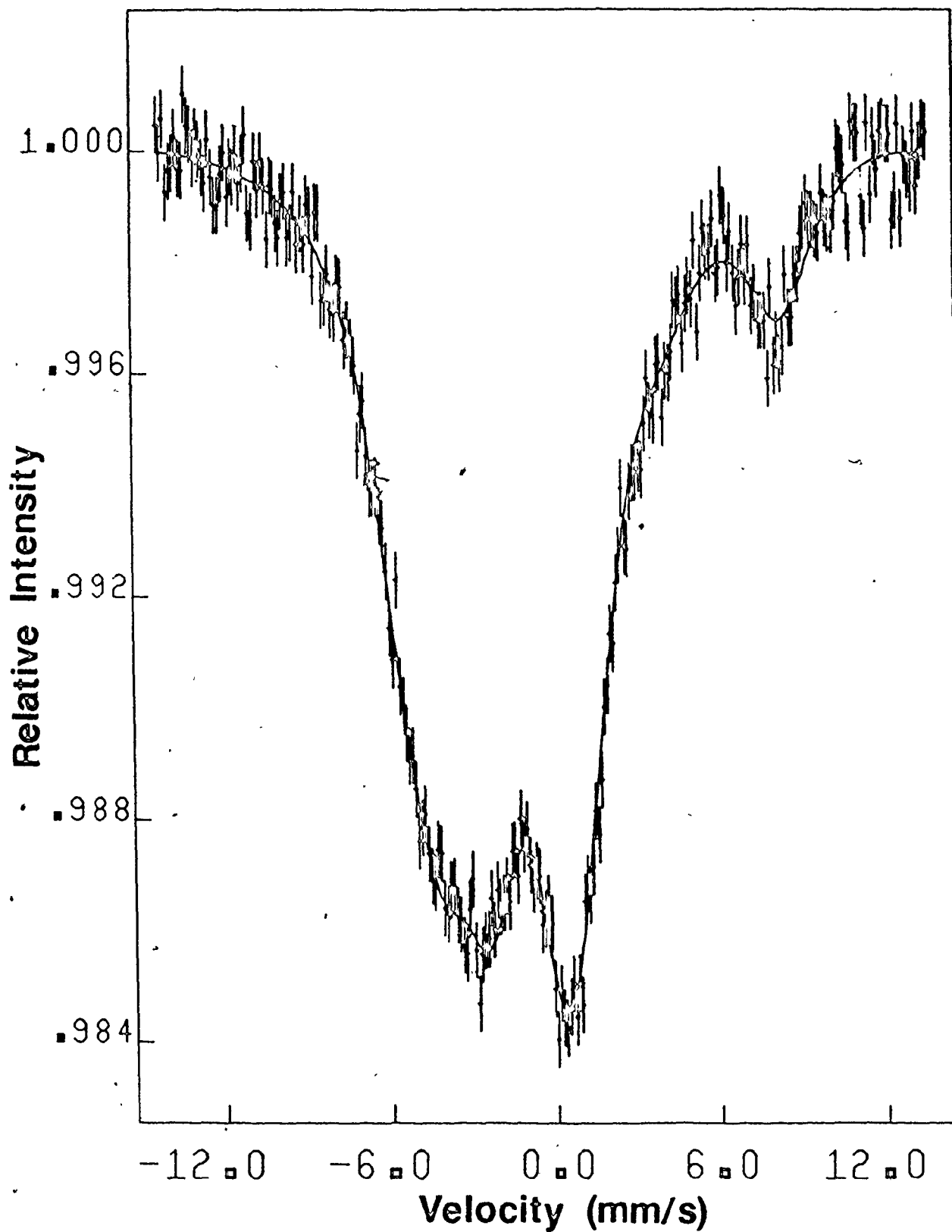
Figure 8.1. ^{127}I Mössbauer spectrum of $[I_2][Sb_2F_{11}]$ at 4.2°K.   The solid

line represents the best fit to the data.
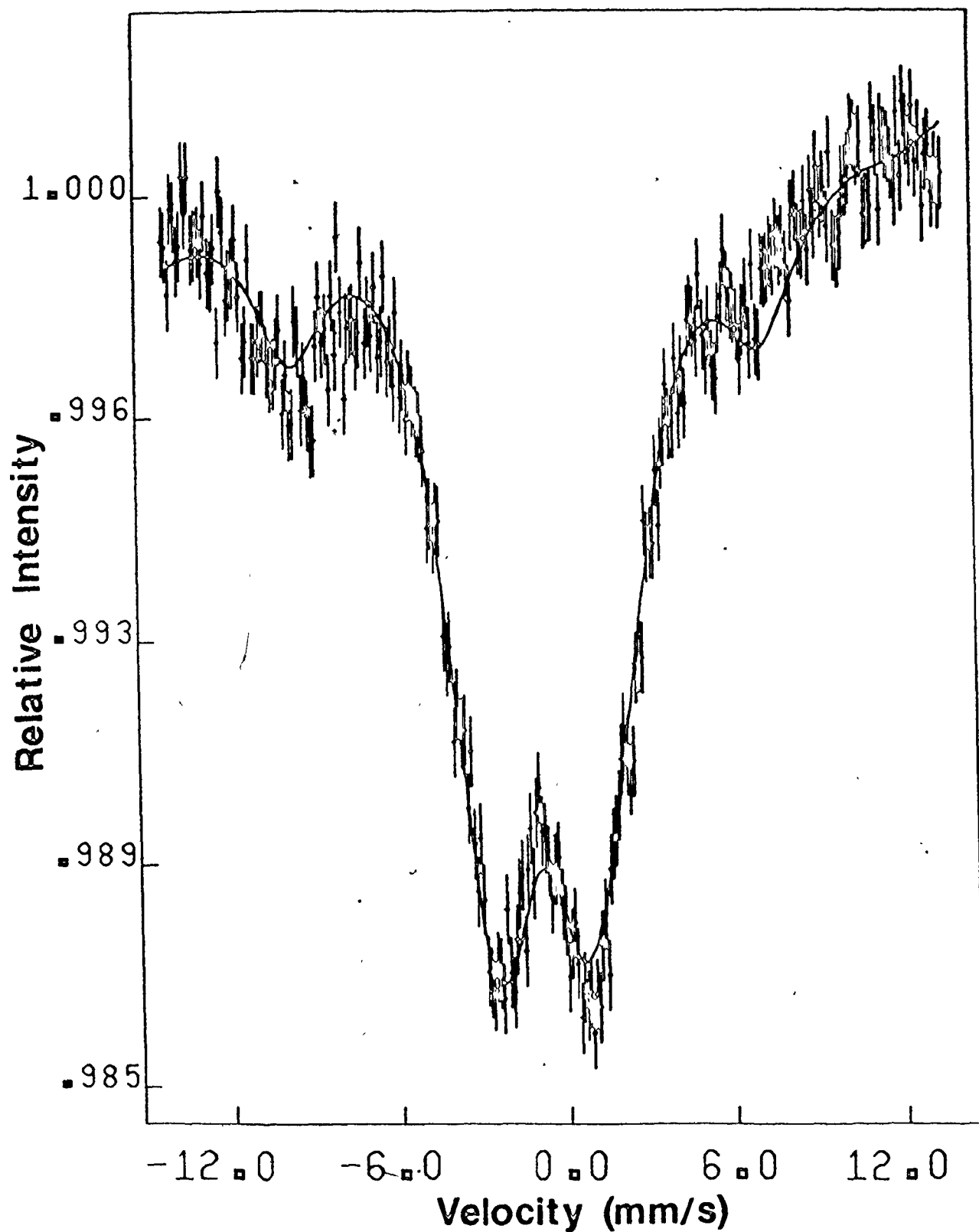
Figure 8.2. ^{127}I Mössbauer spectrum of $[I_2][Sb_2F_{11}]$ dissolved in HSO_3F measured at 4.2°K. The solid line represents the best fit to the data.

and that the principal axis of the electric field gradient is along the
iodine-iodine axis. This is consistent with the X-ray crystal structure
of $[I_2][Sb_2F_{11}]$.[17] The Mössbauer spectrum of the frozen solution of
$[I_2][Sb_2F_{11}]/HSO_3F$ (Figure 8.2) is dramatically different from that of
the pure solid $[I_2][Sb_2F_{11}]$. It is immediately evident that the sign of
$e^2q^{127}Q_g/h$ has reversed from negative to positive and that eta has become
very large. The magnitude of the quadrupole coupling constant however,
is essentially unchanged (Table 8.1) as is the isomer shift. These
Mössbauer parameters of the frozen solution of $[I_2][Sb_2F_{11}]$ are
consistent with a structure for the dimer which is square- or
rectangular-planar (I). The iodine atoms in this arrangement are
envisaged as being in a distorted square-planar arrangement as a result
of the interaction

$$--- \;\stackrel{\vdots}{I} --- \stackrel{\vdots}{I}\; ---$$

$$--- \;\stackrel{\vdots}{I} --- \stackrel{\vdots}{I}\; ---$$

(I)
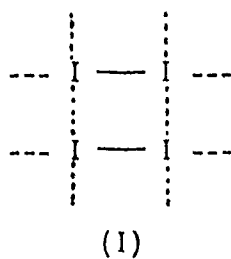
between the two $[I_2]^+$ monomer units, with further longer range inter-
actions to fluorine atoms of the $[Sb_2F_{11}]^-$ anion or even to fluorosulfate
groups. The large value of eta (0.88) is consistent with this structural
arrangement since each iodine atom would experince one strong interaction
to another iodine atom while the remaining interaction would be
presumably much weaker. It is not too surprising that the magnitude of

$e^2q^{127}Q_g/h$ and the isomer shift have not changed relative to $[I_2]^+$, since the immediate environment of the iodine atoms has not changed dramatically from that in the solid state. The other two possible structures which were suggested for the dimer, namely a tetrahedron of iodine atoms and an acyclic chain can be discounted since in the former case the sign of $e^2q^{127}Q_g/h$ would probably be negative, while in the latter case there would likely be at least two different iodine environments, which would give rise to a very complex Mössbauer spectrum.

These Mössbauer results on the $[I_4]^{2+}$ cation in solution have been verified in the solid state in collaboration with Gillespie and Kapoor.[175] These workers have reinvestigated the reactions of I_2 with the Lewis acids SbF_5 and AsF_5. The reaction of I_2 with AsF_5 using the stoichiometry of equation (8.1) produced a very dark crystalline material whose ^{127}I Mössbauer spectrum and parameters are essentially the same as those of $[I_2]^+$ in frozen fluorosulfuric acid solution. Preliminary X-ray crystallographic data have shown the material to contain a rectangular-planar arrangement of iodine atoms with the bond distances indicated in (II).

$$\begin{array}{cc} & 2.573(6) \\ I &\!\!\!\!—\!\!\!\! I \\ | & \quad | \quad 3.270(7) \\ I &\!\!\!\!—\!\!\!\! I \end{array}$$

(II)
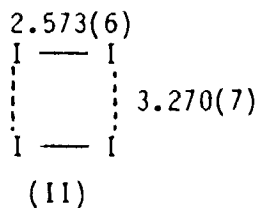
Equation (8.2) shows the correct stoichiometry for this reaction. Even though the reaction

$$2I_2 + 3AsF_5 \xrightarrow{SO_2} [I_4][AsF_6]_2 + AsF_3 \qquad (8.2)$$
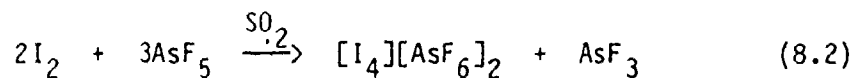
was initially carried out with a large excess of AsF_5 the anion generated is $[AsF_6]^-$ and not $[As_2F_{11}]^-$. In fact there are no examples of compounds which contain the $[As_2F_{11}]^-$ anion, presumably because of the weaker Lewis acidity of AsF_5 compared to SbF_5. The same reaction in SO_2ClF rather than SO_2 solvent produced an amorphous powder whose Mössbauer parameters are similar to those of the crystalline material produced in SO_2. It is possible that the crystalline material was slightly contaminated. The compound is much less soluble in SO_2ClF and when it forms it immediately precipitates in an amorphous state. This behaviour indicates that $[AsF_6]^-$ cannot stabilize the $[I_2]^+$ cation and since $[AsF_6]^-$ is unable to dimerize to $[As_2F_{11}]^-$ the stability of the cation is enhanced by its own dimerization. Since it has been shown [174] that solutions of $[I_2]^+$ become diamagnetic at low temperatures, the $[I_4]^{2+}$ cation should also be diamagnetic by virtue of the pairing of the single unpaired electron of each $[I_2]^+$ cation. It is interesting to note that the dimerization of the $[I_2]^+$ cation produces another symmetric cation.

Gillespie and Kapoor [175] have also repeated the reaction of I_2 with SbF_5 according to the stoichiometry of equation (8.2) producing a dark crystalline material whose ^{127}I Mössbauer spectrum also indicates the presence of $[I_4]^{2+}$. It is not possible to determine at this point

whether the anion in this compound is $[Sb_2F_{11}]^-$ or whether it has remained as $[SbF_6]^-$. It is clear that in the original reaction to produce $[I_2][Sb_2F_{11}]$ (equation (8.1)) the excess of SbF_5 present allows the $[Sb_2F_{11}]^-$ anion to form which is capable of stabilizing the $[I_2]^+$ cation.

The Mössbauer parameters of the various $[I_4]^{2+}$ compounds (Table 8.1) are all very similar and nearly the same as those of $[I_2]^+$ in frozen fluorosulfuric acid solution, indicating that the same species is present in all cases, namely $[I_4]^{2+}$. The spectra of the compounds containing the $[I_4]^{2+}$ cation are not fitted quite as well as $[I_2]^+$ as shown by the high x^2 values and this could perhaps indicate the present of some impurities particularly in the compound designated as $[I_4][SbF_6]_2$. The small differences in isomer shift could be a result of the different anions in the compounds, which might cause small structural differences. Also the $[I_2]^+$ cation in frozen HSO_3F which dimerizes to $[I_4]^{2+}$ will probably be completely solvated. As Table 8.1 indicates, the isomer shifts of the $[I_4]^{2+}$ cations are generally slightly more negative than that of $[I_2]^+$. This indicates a somewhat higher s-electron density which is probably caused by withdrawal of p-electrons as a result of the bonds formed between monomer units. The sign of $e^2q^{127}Q_g/h$ in these compounds is somewhat ambiguous because of the large value of eta. However slightly better computer fits of the spectra were achieved with a positive quadrupole coupling constant as shown in Table 8.1. Also the rectangular-planar structure of the cation indicated by the preliminary X-ray crystal structure data for $[I_4][AsF_6]_2$ is consistent with a negative electric

field gradient, i.e. an excess of electron density along the z axis, which is perpendicular to the plane of the molecule, and hence $e^2q^{127}Q_g/h$ would be expected to be positive on these grounds.

The $[I_4]^{2+}$ cation in the rectangular-planar structure contains 28-2=26 electrons or 13 electron pairs. The two $[I_2]^+$ monomer units account for two bonding electron pairs and eight non-bonding pairs for a total of 20 electrons. Thus there are three pairs of electrons remaining. If the interaction between the two $[I_2]^+$ monomer units were strong a further two electron pairs could be assigned to these two bonds thereby leaving two electrons unaccounted for. If the dimer was square-planar with all the I-I bond distances the same, the cation could be viewed as a 4n+2 aromatic system where n=0. However since the distances between the $[I_2]^+$ units are much longer than the I-I distance in $[I_2]^+$ this model does not apply. Both the X-ray crystallographic and Mössbauer evidence suggest that the interaction between the $[I_2]^+$ monomer units is weak but it is well within the van der Waals contact distance of 3.96Å.[134]

C. Introduction

(i) The Electronegativity of the -OTeF₅ Ligand

Since the first synthesis of HOTeF$_5$ by Engelbrecht and Sladky [176] a substantial number of derivatives of the elements containing -OTeF$_5$ groups have been prepared.[177] In general, the -OTeF$_5$ group appears to be capable of stabilizing the same oxidation states as -F and indeed nearly

all of the chemistry of $-OTeF_5$ compounds has been developed by analogy with the existing fluorides. For example, the $-OTeF_5$ analogs of XeF_2,[178,179] XeF_4,[180] $XeOF_4$ [181] and XeF_6 [181] have all been reported though $Xe(OTeF_5)_6$ has not been fully characterized.

In view of the large number of $-OTeF_5$ compounds, the question of the effective group electronegativity of $-OTeF_5$ relative to that of $-F$ has been speculated upon a number of times. An estimate of the electronegativity of the $-OTeF_5$ group has been made using ^1H NMR spectroscopy by the application of the equation of Dailey and Shoolery [182] (re-evaluated here using Pauling electronegativities). A linear plot of the difference between the chemical shifts of the methyl and methylene protons of XCH_2CH_3 (X = I, Br, Cl, $OTeF_5$ or F) [183] yields a group electronegativity of 3.88 for $-OTeF_5$ (coefficient of determination, R^2 = 0.99). Although. HF is capable of displacing $HOTeF_5$ from its compounds, it has been argued that the $-OTeF_5$ group possesses an electronegativity greater than that of $-F$.[96] The latter electronegativity order is based upon the observation that in the reaction of IF_5 with the ligand-transfer agent $B(OTeF_5)_3$, the square-pyramidal shapes of the resulting structures i.e., $F_aIF_{4-n}(OTeF_5)_n$ were maintained, but no axial fluorine substitution was observed. These results seem to conform to the valence shell electron pair repulsion (VSEPR) predictions,[18] although nowhere in the literature is it clearly noted that the least electronegative ligand occupies the axial position of a square-based pyramidal molecule. This conclusion regarding the stereochemistry observed in AX_5E-type molecules has apparently been inferred by extending arguments pertaining to trigonal bipyramidal

molecules, which conform without exception to VSEPR predictions. Steric effects resulting from mutual hindrance of the $-OTeF_5$ groups, which might account for preferential occupation of the equatorial positions by $-OTeF_5$ groups, appear to have been ruled out on the basis of the crystal structures of the related trans-$F_2Te(OTeF_5)_4$ [184] and $Te(OTeF_5)_6$ [185] compounds.

Attempts to quantify relative group electronegativities by examining the P=O stretching frequencies, ^{31}P chemical shifts and [31]P-^{19}F spin-spin coupling constants of the series $O=PF_2X$ (X = F, $OTeF_5$, $OSeF_5$, Cl) have led to the ambivalent conclusion that the electronegativities of $-OSeF_5$ and $-OTeF_5$ are approximately equal to that of -F. [96]

In order to establish the relative electronegativity of $-OTeF_5$ versus -F, a series of compounds were examined using [129]Xe and [125]Te NMR, and [129]Xe and [127]I Mössbauer spectroscopy. Both techniques are sensitive to changes in electron density at the nucleus of interest and are therefore ideally suited to an investigation of relative effective electronegativities of the directly bonded ligands. In the case of the [129]Xe nucleus, the Mössbauer results are complimented by NMR results on the same nucleus. The compounds to be discussed were prepared using published methods [96,179-181,185-190] by Prof. G. J. Schrobilgen of the Chemistry Department at McMaster University, who also measured the [129]Xe and [125]Te NMR spectra. The [129]Xe Mössbauer spectra were measured by H. de Waard at the Laboratorium voor Algemene Natuurkunde, Rijksuniversteit, Westersingel 34, 9718 CM, Groningen, The Netherlands.

D. Results and Discussion

(i) The Electronegativity of the $-OTeF_5$ Ligand

Both tellurium and xenon possess isotopes having nuclear spins of 1/2 and natural abundances and sensitivities which allow ready observation by FT NMR spectroscopy, i.e., ^{123}Te, 0.87%, D^C = 0.89; ^{125}Te, 6.99%, D^C = 12.5; ^{129}Xe, 26.44%, D^C = 31.8 (D^C = natural abundance sensitivity relative to natural abundance ^{13}C).

The present body of experimental data shows that the range of chemical shifts not only increases with Z for a particular group but also increases with Z for a particular period. It may also be anticipated that the chemical shifts of these heavy nuclei will exhibit greater sensitivity to the effects of substituents than lighter NMR nuclei. It is partly for this reason that ^{125}Te and ^{129}Xe where chosen as NMR probes for assessing the relative electronegativities of $-F$ and $-OTeF_5$.

Of the known xenon fluorides and oxyfluorides, XeF_2, XeF_4 and $XeOF_4$ have been shown to possess well-defined $-OTeF_5$ analogs, i.e., $Xe(OTeF_5)_2$,[179] $Xe(OTeF_5)_4$[180] and $O=Xe(OTeF_5)_4$.[181] Fluorine-19 and xenon-129 NMR parameters have been reported for these species. However, a common solvent for the fluoride and its $-OTeF_5$ analog has not been used in the majority of cases and in the case of $Xe(OTeF_5)_4$ and $O=Xe(OTeF_5)_4$, two different chemical shift conventions seem to have been used. It has been demonstrated that xenon chemical shifts are very sensitive to solvent effects and that this sensitivity increases with increasing number of xenon lone pairs. In some instances, solvent effects can account for up to 200 ppm shifts [191] (c.f. chemical shifts of XeF_2 and $Xe(OTeF_5)_2$ in $CFCl_3$ and SO_2ClF solvents at room temperature, (Table 8.2)). In order to

compare the relative effective electronegativities of -F and -OTeF$_5$, in a meaningful way, the ^{129}Xe chemical shifts of the -F and -OTeF$_5$ analogs were measured in the same solvent at the same temperature and referenced to pure liquid XeOF$_4$, the accepted reference for ^{129}Xe chemical shifts.[192] The ^{125}Te chemical shifts of TeF$_4$, Te(OTeF$_5$)$_4$ and Te(OTeF$_5$)$_6$ were also measured for the first time (Table 8.2). The ^{125}Te NMR parameters for TeF$_6$ have been reported previously elsewhere,[193] but were remeasured here under the same temperature and solvent conditions as for Te(OTeF$_5$)$_6$.

Differences between ^{125}Te and ^{129}Xe chemical shifts for the -F and -OTeF$_5$ analogs consistently show that the -OTeF$_5$ group is significantly more shielding towards the central NMR nucleus than -F (Table 8.2). This strongly argues in favor of an -OTeF$_5$ group that is less electronegative than -F.

The ^{129}Xe chemical shift differences ($\Delta\delta = \delta$F derivative - δOTeF$_5$ derivative) for [XeF]$^+$ and [XeOTeF$_5$]$^+$ (898 ppm) and that for Xe(OTeF$_5$)$_2$ and XeF$_2$ (438 ppm; 219 ppm/group) not only reflect the lower effective electronegativity of -OTeF$_5$, they are also in accord with the anticipated relative bond orders derived from a simplified MO treatment,[114] i.e. [XeX]$^+$ (X = -F or -OTeF$_5$) is described in terms of a two center-two electron bond (bond order, 1) and XeX$_2$ in terms of a three center-four electron bond (bond order, 1/2). Hence, the chemical shift changes per group are greater for systems of greater bond order, e.g., 2c-2e bonds such as in [XeX]$^+$ and TeX$_4$ (in the case of TeF$_4$ and Te(OTeF$_5$)$_4$, the chemical shift contribution from one 3c-4e bond is averaged with

Table 8.2. ^{125}Te and ^{129}Xe NMR Data for $-\text{?}$ and $-OTeF_5$ Derivatives of Tellurium and Xenon †

solute	$\delta_{^{125}Te}$ [a,b]	$\delta_{^{129}Xe}$ [a,c]	$^{125}Te-^{19}F$ [d]	$^{129}Xe-^{19}F$ [d]	$^{125}Te-^{125}Te$	$^{125}Te-^{129}Xe$	solvent	temp. °C	concn. molal
				J, Hz					
Te(OTe'F5)4	Te, 394.0 Te', -157.6		F, 3639 F', 3403		544		CH₃CN	24	1.00
Te(OTe'F5)4	Te, 633.3 Te', -160.8		F, 31.8 F', h F, 3665 F', 3555				SO₂ClF	24	0.18
Te(OTe'F5)6	Te, 630 Te'(A) -154.3 [f] Te'(E) -167.1 [f]		F, 3600 F', 3600 F, 3725 F', 3650				SO₂ClF	-110	~0.18
TeF4	559.8		e				CH₃CN	24	4.35
Te(OTe'F5)6	Te, -235.8 Te', -174.5		F, 3710 F', 3662		1302		C₂F₃Cl₃ [g]	110	0.33
TeF6	-164.3 -164.9		3727 3736				C₂F₃Cl₃ [g] C₂F₃Cl₃ [g]	110 24	1.32
Xe(OTeF5)2		≳2447.4		F, 31 F', h		476	CFCl₃	26	0.61

Table 8.2: (Contd.)

solute	$\delta_{125\text{Te}}$ [a,b]	$\delta_{129\text{Xe}}$ [a,c]	$^{125}\text{Te}-^{19}\text{F}$ [d]	$^{129}\text{Xe}-^{19}\text{F}$ [d]	$^{125}\text{Te}-^{125}\text{Te}$	$^{125}\text{Te}-^{129}\text{Xe}$	solvent	temp. °C	concn. molal
XeF$_2$		−2009		5579			CFCl$_3$	26	satd
Xe(OTeF$_5$)$_2$		−2327	F, 30 F', h		470				
FXeOTeF$_5$		−2051	F, 34 F', h	5743 [J]	560±20		SO$_2$ClF	26	1.54 [J]
XeF$_2$		−1913		5621					
[XeOTeF$_5$]$^+$ [k]	−134.9	−1472		F, 18.5 F', h			SbF$_5$	26	0.74
[XeF]$^+$ [j]		−574		7210			SbF$_5$	26	0.71
(structure)		Xe, −1146 Xe', −1633		5747 [m]					
(structure)		−1059		F$_b$, 4828 F$_t$, 6662			BrF$_5$	−60	0.30 [n]

Table 8.2: (Contd.)
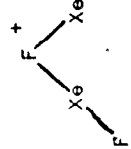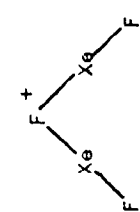
solute	δ_{125Te} [a,b]	δ_{129Xe} [a,c]	J, Hz				solvent	temp. °C	concn. molal
			$^{125}Te-^{19}F$ [d]	$^{129}Xe-^{19}F$ [d]	$^{125}Te-^{125}Te$	$^{125}Te-^{129}Xe$			
Xe(OTeF$_5$)$_4$		− 662.8		F, 63 F', h		988	CFCl$_3$	24	~0.2
XeF$_4$		166.1		3801			CFCl$_3$	24	sat'd
O=Xe(OTeF$_5$)$_4$		− 211.8		F, 54 F', h		1304	CFCl$_3$	24	~0.4
O=XeF$_4$		0.0		1123			neat	24	16.4

Footnotes to Table 8.2:

a IUPAC conventions have been used in reporting chemical shift data
(Pure Appl. Chem., 1972, 29, 627; 1976, 45, 217), i.e., a positive.
chemical shift denotes a positive frequency and vice versa.

b Tellurium-125 spectra have been referenced with respect to saturated
aqueous $Te(OH)_6$ at 24°C where the chemical shift conversion with ,
respect to neat $(CH_3)_2Te$ is given by $\delta[(CH_3)_2Te] = \delta[(OH)_6Te] + 710.9$.

c Xenon-129 spectra have been referenced with respect to liquid $XeOF_4$ at
24°C.

d F and F' denote the equatorial and axial fluorines, respectively, of
the $OTeF_5$ group.

e ^{125}Te-^{19}F coupling not observed due to rapid fluorine chemical
exchange.

f A and E denote axial and equatorial $OTeF_5$ groups, respectively.

g 1,1,2-trichlorotrifluoroethane.

h Coupling between the central atom nucleus and F' of the $OTeF_5$ group
could not be resolved.

i The value represents the directly bonded ^{129}Xe-^{19}F spin-spin coupling
constant.

j Initial concentrations of $FXeOTeF_5$; the latter compound
disproportionates in SO_2ClF solvent yielding an equilibrium mixture
of XeF_2, $FXeOTeF_5$ and $Xe(OTeF_5)_2$.

k Reference (193).

l Reference (191-192).

m Owing to the lability of the XeF_2 group on the NMR time scale, only
one ^{129}Xe-^{19}F spin-spin coupling is observed (see ref. (193)).

n Initial concentrations of $[XeOTeF_5][AsF_6]$ dissolved at -48°C, not
warmed above -48°C prior to recording the spectrum.

o F_b and F_t denote the bridging and terminal fluorines respectively.

† NMR spectra were recorded by G. Schrobilgen.

contributions from two 2c-2e bonds). The bonding in TeX_6-type molecules

may be approximately described in terms of three 3c-4e bonds, conse-

quently, the ^{125}Te chemical shift difference for TeX_4 (166 ppm; 41.5 ppm/

group) is expected to be larger than for TeX_6 (71.5 ppm; 11.9 ppm/group)

owing to the higher average bond orders anticipated for TeX_4 species. It

is interesting to note that the ^{129}Xe chemical shift difference per group

for XeF_4 and $Xe(OTeF_5)_4$ (207 ppm/ group) is nearly identical to that for

XeX_2. This is in accord with a description of the bonding in XeX_4 in

terms of two 3c-4e bonds. Although the Xe-X bonds of $XeOX_4$ may be

described in terms of two 3c-4e bonds, the value derived for $XeOX_4$ is

small (53 ppm/group) compared to those of XeX_2 and XeX_4. The Xe=O bond

serves to diminish the difference in deshielding effects between $-OTeF_5$

and -F. The less electronegative $-OTeF_5$ groups place more electron

density onto the central xenon. A greater contribution from the valence

bond structure $\overset{+}{Xe}-\overset{-}{O}$ results, and serves to remove much of the additional

electron density on the xenon of the $-OTeF_5$ compound. This is supported

by a somewhat lower Xe=O stretching frequency for the $-OTeF_5$ compound

($O=XeF_4$, 920 cm^{-1}; $O=Xe(OTeF_5)_4$ 882 cm^{-1}, this work).

Table 8.3 summarizes the ^{129}Xe and ^{127}I Mössbauer data for

pairs of structurally related molecules in which the axial fluorines in

XeF_2 and the equatorial fluorines in XeF_4, $O=XeF_4$ and IF_5 molecules are

replaced by the $-OTeF_5$ group. The geometry remains the same in each pair

and the Mössbauer parameters should then reflect the effect of

replacing a fluorine by the $-OTeF_5$ group. The influence that these

ligands have upon the parameters will depend upon their relative electron

Table 8.3.

Mössbauer Data for -F and -OTeF$_5$ Derivatives of Xenon and Iodine

Compound	Isomer shift (mms^{-1})	Quadrupole splitting ΔE_Q (mms^{-1})	Line width Γ (mms^{-1})
XeF$_2$ [b]	0.2(2)	39.7(4)	
Xe(OTeF$_5$)$_2$ [b]	0.1(3)	38.3(3)	
XeF$_4$ [b]	0.40(4)	41.04(7)	
Xe(OTeF$_5$)$_4$	0.9(1)	36.1(2)	8.8(2)
O=XeF$_4$ [b]	0.5(3)	18.1(5)	
O=Xe(OTeF$_5$)$_4$	0.7(1)	15.7(1)	8.8(2)
IF$_5$	-1.39(4) [c]	1171(33) [d]	2.73(20)
FI(OTeF$_5$)$_4$	-1.36(4) [c]	910(37) [d]	2.31(18)

[a] ^{129}Xe isomer shifts are relative to the xenon β-hydroquinone clathrate and were recorded by H. de Waard.

[b] Data from reference (194).

[c] ^{127}I isomer shifts are relative to KI.

[d] ^{127}I quadrupole couplings are given in the more usual form of $e^2q^{127}Q_g/h$ in units of MHz; for ^{127}I 1 mms^{-1} = 46.46 MHz.

withdrawing powers, i.e., upon their relative electronegativities and upon the nature of the bonding in these molecules. Three types of molecules are represented here which may be described according to VSEPR rules,[18] as AX_2E_3, AX_4E_2 and AX_5E. In valence bond terms the bonding could be described as sp^3d and sp^3d^2. However, it has already been established,[194] based upon the trends in the isomer shifts of a large series of xenon compounds, that the bonds between the central xenon and the ligands only have a very small degree of s-character. The isomer shifts reported here, which are a measure of s-electron density, confirm this conclusion. The isomer shifts for the iodine compounds are quite negative, indicating a high s-electron density at the iodine nucleus. This suggests that the I-F bonds are principally of p-character and that there is little involvement of the iodine 5s-electrons in the bonding.

With one exception, the isomer shift differences between the fluorides and the $-OTeF_5$ analogs lie within the errors of measurement for both the xenon and iodine compounds. In all cases the changes in isomer shift are only a small fraction of the widths of the observed resonance and as a result no realistic interpretation can be given for the changes in this parameter.

Fortunately, the changes in the quadrupole splitting are much greater than the errors in the measurement and this parameter is therefore much more useful as a structural tool. The fact that the quadrupole splittings for the $-F$ and $-OTeF_5$ analogs are very similar is added confirmation that their structures are of the same type, i.e., $Xe(OTeF_5)_2$ is linear like XeF_2 while $FI(OTeF_5)_4$ has a square-based

pyramidal geometry like IF_5. The largest quadrupole splittings are observed in those cases where the bonding ligands, -F or $-OTeF_5$, are along one axis, $Xe(OTeF_5)_2$, or in the same plane, $Xe(OTeF_5)_4$, while non-bonding electron pairs occupy the remaining positions in the structure. These arrangements create the largest electric field gradients and have the largest quadrupole splittings. The quadrupole coupling constants in the XeX_2 and XeX_4 (X = -F or $-OTeF_5$) compounds should of course have opposite signs since V_{zz} is in the equatorial plane for XeF_2 but in the axial direction for XeX_4. In going from $Xe(OTeF_5)_4$ to $O=Xe(OTeF_5)_4$, the quadrupole splitting drops by 20.4 mms^{-1} while in the $XeF_4/XeOF_4$ pair the drop is 23.9 mms^{-1}. This is the effect of replacing a non-bonded electron pair (zero electronegativity [18]) by an electronegative oxygen. Figure 8.3 shows the ^{129}Xe Mössbauer spectrum of a mixture of $Xe(OTeF_5)_4$ and $O=Xe(OTeF_5)_4$. The identity of these species was confirmed by NMR as discussed earlier.

One can see from Table 8.3 that for a given fluoride, replacement of -F by $-OTeF_5$ results in a decrease in the magnitude of the quadrupole splitting. This occurs whether the central atom is xenon or iodine and is a reflection of the relative electron withdrawing power of the -F compared to the $-OTeF_5$ group. The greater the electron withdrawal in the x- and y- directions as compared to the z-direction (which contains the non-bonding electron pair(s) in the AX_4E_2 or AX_5E compounds) the greater the quadrupole splitting. The reverse is true for XeF_2 and $Xe(OTeF_5)$ where the ligands are along the z-axis and the non-bonded electron pairs are in the xy-plane. Clearly, these results establish that -F is a more

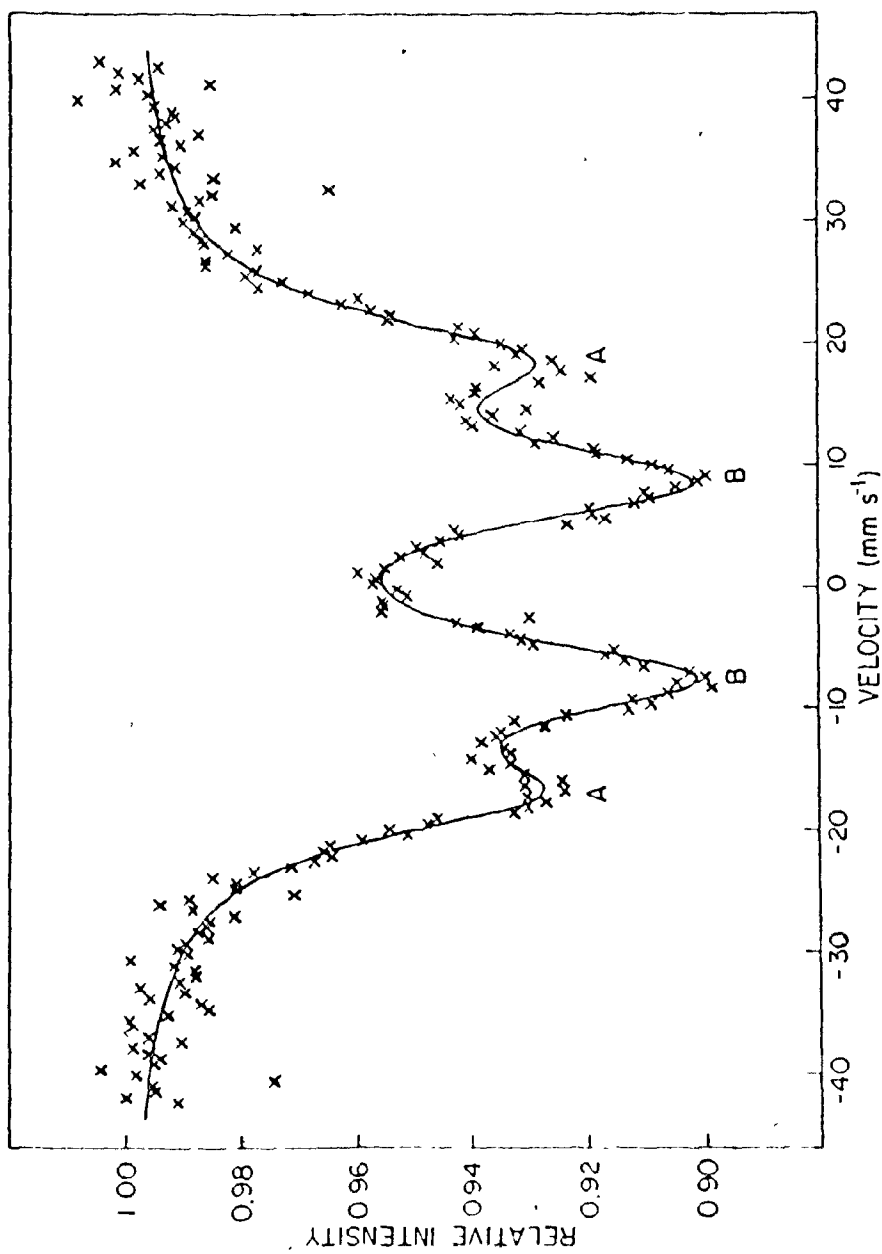Figure 8.3. ^{129}Xe Mössbauer spectrum of a O=Xe(OTeF$_5$)$_4$/Xe(OTeF$_5$)$_4$ (∿2:1) mixture at 4.2° K.   The spectrum was measured as described by reference 191.   The solid line represents the best fit to the data.   This spectrum was recorded by H. de Waard.

electronegative ligand than $-OTeF_5$. From the nearly linear relationship between the quadrupole splittings of XeF_2, $XeCl_2$ and $XeBr_2$ [195] and the Pauling electronegativities of the ligand atoms (coefficient of determination, $R^2 = 0.98$), the corresponding Pauling electronegativity of $-OTeF_5$ can be estimated. The interpolated value for $-OTeF_5$ derived from the observed quadrupole splitting for $Xe(OTeF_5)_2$ is 3.87 compared to 3.98 for $-F$. This compares to a value of 3.88 obtained from the NMR method as mentioned previously.

The Mössbauer spectrum of IF_5 has been reported by Bukshpan, et al.[196] who used the ^{129}I isotope. This isotope gives much better resolved spectra than the ^{127}I isotope, but because the earlier workers were not sure of the purity of their sample, the spectrum of a pure sample was measured using the natural isotope. The Mössbauer parameters obtained for IF_5 agree reasonably well with the earlier data after converting the ^{129}I data to their ^{127}I equivalents. The computed line width for the $^{127}IF_5$ spectrum is substantially greater than the natural line width, i.e., 2.73 compared to 1.27 mms^{-1}. This large line width is attributed to the fact that in the solid state, at $-80°C$ there are three crystallographically discrete, albeit chemically equivalent, iodine sites.[197] This interpretation is consistent with the results obtained by Kuz'min et al.[198] who measured the ^{127}I NQR spectrum of IF_5 at 77° K. These workers were able to resolve three crystallographically non-equivalent iodine atom positions having a population ratio of ca. 3:4:3, whose resonance frequencies were 1025, 1031, and 1067 MHz. The ^{127}I spectrum of $FI(OTeF_5)_4$ shown in Figure 8.4 gives a more acceptable
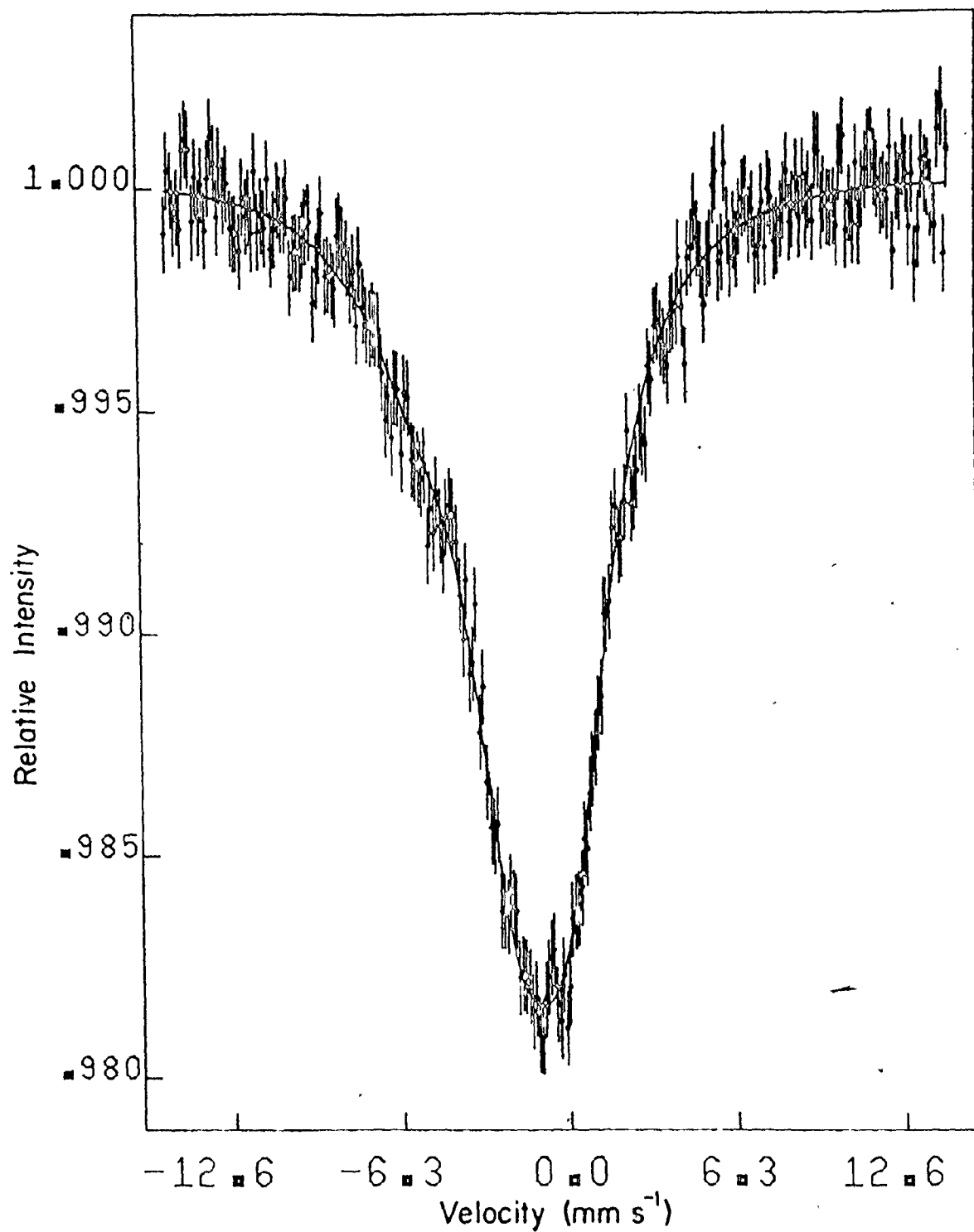
Figure 8.4. ^{127}I Mössbauer spectrum of $F-I(OTeF_5)_4$ at 4.2°K. The solid

line represents the best fit to the data.

line width, suggesting that only one iodine site is present. The shape of the iodine spectrum immediately gives the sign of the quadrupole coupling constant, which is positive, indicating that there is an excess of electron density in the z-direction, i.e., that direction which contains the non-bonded electron pair and the axial fluorine. In the case of the xenon spectra, the sign of the interactions cannot be determined by inspection and must be inferred from the geometry of the compound.

NMR and Mössbauer spectroscopy have shown that -F is more electronegative than $-OTeF_5$. On the basis of the observed geometry of $FI(OTeF_5)_4$ and VSEPR implications it was previously concluded that $-OTeF_5$ is more electronegative than -F. In the case of the trigonal bipyramid where the axial and equatorial regions of space are clearly geometrically unique there appears to be no exception to VSEPR which predicts that the axial position is always occupied by the most electronegative ligand.[18] In the case of the square-based pyramid however, which may be regarded as a pseudo-octahedron, the difference between equatorial and axial positions is more subtle, such that a ligand's preference for a particular region is less demanding, thereby making predictions more difficult.

It is difficult to find suitable examples with which to compare $FI(OTeF_5)_4$ and $\underline{trans}$-$F_2Te(OTeF_5)_4$. It has been found for the series of compounds $R-IF_4$ (R = OCH_3, CF_3, C_2F_5, etc.) that the least electronegative R group remains axial,[199] as might have been expected. However, there also exist examples in the main group, where VSEPR has enjoyed most of its success, in the transition metals, and even in the

actinides, where the most electronegative ligand in fact occupies the axial position of a pseudo-octahedral molecule, to which the square-based pyramid may be classed. In $IO_2F_4^-$ [200] both cis and trans isomers are known to exist despite the fact that doubly bonded oxygen normally prefers to adopt pseudo-axial positions (double-bonded oxygen is thought to exhibit steric characteristics similar to a non-bonded pair of electrons).[201] Similarly, the reactions of TeF_6 with various alcohols [202] result in the formation of di-substituted products where, although the cis isomer predominates, some trans isomer is also formed. The reaction of telluric acid with anhydrous HF [203] results in fluoro-substituted species whose ^{19}F NMR spectra are consistent with the presence of $(HO)_5TeF$, trans-$(HO)_4TeF_2$, fac-$(HO)_3TeF_3$ and mer-$(HO)_3TeF_3$. Tötsch and Sladky [204] have recently isolated cis- and trans-$(HO)_2TeF_4$, $HOTeF_4OCH_3$ and $(CH_3O)_2TeF_4$ and have demonstrated that the isomer ratio of $(HO)_2TeF_4$ is kinetically and not thermodynamically controlled. In the tungsten hexahalide system WF_xCl_{6-x} [205] all compounds in the series are known, including all geometric isomers. Fluorine-19 NMR studies [206] have also shown that all isomers of the $F_xU(OTeF_5)_{6-x}$ system exist in solution.

Thus, in pseudo-octahedral molecules there appears to be no strong preference for the least electronegative ligand to remain in the pseudo-axial position. The above examples suggest that it is perhaps not a good idea to base electronegativity differences of attached ligands solely upon the observed stereochemistry and VSEPR arguments since other effects (kinetic, thermodynamic, etc.) may become important, particularly when these differences are small.

CHAPTER 9

Summary and Conclusions

A. Summary

This thesis has undertaken an extensive study of several different series of iodine compounds by means of ^{127}I Mössbauer spectroscopy in order to obtain more detailed information about the bonding in these molecules. Initially a number of apparently octahedral or cubic inorganic iodine compounds were examined so that a suitable single line absorber could be selected as a reference compound. The literature data to date have been reported either with no reference compound, i.e. against the source, or against a variety of compounds. This of course makes comparisons with the literature data very difficult since the shifts are usually very small. Many of the compounds examined (Table 3.1) gave very broad resonances and close examination of existing X-ray crystallographic data for these compounds revealed that small distortions from true cubic symmetry were present. CuI, a compound generally thought to contain iodine in a cubic environment exists in many different phases and polytypes, which results in a resonance having a very broad and variable line width. As a result of this study it was concluded that KI is the best available reference material and hence it is recommended that this compound be adopted as the universal reference material for ^{127}I Mössbauer spectroscopy. All the isomer shifts in this thesis are quoted with respect to KI unless otherwise stated.

It has become customary to use the semi-empirical relationships presented in Chapter 1 to convert isomer shifts and quadrupole coupling constants into s- and p-orbital populations. It was felt that the general applicability of equation (1.29) was questionable since it was established [47] using only a limited number of iodine compounds. This expression has been re-evaluated (Chapter 4) and equation (4.6) was the result. It was found that there was considerable scatter in the data used to establish (4.6) and the agreement between the values of h_p derived from this equation, and U_p from the quadrupole coupling constants was generally poor. Equation (4.6) was also used to calculate values for h_p and h_s for the data presented in Chapters 5 and 7 and again the results were not very good. It was concluded that an expression of this type does not have general applicability and is not very useful at all when discussing different classes of compounds where the bonding is likely to be quite different. Equation (1.29) was established by assuming that the isomer shift and quadrupole coupling constant are linearly dependent parameters but the results presented in this thesis clearly show that the isomer shift and quadrupole coupling constant do not always respond equally to changes induced by the ligands surrounding the iodine atom.

During the course of examining some interhalogen cations of iodine by ^{127}I Mössbauer spectroscopy (Chapter 5), several new cations were prepared and characterized. In view of the data presented here on some interhalogen cations of iodine it was concluded that the existence, in the solid state, of the asymmetric $[I_2X]^+$ (X = Cl, Br) cations is

doubtful. The cations $[I_2]^+$ [17] and $[Br_2]^+$ [140] are known and have been characterized by X-ray crystallography but it is doubtful that $[IBr]^+$ exists even though according to Evans and Orchard,[207] the adiabatic first ionization potential of IBr is less than that of Br_2. It is suggested in this thesis that asymmetric cations are unlikely to exist and that $[IBr]^+$ would rapidly rearrange to a more symmetric species. The asymmetric cation $[BrICl]^+$ has still not been identified by X-ray crystallography and an attempt to prepare this cation in the present work resulted in a disordered cation of approximate stoichiometry $[IBr_{0.75}Cl_{1.25}]^+$. This cation is thought to be a crystallographic mixture of $[IBr_2]^+$ and $[ICl_2]^+$ but the presence of some $[BrICl]^+$ cation cannot be unambiguously ruled out.

This thesis has demonstrated that ^{127}I Mössbauer spectroscopy is a good diagnostic tool for determining the effect of various ligands on the central iodine atom and also for determining the gross geometry around the iodine atom by allowing a determination of the sign of the quadrupole coupling constant. The degree of asymmetry in the structure is also reflected by the magnitude of the asymmetry parameter, eta. ^{127}I Mössbauer spectroscopy was demonstrated to be invaluable in determining the nature of the species formed when solutions of $[I_2]^+$ are cooled, and also in ascertaining the electronegativity of the $-OTeF_5$ ligand relative to $-F$.

B. Future Direction of Research

The work presented in this thesis has opened up several new avenues of interest which could be pursued in future work. The Mössbauer spectra of three fluorine containing linear triatomic anions of iodine, namely $[ClIF]^-$, $[BrIF]^-$ and $[IF_2]^-$ were presented and in view of the very unusual Mössbauer parameters obtained, the X-ray crystal structures of these compounds would be of great interest. Similarly it would be useful to extend the $[IX_2]^+$ (X = Cl, Br, I) series of cations to include the $[IF_2]^+$ cation since $[IF_2][SbF_6]$ has been identified by ^{19}F NMR spectroscopy.[25] If this cation follows the trend established by the former cations it would be expected to have a quadrupole coupling constant larger than that of $[ICl_2]^+$.

Since $[I_2]^+$ is paramagnetic it would also be very interesting to examine the Mössbauer spectrum of this cation in a very large external magnetic field. The magnitude of the resultant splitting in the Mössbauer spectrum should be a reflection of the applied field and the induced field caused by the unpaired electron on iodine. Although many paramagnetic compounds have been examined in magnetic fields by Mössbauer spectroscopy, this would be the first example involving a main group element. These experiments may also shed some light upon the antiferromagnetism of $[I_2][Sb_2F_{11}]$ which has been suggested by Aubke and co-workers.[173] Subsequent experiments would of course involve the examination of the frozen solution of $[I_2]^+$ as well as of solid $[I_4]^{2+}$ in a magnetic field. The diamagnetism suggested for the $[I_4]^{2+}$ cation of Gillespie and Kapoor [175] could most easily be established by bulk susceptibility measurements on the solid compounds.

REFERENCES

1. B. Pelletier and J.B. Caventou, Ann. Chem. Phys., $\underline{10}$, 164 (1819).

2. A.I. Popov, "Halogen Chemistry", Ed. V. Gutmann, Academic Press, London (1967).

3. R.C.L.·Mooney, Z. Kristallogr., $\underline{90}$, 143 (1935).

4. H.A. Tasman and K.H. Boswijk, Acta. Cryst., $\underline{8}$, 59 (1955).

5. J. Runsink, S. Swen-Walstra, and T. Migchelsen, ibid., $\underline{B28}$, 1331 (1972).

6. R.C.L. Mooney, Z. Kristallogr., $\underline{100}$, 519 (1939).

7. G.L. Breneman and R.D. Willett, Acta. Cryst., $\underline{B25}$, 1073 (1965).

8. J.E. Davies and E.K. Nunn, Chem. Comm., 1374 (1969).

9. U. Müller, Z. Naturforsch, $\underline{34b}$, 1064 (1979).

10. H.W. Cremer and D.R. Duncan, J. Chem. Soc., 2243 (1931).

11. G.C. Hayward and P.J. Hendra, Spectro. Acta., $\underline{23A}$, 2309 (1967).

12. A.G. Maki and R. Forneris, ibid., $\underline{23A}$, 867 (1967).

13. W. Gabes and H. Gerding, J. Mol. Struct., $\underline{14}$, 267 (1972).

14. G.J. Perlow and M.R. Perlow, J. Chem. Phys., $\underline{45}$, 2193 (1966).

15. B.S. Ehrlich and M. Kaplan, ibid., $\underline{51}$, 603 (1969).

16. J. Shamir, Structure and Bonding, $\underline{37}$, 141 (1979).

17. C.G. Davies, R.J. Gillespie, P.R. Ireland, and J.M. Sowa, Can. J. Chem., $\underline{52}$, 2048 (1974).

18. R.J. Gillespie, "Molecular Geometry", Van Nostrand Reinhold, London (1972).

19. C.G. Vonk and E.H. Wiebenga, Acta. Cryst., $\underline{12}$, 859 (1959).

20. A.J. Edwards and G.R. Jones, Chem. Comm., 1304 (1967).

21. A.J. Edwards and G.R. Jones, J. Chem. Soc., A, 1467 (1967).

22. A.J. Edwards and K.O. Christe, J. Chem. Soc. Dalton Transact., 175 (1976).

23. H. Lynton and J. Passmore, Can. J. Chem., 49, 2539 (1971).

24. A.J. Edwards and R.J.C. Sills, J. Chem. Soc. A, 2697 (1970).

25. M. Schmeisser, W. Ludovici, D. Naumann, P. Sartori, and E. Scharf, Chem. Ber., 101, 4214 (1968).

26. W.W. Wilson and F. Aubke, Inorg. Chem., 13, 326 (1974).

27. W.W. Wilson, J.R. Dalziel, and F. Aubke, J. Inorg. Nucl. Chem., 37, 665 (1975).

28. I. Masson, J. Chem. Soc., 1708 (1938).

29. R.J. Gillespie and J.B. Milne, Inorg. Chem., 5, 1577 (1966).

30. J. Arotsky, H.C. Mishra, and M.C.R. Symons, J. Chem. Soc., 2582 (1962).

31. R.A. Garrett, R.J. Gillespie, and J.B. Senior, Inorg. Chem., 4, 563 (1965).

32. J. Passmore, G. Sutherland, and P.S. White, ibid., 20, 2169 (1981).

33. O. Ruff, Chem. Ber., 48, 2068 (1915).

34. Y.A. Fialkov and I.L. Abarbarchuk, Ukr. Khim. Zh., 15, 372 (1949).

35. Y.A. Fialkov, Izv. Akad. SSSR, Utd. Khim. Nauk., 972 (1954).

36. Y.A. Fialkov and O.I. Schorr, J. Gen. Chem. SSSR, 19, a235 (1949).

37. R.J. Gillespie, M.J. Morton, and J.M. Sowa, Adv. Raman Spectrosc., 1, 539 (1972).

38. J. Shamir and M. Lustig, Inorg. Chem., 12, 1108 (1973).

39. D.J. Merryman, P.A. Edwards, J.D. Corbett and R.E. McCarley, J. Chem. Soc. Chem. Comm., 779 (1972).

40. D.J. Merryman, J.D. Corbett, and P.A. Edwards, Inorg. Chem., 14, 428 (1975).

41. R.L. Mössbauer, Z. Physik, 151, 124 (1958).

42. F.R. Metzger, Progr. Nucl. Phys., 7, 54 (1959).

43. T.C. Gibb, "Principles of Mössbauer Spectroscopy", Chapman and Hall, London (1976).

44. J. Petzold, Z. Physik, 163, 71 (1961).

45. W.M. Visscher, Ann. Phys., 9, 194 (1960).

46. H. Frauenfelder, "The Mössbauer Effect", W.A. Benjamin Inc., New York (1963).

47. N.N. Greenwood and T.C. Gibb, "Mössbauer Spectroscopy", Chapman and Hall, London (1971).

48. P. Jung and W. Triftshäuser, Phys. Rev., 175, 512 (1968).

49. S.L. Ruby and G.K. Shenoy, ibid., 186, 326 (1969).

50. G.J. Perlow and S.L. Ruby, Phys. Lett., 13, 198 (1964).

51. J.R. Gabriel and S.L. Ruby, Nucl. Instr. Meth., 36, 23 (1965).

52. K. Ruebenbauer and T. Birchall, Hyperfine Interact., 7, 125 (1979).

53. S. Margulies and J.R. Ehrman, Nucl. Instr. Meth., 12, 131 (1961).

54. E.U. Condon and G.H. Shortley, "The Theory of Atomic Spectra", Cambridge University Press, New York (1963).

55. M.S. Lazarus and T.D. Thomas, J. Chem. Phys., 60, 4682 (1974).

56. G.K. Shenoy and J.M. Friedt, Nucl. Instr. Meth., 116, 573 (1974).

57. G.K. Shenoy and J.M. Friedt, Phys. Rev. Lett., 31, 419 (1973).

58. D.W. Hafemeister, G. de Pasquali, and H. de Waard, Phys. Rev., 135, B1089 (1964).

59. C.H. Townes and B.P. Dailey, J. Chem. Phys., 17, 782 (1949).

60. T.P. Das and E.L. Hahn, "Nuclear Quadrupole Resonance Spectroscopy, Supplement I of Solid State Physics, Ed. F. Zeitz and D. Turnbull, Academic Press, New York (1958).

61. H. de Waard, "Mössbauer Effect Data Index", Ed. J.G. Stevens and V. Stevens (1973).

62. R. Livingston and H. Zeldes, Phys. Rev., 90, 609 (1953).

63. S. Jha, R. Segnan, and G. Lang, Phys. Rev., 128, 1160 (1962).

64. F. de S. Barros, N. Ivantchev, S. Jha, and K.R. Reddy, Phys. Lett., 13, 142 (1964).

65. J.S. Geiger, R.L. Graham, I. 'ergström, and F. Brown, Nucl. Phys., 68, 352 (1965).

66. P.A.W. Dean, R.J. Gillespie, and P.K. Ummat, Inorg. Synth., 15, 213 (1974).

67. G.J. Schrobilgen, Ph.D. Thesis, McMaster University (1973).

68. S.L. Ruby, "Mössbauer Effect Methodology", Proc. of the Eighth Symposium, Ed. I.J. Gruverman, 8, 263 (1973).

69. R.J. Gillespie and G.J. Schrobilgen, Inorg. Chem., 15, 22 (1976).

70. R.J. Gillespie, P. Spekkens, J.B. Milne, and D. Moffett, J. Fluorine Chem., 7, 43 (1976).

71. G. Turner, Ph.D. Thesis, McMaster University (1976).

72. G.H. Stout and L.H. Jensen, "X-ray Structure Determination", Macmillan, London (1968).

73. G.M. Sheldrick, "SHELX System of Crystallographic Programs", Cambridge University (1976).

74. "X-ray System of Crystallographic Programs", Technical Report TR-446, University of Maryland, College Park, Md. (1976).

75. C.G. Vonk and E.H. Wiebenga, Rec. Trav. Chim., 78, 913 (1959).

76. R.C. Thompson, Ph.D. Thesis, McMaster University (1962).

77. R.J. Gillespie and G.J. Schrobilgen, Inorg. Chem., 13, 1230 (1974).

78. F.D. Chattaway and G. Hoyle, J. Chem. Soc., 123, 654 (1923).

79. A.I. Popov and R.E. Buckles, Inorg. Synth., 5, 167 (1957).

80. E.H. Wiebenga, E.E. Havinga, and K.H. Boswijk, Advan. Inorg. Chem. and Radiochem., 3, 133 (1961).

81. G.B. Carpenter, Acta. Cryst., 20, 330 (1966).

82. R.C.L. Mooney, Phys. Rev., 53, 851 (1938).

83. H. Meinert and H. Klamm, Z. Chem., 5, 468 (1965).

84. E. Birk, Angew. Chem., 41, 751 (1928).

85. G. Brauer, "Handbook of Preparative Inorganic Chemistry", Vol. 1, Academic Press, New York (1963).

86. F.M. Beringer, M. Drexler, E.M. Gindler, and C.C. Lumpkin, J. Amer. Chem. Soc., 75, 2705 (1953).

87. (a) J. Passmore, P. Taylor, T.K. Whidden, and P.S. White, J. Chem. Soc. Chem. Comm., 689 (1976);

    (b) J. Passmore, G. Sutherland, P. Taylor, T.K. Whidden, and P.S. White, Inorg. Chem., 20, 3839 (1981).

88. J. Passmore, G. Sutherland, and P.S. White, J. Chem. Soc. Chem. Comm., 330 (1980).

89. J. Passmore, G. Sutherland, and P.S. White, ibid., 901 (1979).

90. J. Passmore, G. Sutherland, T. Whidden, and P.S. White, ibid., 289 (1980).

91. J. Passmore, unpublished results.

92. J. Passmore and P. Taylor, J. Chem. Soc. Dalton Transact., 804 (1976).

93. J. Passmore, G. Sutherland, and P.S. White, unpublished results.

94. A. Rogstad and E. Augdahl, Acta. Chem. Scand., 25, 225 (1971).

95. A. Arotsky and M.C.R. Symons, Quart. Rev., 16, 282 (1962).

96. D. Lentz and K. Seppelt, Angew. Chem. Int. ed., 17, 355 (1978).

97. J. Krasznai, Ph.D. Thesis, McMaster University (1975).

98. W.L. Gettys and J.G. Stevens, J. de Physique Coll., 41, C1-137 (1980).

99. K.R. Reddy, F. de S. Barros, and S. Debenedetti, Phys. Lett., 20, 297 (1966).

100. R.N. Kurdyumova and R.V. Baranova, Soviet Physics - Crystallography, 6, 318 (1961).

101. R. Batchelor and T. Birchall, Acta. Cryst., in press.

102. J.G. Stevens and W.L. Gettys, "Mössbauer Isomer Shifts", Ed. G.K. Shenoy and F.E. Wagner, North-Holland Publishing Company, New York (1978).

103. Y.D. Feikema, Acta. Cryst., 14, 315 (1961).

104. Y.D. Feikema, ibid., 20, 765 (1966).

105. L. Helmholz, J. Amer. Chem. Soc., 59, 2036 (1937).

106. E.A. Hazlewood, Z. Kristallogr., 98, 439 (1938).

107. A. Kalman and D.W.J. Cruickshank, Acta. Cryst., B26, 1782 (1970).

108. A. Weiss and W. Weyrich, Z. Naturforsch, A24, 474 (1969).

109. P.K. Burkert, ibid., 35b, 1349 (1980).

110. P.K. Burkert and F.M. Hutter, ibid., 32b, 15 (1977).

111. R.W.G. Wyckoff, "The Structure of Crystals", J.J. Little and Ives Company, New York (1931).

112. C.H.W. Jones, J. Chem. Phys., 62, 4343 (1975).

113. C.H.W. Jones and J.L. Warren, ibid., 53, 1740 (1970).

114. R.E. Rundle, J. Amer. Chem. Soc., 85, 112 (1963).

115. S. Bukshpan, C. Goldstein, T. Sonnino, L. May, and M. Pasternak, J. Chem. Phys., 62, 2606 (1975).

116. O. Hassel and H. Hope, Acta. Chem. Scand., 15, 407 (1961).

117. E.L. Ahlsen and K.O. Stromme, ibid., A28, 175 (1974).

118. M. Pasternak and T. Sonnino, J. Chem. Phys., 48, 1997 (1968).

119. M.J. Potasek, Phys. Lett., 45A, 489 (1973).

120. G.B. Carpenter and S.M. Richards, Acta. Cryst., 15, 360 (1962).

121. K.H. Boswijk, J. vander Heide, A. Vos, and E.H. Wiebenga, ibid., 9, 274 (1956).

122. B.S. Ehrlich and M. Kaplan, J. Chem. Phys., 50, 2041 (1969).

123. K.O. Christe and O. Naumann, Inorg. Chem., 12, 59 (1973).

124. P.A. Agron, G.M. Begun, H.A. Levy, A.A. Mason, C.G. Jones, and D.F. Smith, Science, 139, 842 (1963).

125. W. Holzer, W.F. Murphy, and H.J. Bernstein, J. Chem. Phys., 52, 399 (1970).

126. R.C. Paul, C.L. Arora, and K.C. Malhotra, J. Inorg. Nucl. Chem., 33, 991 (1971).

127. P.A. Yeats, W.W. Wilson, and F. Aubke, Inorg. Nucl. Chem. Lett., 9, 209 (1973).

128. N.W. Alcock and R.M. Countryman, J. Chem. Soc. Dalton Transact., 217 (1977).

129. R.D. Myers, McMaster University Thesis Tables #1, Available from Thode Library, McMaster University.

130. K.H. Boswijk and E.H. Wiebenga, Acta. Cryst., 7, 417 (1954).

131. R.J. Elema, J.L. de Boer, and A. Vos, ibid., 16, 243 (1963).

132. A.J. Edwards, J. Chem. Soc. Dalton Transact., 1723 (1978).

133. E.H. Wiebenga and D. Kracht, Inorg. Chem., 8, 738 (1969).

134. N.W. Alcock, Adv. Inorg. Chem. Radiochem., 15, 1 (1972).

135. R.D. Burbank and G.R. Jones, Inorg. Chem., 13, 1071 (1974).

136. T. Birchall and J.G. Ballard, J. Phys., Colloq. (Orsay, Fr.), 12, C6-513 (1976).

137. J.G. Ballard, T. Birchall, and D.R. Slim, J. Chem. Soc. Dalton Transact., 1469 (1977).

138. J.G. Ballard and T. Birchall, Can. J. Chem., 56, 2947 (1978).

139. L.E. Selin, Naturwissenschaften, 47, 104 (1960).

140. A.J. Edwards, G.R. Jones, and R.J.C. Sills, J. Chem. Soc. Chem. Comm. 1527 (1968).

141. J.B. Senior and J.L. Grover, Can. J. Chem., 49, 2688 (1971).

142. "International Tables for X-ray Crystallography"; Kynoch Press, Birmingham, England (1962).

143. G.J. Visser and A. Vos, Acta Cryst., 17, 1336 (1964).

144. R.C.L. Mooney Slater, ibid., 12, 187 (1959).

145. R. Forneris and Y. Tavares-Forneris, J. Mol. Struct., 23, 241 (1974).

146. W. Holzer, W.F. Murphy, and H.J. Bernstein, J. Chem. Phys., 52, 399 (1970).

147. E. Hulthen, N. Johansson, and U. Pilsäter, Arkiv, Fys., 14, 31 (1959).

148. R.J. Gillespie and M.J. Morton, Inorg. Chem., 9, 616 (1970).

149. S. Pohl and W. Saak, Z. Naturforsch, 36b, 283 (1981).

150. N. Thorup and J. Shamir, Inorg. Nucl. Chem. Lett., 17, 193 (1981).

151. J. Passmore, P. Taylor, T. Whidden, and P.S. White, Can. J. Chem., 57, 968 (1979).

152. K.F. Tebbe, "Homoatomic Rings, Chains, and Macromolecules of Main Group Elements", Ed. A.L. Rheingold, Elsevier Scientific Publishing Co., New York (1977).

153. I.D. Brown, Chem. Soc. Rev., 7, 359 (1978).

154. K. Nakamoto, "Infrared Spectra of Inorganic and Coordination Compounds", Wiley Interscience, New York (1970).

155. Unit cell parameters for $[I_2Cl][SbCl_6]$ obtained from the diffracting positions of 11 high angle ($17° < 2\theta < 35°$) reflections: triclinic, PT, a = 9.839(4), b = 7.119(3), c = 7.732(2)$\overset{o}{A}$, α = 91.15(3), β = 134.31(2), γ = 95.47(3)°, V = 382.9(2)$\overset{o}{A}^3$.

156. R. Forneris, J. Hiraishi, F.A. Miller, and M. Vehara, Spectro. Acta., 26A, 581 (1970).

157. present work.

158. D.J. Merryman, P.A. Edwards, J.D. Corbett, and R.E. McCarley, Inorg. Chem., 13, 1471 (1974).

159. D.J. Merryman and J.D. Corbett, ibid., 13, 1258 (1974).

160. H.A. Tasman and K.H. Boswijk, Acta. Cryst., 8, 59 (1955); 8, 857 (1955).

161. W.E. Dasent, "Non-Existent Compounds", Marcel Dekker, New York (1965).

162. V.G. Vahl and R. Minkwitz, Z. Anorg. Allg. Chem., 443, 217 (1978).

163. G. Krummel and R. Minkwitz, Inorg. Nucl. Chem. Lett., 13, 213 (1977).

164. L. Field and J.E. White, Proc. Nat. Acad. Sci., 70, 328 (1973).

165. D.L. Nosco, M.J. Heeg, M.D. Glick, R.C. Elder, and E. Deutsch, J. Amer. Chem. Soc., 102, 7784 (1980).

166. H. Sakai, J. Sci. Hiroshima Univ., Ser. A, 36, 47 (1972).

167. J. Trotter, Z. Kristallogr., 121, 81 (1965).

168. J. Trotter and T. Zobel, ibid., 123, 67 (1966).

169. T. Okuda, K. Yamada, Y. Furukawa, and H. Negita, Bull. Chem. Soc. Japan, 48, 3480 (1975).

170. C.H.W. Jones and M. Mauguin, J. Chem. Phys., 68, 3067 (1978).

171. V. Paulat and B. Krebs, Angew. Chem. Int. ed., 15, 39 (1976).

172. R.J. Gillespie and M.J. Mort, ... 969).

173. W.W. Wilson, R.C. Thompson .... (1980).

174. R.J. Gillespie, J.B. Mil............... on Inorg Chem., ..., (1968).

175. R.J. Gillespie and R. Kap ....

176. A. Engelbrecht and F. Sladk .... 4).

177. A. Engelbrecht and F. Sladky, ..., MTP Review of Science, H.J. Emeleus, ... Ltd., London, Vol. 2, Chapt. 5 (1972).

178. F. Sladky, Mh. Chem., 101, 1578 (1970).

179. F. Sladky, ibid., 101, 1559 (1970).

180. D. Lentz and K. Seppelt, Angew. Chem. Int. ed., 17, 356 (1978).

181. D. Lentz and K. Seppelt, ibid., 18, 66 (1979).

182. B.P. Dailey and J.N. Schoolery, J. Amer. Chem. Soc., 77, 3977 (1955).

183. F. Sladky and H. Kropshofer, Inorg. Nucl, Chem. Lett., 8, 195 (1972).

184. D. Lentz, H. Pritzkow, and K. Seppelt, Inorg. Chem., 17, 1926 (1978).

185. H. Pritzkow, and K. Seppelt, ibid., 16, 2685 (1977).

186. K. Seppelt and D. Nöthe, ibid., 12, 2727 (1973).

187. F. Slady, H. Kropshofer, and O. Leitzke, J. Chem. Soc. Chem. Comm., 134 (1973).

188. S.M. Williamson, Inorg. Synth., 11, 147 (1968).

189. J.G. Malm and C.L. Chernick, ibid., 8, 254 (1966).

190. C.L. Chernick, H.H. Classen, J.G. Malm, and P.L. Plurien, "Noble-Gas Compounds", H.H. Hyman, Ed., University of Chicago Press, Chicago, Ill., p. 106 (1963).

191. G.J. Schrobilgen, J.H. Holloway, P. Granger, and C. Brevard, Inorg. Chem., $\underline{17}$, 980 (1978).

192. G.J. Schrobilgen, "N.M.R. and the Periodic Table", R.K. Harris and B.E. Mann, Ed., Academic Press, London, Chapter 14 (1978).

193. N. Keller and G.J. Schrobilgen, Inorg. Chem., $\underline{20}$, 2118 (1981).

194. H. de Waard, S. Bukshpan, G.J. Schrobilgen, J.H. Holloway, and D. Martin, J. Chem. Phys., $\underline{70}$, 3247 (1979).

195. G.J. Perlow and H. Yoshida, ibid., $\underline{49}$, 1474 (1968).

196. S. Bukshpan, C. Goldstein, J. Soriano, and J. Shamir, ibid., $\underline{51}$, 3976 (1969).

197. R.D. Burbank and G.R. Jones, Inorg. Chem., $\underline{13}$, 1071 (1974).

198. A.I. Kuz'min, V.I. Shpanko, G.N. Eviadadze, V.F. Sukhoverkhov, V.S. Barkman, and B.E. Dzevitskii, Russian Journal of Inorg. Chem., $\underline{22}$, 1290 (1977).

199. (a) G. Oates, J.M. Winfield, and O.R. Chambers, J. Chem. Soc. Dalton Transact., 1380 (1974).

    (b) G. Oates and J.M. Winfield, ibid., 119 (1974).

200. A. Engelbrecht and P. Peterfy, Angew. Chem. Int. ed., $\underline{8}$, 768 (1969).

201. K.O. Christe and H. Oberhammer, Inorg. Chem., $\underline{20}$, 296 (1981).

202. G.W. Fraser and J.B. Millar, J. Chem. Soc. Dalton Transact., 2029 (1974).

203. U. Elgad and H. Selig, Inorg. Chem., $\underline{14}$, 140 (1975).

204. W. Tötsch and F. Sladky, Chem. Soc. Chem. Comm., 927 (1980).

205. G.W. Fraser, C.J.W. Gibbs, and R.D. Peacock, J. Chem. Soc. A, 1708 (1970).

206. K. Seppelt, Chem. Ber., $\underline{109}$, 1046 (1976).

207. S. Evans and A.F. Orchard, Inorg. Chim. Acta., $\underline{5}$, 81 (1971).